Headcut Retreat Resulting from Plunge Pool Erosion in a 3D Landscape Evolution Model

by

Javier Homero Flores Cervantes

Submitted to the Department of Civil and Environmental Engineering
in partial fulfillment of the requirements for the degree of

Master of Science in Civil and Environmental Engineering

at the

MASSACHUSETTS INSTITUTE OF TECHNOLOGY

June 2004

© 2004 Massachusetts Institute of Technology. All rights reserved.

Author .....
Department of Civil and Environmental Engineering
May 7, 2004

Certified by .....
Rafael L. Bras
Bacardi and Stockholm Water Foundations Professor
Professor of Civil and Environmental Engineering
Thesis Supervisor

Accepted by .....
Heidi Nepf
Chairman, Department Committee on Graduate Students

BARKER

MASSACHUSETTS INSTITUTE OF TECHNOLOGY
JUN 07 2004
LIBRARIES

Headcut Retreat Resulting from Plunge Pool Erosion in a 3D Landscape Evolution Model

by

Javier Homero Flores Cervantes

Submitted to the Department of Civil and Environmental Engineering
on May 7, 2004, in partial fulfillment of the
requirements for the degree of
Master of Science in Civil and Environmental Engineering

Abstract

Headcut retreat produced by plunge pools is represented using existing concepts about this type of erosion. The model estimates retreat rates, given flow, height of the headcut, upstream slope and Manning's roughness, and the relevant soil parameters (erodibility and critical shear stress). The model was analyzed to study its behavior as its input parameters changed, and its output was compared to experimental observations. Next, the plunge pool mechanism was implemented in an existing 3D landscape evolution model (CHILD) that includes other mechanisms of erosion like fluvial erosion and diffusion. The effects of headcut retreat on the landscape and of the landscape on the headcut retreat mechanism were investigated to learn what factors promote gully erosion and the extent of the impact of this type of erosion on the landscape. The results indicate that headcut retreat is most significant in zones comprising either gentle slopes or large headcut heights. Additional hydraulic conditions promoting to headcut retreat due to plunge pool erosion were found.

Thesis Supervisor: Rafael L. Bras
Title: Bacardi and Stockholm Water Foundations Professor
Professor of Civil and Environmental Engineering

Acknowledgments

I gratefully acknowledge the support provided by the Department of Civil and Environmental Engineering through the Schoettler Fellowship and the support provided by the U. S. Army Research Office (agreement DAAD 19-01-1-0513).

I am grateful to Rafael for the opportunity to work with him and to immerse myself in this field of research, for being my mentor and for being supportive not only in research and classes, but also in other aspects of life outside of MIT. It has been great to work with him.

I am grateful to my research group, present and past, for their listening, their counsel, and their camaraderie (Enrique, Valeri, Nicole, Daniel, Vanessa, Frederic, Jean, Bill, Erkan, Lejo, Jing Feng and Giacomo).

I am grateful to Greg Tucker, who always has been in touch regarding this project and who led our field work in Colorado. Thanks to my field trip companions (Daniel, Erkan and Bill from MIT, Lee, Peter and Vanessa from Oxford) for the food, help, suggestions and sharing of the lovely hot summer days. I thank the Directorate of Environmental Compliance and Management of the U. S. Army (DECAM) personnel for their assistance during our field work at Fort Carson and the Piñon Canyon Maneuver Site.

I also am grateful to John Germaine for the support he provided me to do the soil experiments for this project at the Geotechnical Laboratory at the Department of Civil and Environmental Engineering, and the valuable conversations we had.

Thanks to my office partners for the good vibes they always radiated: Marine, Amy and Janelle. These vibes always make life better.

Thanks to professors within and out of the Department, who shared their experience and taught me things I found very interesting.

Thanks to my international friends, who always shared their perspectives of life and from whom I am always learning something new.

To Xanat, who is always close and wise.

To Laila, who is always close and listening.

To my mother, who always sends good vibes and pushes me towards finishing what I begin, and to my father, who always listens and counsels me well.

To Mexico: I always remember where I come from.

Contents

1 Introduction **19**

1.1 Motivation 19

1.2 Outline of the thesis 21

2 Background **23**

2.1 The importance of the landscape 23

2.2 Hillslope processes 24

2.3 Processes by which water removes material from a hillslope 25

2.4 Gullying 27

2.5 Mass wasting 29

2.6 Retreating process 30

2.7 Work on which the headcut-retreat model is based 32

3 Field exploration **37**

3.1 Introduction 37

3.2 Observations and measurements 39

3.2.1 The processes 39

3.2.2 Vegetation, soil and water fluxes in the areas where gullying occurs 40

3.2.3 Plunge pool erosion and headcut retreat 52

3.2.4 Stability and stabilization of slopes 57

3.2.5 Combination of mechanisms 64

4 Headcut Retreat Model through Plunge Pool Erosion **67**

4.1 Introduction 67

4.1.1 The novelty of the plunge pool approach 67

4.2 Description of the retreat rate model 68

4.2.1 Overview 69

4.2.2 Flow characteristics 73

4.2.3 Impingement region 76

4.2.4 Erosion and retreat 78

4.3 Implementation of the headcut retreat through plunge pool erosion model into CHILD 79

4.3.1 CHILD as a framework 79

4.3.2 The eroding model for retreat 80

4.3.3 Defining a headcut in CHILD. 81

4.4 Limits of the retreat rate model 82

5 Model sensitivity and conditions for plunge pool erosion **89**

5.1 Introduction 89

5.2 Sensitivity of the retreat to q, H, n, and S 89

5.2.1 The diffusion/non-diffusion boundary 90

5.2.2 Diffusion state 92

5.2.3 Non-diffusion state 94

5.2.4 Shear stress in terms of q, n, and S 94

5.3 Conditions for plunge pool erosion 99

6 Comparison of the model output with observations from flume experiments **105**

6.1 Introduction 105

6.2 The trends of the headcut retreat rates as the parameters S, initial H and q change 107

6.2.1 Variations in S 108

6.2.2 Variations in H 110

6.2.3 Variations in q 114
6.3 Summary 116

7 Results of CHILD runs **117**
7.1 Introduction 117
7.2 Design of the experiments 118
7.2.1 The 1D model analysis of shear stress 119
7.2.2 The experiments in CHILD 125
7.3 Results from the CHILD simulations 126
7.4 Conclusions 131

8 Conclusions **133**
8.1 Summary of the work 133
8.2 The retreat rate model 134
8.3 The comparative analyses 134
8.4 Zones of the landscape where headcut retreat through plunge pool erosion is likely to happen 135
8.5 Future work 136

List of Figures

3-1 Fort Carson and PCMS training sites. 38

3-2 Big Arroyo in PCMS. The top photograph shows the site in the summer of 2002, while the lower photographs show the same site in the summer of 2003, when more rain occurred. 42

3-3 Location of the soil sampling and of the headcut measurements. . . . 44

3-4 Vertical walls of gullies. On the left, "Horton Gully", a gully formed on the east of Fort Carson's Route 11 and whose location is shown in Figure 3-3. On the right, a hanging wall in Big Valley, Fort Carson, formed in a soft cohesive bedrock. 48

3-5 Cohesion and headcut height H of several headcuts, reported in Table 3.1. 49

3-6 Pipes observed in Big Valley (left) and in the Big Arroyo headwaters (right) in Fort Carson. Dispersion of soils is a major cause of the formation of natural pipes in soils. A notebook serves as scale on the photograph on the right. 50

3-7 Sketch of a field plunge pool. This is the general plunge pools' profile observed at the Little Grand Canyon, in Fort Carson. 53

3-8 Plunge pools observed at the Little Grand Canyon in Fort Carson (top) and Big Arroyo in PCMS. The top gully drains into a larger incising channel. The channel formed by the retreating headcut shown at the bottom disappears a few meters downstream. 54

3-9 Shape factor S_f of the last ten headcuts described in Table 3.1 and their corresponding headcut height H. 55

3-10 Scheme of a series of plunge pool observed in the Little Grand Canyon, in Fort Carson. 58

3-11 Series of retreating scarps along an incising channel shown by the white arrows, in Big Arroyo (PCMS). 59

3-12 A section of Taylor Arroyo (PCMS) showing a gentle slope covered with vegetation in the foreground, and vertical slopes with no vegetation at all in the background. 61

3-13 A section of Taylor Arroyo (PCMS). The slope retreats when its toe is incised and made unstable. 62

3-14 A branch of "Horton Gully" in Fort Carson. One side has vertical scarps, while the other has gentle slopes and vegetation. 63

4-1 Hydraulic characteristics considered in the headcut-retreat model. . . 68

4-2 Plunge pool retreat schematic. 69

4-3 Shape of an idealized plunge pool. 71

4-4 Relationship between the volume and shape of a plunge pool, from Stein and Julien, 1993 [36]. 72

4-5 Flow characteristics before it penetrates the plunge pool. 75

4-6 Jet impinging a plunge pool, modified from Stein *et al.*, 1993 [37]. . . 76

4-7 Schematic of a section of the flow network created by CHILD. 81

4-8 Example of the retreat of a cell. 82

4-9 Flow at the brink under fast flow conditions. The figure shows the flow at the brink (h_{brink}) and the upstream normal flow (h_n), for the fast (a small flow depth) and slow (a large flow depth) flow conditions. These flow conditions delimit the possible depths at the brink for the specified ranges of n and S. 84

4-10 Shear stress at the bottom of the pool for $H = 0.5m$ as q increases. Two flow conditions are shown: the slow flow conditions correspond to the maximum roughness n and minimum slope S of the previously specified range for these parameters; the fast flow conditions correspond to the minimum roughness and maximum slope within the previously specified range. The break in the slope of the line corresponding to the slow flow conditions marks a transition from a diffusion to a non-diffusion state. This transition is further explored in Chapter 5. 85

4-11 h_t/D ratio, calculated with $h_t = h_n$. This figure illustrates how negligible or significant h_t is. Fast(small depths) and slow (large depths) flow conditions are shown. As H becomes smaller, the ratio h_t/D increases and h_t becomes more significant. In this example the shape factor, Sf, is 0.2. 86

4-12 Flow depth at different points along the headcut-plunge pool system. 86

4-13 Depth of the flow downstream of the plunge pool, h_t, that should be smaller than $H_{original}$ in order to satisfy the ventilated jet condition (that is, a non-submerged jet). Fast(small depths) and slow (large depths) flow conditions are shown. 87

5-1 Boundary between the diffusion and non-diffusion zones. This example corresponds to a subcritical flow regime. In this example $S_f = 0.5$. . . 91

5-2 Flow characteristics before it penetrates the plunge pool. 92

5-3 Jet impinging a plunge pool, modified from Stein *et al*, 1993 [37]. . . 93

5-4 Velocity component vectors of the water jet impinging into the plunge pool. 94

5-5 Variation of the boundary between the diffusion and non-diffusion zones as n varies. The boundary moves upward as n increases. A constant H_p is observed in the subcritical regime, where the boundary between the diffusion and non-diffusion zones is independent of n. In this example $S_f = 0.5$. 95

5-6 Variation of the boundary between the diffusion and non-diffusion zones as S varies.The boundary moves downward as S increases. A constant H_p is observed in the subcritical regime, where the boundary between the diffusion and non-diffusion zones is independent of S. In this example $S_f = 0.5$. 96

5-7 Variation of the shear stress in the diffusion zone. Each vertical line represents shear stress in intervals of $10Pa$, increasing as flow increases. In this example $S_f = 0.5$. 97

5-8 Variation of the shear stress in the diffusion zone. Each line represents shear stress in intervals of $10Pa$, increasing in the upward direction. In this example $S_f = 0.5$. 98

5-9 Behavior of the shear stress as q increases and the diffusion/non-diffusion conditions change. In this example the flow regime is subcritical and $S_f = 0.5$. 100

5-10 Behavior of the shear stress as H increases and the diffusion/non-diffusion conditions change. In this example the flow regime is subcritical and $S_f = 0.5$. 101

5-11 Behavior of the shear stress as n increases and the diffusion/non-diffusion conditions change. In this example, the flow regime is supercritical for small values of n, and subcritical for larger values. The horizontal line on the left plot corresponds to the subcritical regime. In this example $S_f = 0.5$. 102

5-12 Behavior of the shear stress as S increases and the diffusion/non-diffusion conditions change. In this example, the flow regime is subcritical for small values of S and supercritical for larger values. The horizontal line on the left plot corresponds to the subcritical regime. In this example $S_f = 0.5$. 103

5-13 Headcut height (H) and flow (q) threshold conditions for plunge pool erosion with $\tau_{cr} = 40Pa$, $S = 0.035$, $n = 0.05$ and $S_f = 0.2$. The flow regime under these flow conditions is subcritical for the range of flows (q) shown. 104

6-1 Observed and calculated retreat rates as S increases. 108

6-2 Values of S_f as S, H and q change. 111

6-3 Values of D as S, H and q change. 112

6-4 Observed and calculated retreat rates as H increases. 113

6-5 Observed and calculated retreat rates as q increases. 115

7-1 Hydraulic characteristics and soil properties considered in the retreat rate model. 120

7-2 Plunge pool and sheetflow shear stresses for slow flow conditions. . . 121

7-3 Plunge pool and sheetflow shear stresses for fast flow conditions. . . . 121

7-4 Plunge pool and sheetflow shear stresses for high [sheetflow] shear stress conditions. 122

7-5 Plunge pool and sheetflow shear stresses for low [sheetflow] shear stress conditions. 122

7-6 Plunge pool and sheetflow shear stresses for a shape factor (S_f) of 0.5 (large shape factor). All the previous examples consider an S_f of 0.2. 123

7-7 Example of a simulated surface in CHILD, view from above, where darker colors represent low elevations and lighter colors high elevations. The left and right figures are the surface conditions after one hundred and one thousand $1hr$ storms have occurred in the simulation, respectively. The dimensions shown are in meters. 126

7-8 Evolution of a profile extracted from the simulated surface. The drainage area corresponding to the outlet of the profile changes as the profile evolves. The vertical and horizontal scales are elevation and negative distance from the outlet, respectively, in meters. 128

7-9 Comparison of the evolution of the profile extracted from two CHILD simulations: High initial H (on the left) and Low initial H (on the right) (see Table 7.3). The vertical and horizontal scales are elevation above and negative distance from the outlet, respectively, in meters. . 129

7-10 Comparison between the evolution of the profile extracted from two CHILD simulations, one considering headcut retreat and the other not considering it, for the same initial conditions (simulations High initial H on the left and No headcut retreat on the right) (see Table 7.3). The vertical and horizontal scales are elevation above and negative distance from the outlet, respectively, in meters. 130

7-11 Comparison of the evolution of the profile extracted from two CHILD simulations: Fast flow conditions and Slow flow conditions (see Table 7.3). The vertical and horizontal scales are elevation above and negative distance from the outlet, respectively, in meters. 130

7-12 Examples of the evolution of two profiles extracted from a CHILD simulation where the initial slopes are little eroded by sheetflow because the slope gradients are small. Both profiles correspond to the simulation Examples of a headcut in a flat zone, summarized in Table 7.3. The vertical and horizontal scales are elevation above and negative distance from the outlet, respectively, in meters. 131

List of Tables

3.1 Headcut field measured dimensions, slopes, cohesion, and drainage areas. 43

3.2 Soil samples characteristics. 45

3.3 Physical properties of the major size fractions in soil [34]. 46

5.1 How retreat varies with n and S, depending on the diffusion state. . . 99

6.1 Conditions of flow q, headcut height H, and upstream of the headcut slope S corresponding to the experiments carried out by Bennett and coworkers. * See Section 6.2.1. 107

6.2 Values of H and n of the experiment when S increases. The values of n were back calculated from the experimental upstream flow conditions. 110

7.1 Conditions of the 1D comparative analysis between the plunge pool and sheetflow shear stresses. 119

7.2 Plunge pool, sheetflow shear stresses, and their difference, corresponding to the 1D shear stress simulations of this comparative analysis, for $q = 0.01m^2/sec$. 124

7.3 Summary of the conditions simulated in CHILD. 126

Chapter 1

Introduction

1.1 Motivation

Gully erosion consists of the removal of soil from a hillslope through the incising of a channel, particularly during short, intense flow events. This type of erosion is common in semiarid regions, in gentle slopes, and forms channels with steep sides and a steeply sloping or vertical head scarp [34]. Gullies often extend through scarp retreat. One type of scarp is the headcut, a step change in bed surface elevation that occurs at the head of a channel where intense localized erosion takes place [3]. Scarps may occur within a channel, in which case they are referred to as knickpoints [3].

From a practical point of view, gully erosion is relevant because often it affects human activities: gullies make agriculture and grazing difficult, deteriorate roads, airport runways and other civil works, affect military training grounds, and produce sediments that might fill water bodies. Ironically, many of today's gullies resulted from the human activities they now undermine such as infrastructure construction, agriculture and grazing.

From the scientific point of view, the gully is an interesting geomorphologic phenomenon that originates during short time events (of a few hours), creates avenues of flow along the landscape, sets channel head locations, and produces features that may persist in the landscape for long periods of time. Because gullies are channel heads that determine channel extension, they are tightly linked to drainage network

development. "Geomorphologists have examined migrating headcuts and knickpoints in relation to rill incision, drainage network development, and alluvial response to base level lowering" (Bennett *et al.*, p. 1911 [3]).

The purpose of this thesis was to improve our understanding of the processes acting on gully erosion via the development and use of numerical models of these processes. Its aim was to create a way to represent gullies in a 3D landscape evolution model. The interest was in learning what triggers gullying, under what circumstances the land is more or less susceptible to it, and what human-induced factors enhance or reduce gully activity, before and after the erosion process begins.

Several mechanisms of erosion interact with each other in the gullying process [33]. Fieldwork in southeastern Colorado, at two military training sites (Fort Carson and Pinõn Canyon Maneuver Site (PCMS)), led to the interest in the study of a particular mechanism of erosion at gully heads, headcut retreat through plunge pool erosion. Plunge pools have been observed at headcuts in these sites as discussed in Chapter 3. In addition, plunge pool erosion has been observed by others at several active gully heads [24, 10], and it has been suggested as one of the major causes of gully headcut retreat [10]. The studies carried out by other researchers regarding headcut retreat through plunge pool erosion, in particular for agricultural purposes [3, 4, 2, 36, 37, 35], provided the bases for the development of this thesis' modeling of headcut retreat through plunge pool.

Through modeling, this thesis aims to explore where in the landscape the plunge pool mechanism is an important erosional process. Here it is hypothesized that plunge pool, as well as other retreat processes, will dominate over diffusion and wash mechanisms in a soil that resists headcuts (i.e., a cohesive soil); where the top soil layers are resistant (e.g., due to vegetation); and/or the hydraulic conditions favor retreating mechanisms, such as zones of gentle slopes, high headcuts, and flow magnitudes that are not extremely large (so that flow depths, and thus shear stresses, are not large enough to wash out the headcut).

1.2 Outline of the thesis

A novel 3D headcut-retreat-model-through-plunge-pool-erosion, henceforth referred to as the headcut-retreat model, was implemented in the Channel-Hillslope Integrated Landscape Development (CHILD) Model [42], a 3D landscape evolution framework where other erosion processes such as wash erosion and diffusion have already been represented. The headcut-retreat model and CHILD are further described in Chapter 4. A background section is provided in Chapter 2, describing the relevance of the studies of landscapes; what hillslope processes are and how they are studied; what gullying is and its link to mass wasting processes; what mass wasting processes are and their link to retreat processes; why plunge pool is studied as a retreat process; and the work of others on which the headcut-retreat model is based.

Chapter 3 describes the fieldwork carried out at the two military training sites in Colorado.

Chapter 5 discusses the way the retreat rate of the headcut-retreat model behaves as the hydraulic characteristics of the flow approaching the headcut vary. Those changes are a function of the location of the headcut in the landscape. Two types of model behavior were observed. One in the diffusion state, the state in which the plunge pool is deep enough so that the water jet falling from the headcut experiences a significant amount of diffusion before it reaches the bottom of the pool and erodes it. The other one is the non-diffusion state. The model behaves differently to changes in hydraulic conditions depending on the state.

Chapter 6 explains how the retreat rate of the headcut-retreat model compares to retreat rates observed in a series of flume experiments.

Chapter 7 describes a series of experiments on the headcut-retreat model implemented in CHILD. The experiments were carried out with the objective of exploring the conditions in which headcut retreat through plunge pool erosion is more or less a relevant erosive process in the landscape, in comparison to sheetwash erosion. The results of these experiments support the hypothesis that headcut retreat is a relevant process in gentle sloped terrain with large headcuts, where water flow concentrates

(but the flow is not strong enough so that headcuts are washed away). Additionally, that in a state of diffusion, headcut retreat is favored by a large surface roughness that may be provided by vegetation.

Chapter 8 provides the thesis' concluding remarks and future lines of research.

Chapter 2

Background

2.1 The importance of the landscape

Understanding the changes and processes that take place in the landscape, in time scales relevant to the evolution of human history and to ongoing human activities, improves our understanding of the interaction between humans and our environment. The evolution of landscapes is studied by geomorphologists from two different perspectives: one focuses on "when" the changes have occurred, and on the sequence of events that in long periods of time (thousands and millions of years) gave place to contemporary landforms. The other focuses on the "why" those landforms developed, and on the processes that act on the land surface and that through time result in landforms and landscapes such as the ones we know today [27]. In the second approach geomorphologists "observe physical phenomena over short time spans" and focus on "the mechanics of agents producing erosion or deposition rather than the landform which they create" (Ritter, p.160 [27]). Thus, the second approach can provide pragmatic knowledge useful in understanding the current interaction between human activities and processes that shape the landscape. Gully erosion is a landshaping process that causes problems to humans as it changes the landscape in short periods of time. Some examples of these problems are given in the Introduction.

Two different zones of action of the landscape shaping processes are generally recognized: the hillslope and the channel [43]. The processes acting on each of these

zones interact at the channel-hillslope interface. Gullying and headcut retreat occur along such interface because they result in the incision of channels into hillslopes. They are considered hillslope processes.

2.2 Hillslope processes

"Hillslopes occupy most parts of the landsurface" (Selby, p.1 [34]) of Earth. Different processes of erosion and deposition occur on them. The evolution of a hillslope is complex as a result of the "many influences of variable intensity ... [on] .. the rate at which hillslope forms change" (Selby, p.1 [34]). Understanding these processes is often complicated because normally they can only be monitored for a few years, while they only produce changes of the order of millimeters in a year, of millimeters in thousands of years, and/or the changes occur during rare, catastrophic events [34].

It is known, as Selby states, that the process of removal of rock and soil from hillslopes "is episodic and depends upon the availability of energy and transporting medium" (Selby, p.4 [34]). It is also known that the frequency and intensity of these processes depend on the forcing events and resistance of the materials. Hillslope studies involve the evaluation of short term changes, through the tracing and measurement of movements of materials from hillslopes through different processes, as well as modifications of the hillslopes by these processes [34]. "In theory this should eventually provide an understanding of how a hillslope evolves" (Selby, p.4 [34]). The sources of energy to erode and transport soil are also studied and related to the magnitudes of changes observed. Measuring the sources of energy of the erosion-deposition systems is even more difficult than measuring the changes in the hillslope.

To compensate for the lack of observations over long time periods of hillslope evolution, process-response models have been developed [34]. The headcut-retreat model of this thesis aims to provide insight about a problem which is difficult to observe over short periods of time, and even more in long periods of time, under natural conditions.

The following three sections (Section 2.3, 2.4 and 2.5) are a description of the

processes that shape hillslopes, headcut retreat by plunge pool erosion being an important one. Selby [34] provides a comprehensive synthesis of these topics, which the following three sections closely follow.

Headcut retreat, even though it is considered a hillslope process, is a process that acts at the channel-hillslope interface and may extend a basin's channel network. Hence, headcut retreat may have implications in the long term evolution of a basin, given the dependence of a basin's geomorphic evolution on its channel network extension. Such implications, however, are beyond the scope of this work.

2.3 Processes by which water removes material from a hillslope

Water removes soil from the hillslopes through wash, rill, piping and gully erosion processes. The first three are described below, gully erosion is further described in the following section. These descriptions are based on the Selby's synthesis of the processes [34]

On the hillslope, the formation of patterns of alternating scour-deposit sequences are observed at different scales. This patchiness results from different processes but happens because of the same fundamental reason: the erosive, transport, and resistant forces vary along the landscape. Where the resistant forces are the largest, little erosion takes place. Where the erosion and transport forces are larger than the resistant forces, erosion and transport occur. Where the transport forces are smaller than that required to transport the sediment in the flow, deposition occurs.

These scour-deposit patterns point to the strong relationship between the hydraulic characteristics and the sediment transport rules of the system, and show that the hydraulic characteristics of an ephemeral and variable flow path are changing constantly. Sediment transport mechanisms are important in the physical development of the hillslope, but are difficult to model and are not considered in this thesis.

Wash erosion is the detachment of soil particles in the hillslope and its trans-

portation as suspended or bedload in the flow. The detachment is due to the action of raindrops on an exposed soil surface and to the shear stress produced by flowing water. Sheetwash erosion is the wash erosion resulting from sheetflow. In the process of wash erosion the hydraulic conditions vary over short distances and, due to such variations, patterns of miniature alternating scour-deposit sequences form [34].

"**Rills** are small channels with cross-sectional dimensions of a few centimeters to a few tens of centimeters[, and] they are usually discontinuous" (Selby, p. 232 [34]). Rills may disappear between storms through diffusion, or within storms when they oversaturate with sediments or their sides collapse due to liquefaction [34]. Rills grow via the scouring of their beds or through rill merging. Rills may enlarge and become gullies or heads of natural drainage systems [34]. Some rills become wider and shallower in their downstream direction, and their sediments, usually sands, deposit in downstream sections [34]. The depositing and scouring of small rills gives place to patterns of alternating scour-deposit sequences, characteristic of wash erosion. Rills, as well as gullies, can form through the collapse of the roof of micropipes and tunnels, which are common in shrink swell clays, particularly in smectite-rich soils.

Rills and gullies, as channels, are efficient avenues of sediment transport. They transport the sediments produced by the erosion of the rill and gully margins as well as the eroded sediments flowing into the channel. Wash and rill erosion is different depending on whether the flow is produced by a short intense rain event, or by a long, low intensity event. In the first case, high shear stresses are produced by the flow, and in the second, resistant forces of the soil are reduced due to saturation of the soil [34].

Piping results from pipe flow, a hydrological process that has been greatly underestimated as an hydrologic process, principally because it is difficult to detect [34] p.217. Pipes may contribute to large amounts of flow and erosion, and result in the main gullying mechanism in certain zones. Few modeling efforts and studies of the phenomenon have been made. Pipes form when water infiltrates through cracks or animal- and vegetation-made conduits, and reaches a permeable layer or dispersible clay through which it begins to slowly flow laterally. When this flow seeps out of

the soil, it accelerates and is more likely to detach particles, and initiate or enlarge a pipe. Gullies promote piping when they incise the land because water will seep through their walls.

Pipes vary in size, between 0.02 and $1m$ in diameter, and between a few meters and more than $1km$ in length [34]. They are more likely under the following conditions: a seasonal or highly variable rainfall; a soil with cracking periods; a reduction in vegetation cover; a relatively impermeable layer in the soil profile; a hydraulic gradient; and a dispersible soil layer [34]. Therefore they are common in semiarid badlands and on smectite clays, which have strong swelling and shrinkage properties, and may have a high exchangeable sodium content, often associated with dispersible soils [34]. Pipes are also common in loess and loessic colluvium with high sodium content [34].

2.4 Gullying

A gully is "a recently extended drainage channel that transmits ephemeral flow, has steep sides, a steeply sloping or vertical head scarp, a width greater than 0.3 m and a depth greater than about 0.6 m" (Brice 1966, p.290, cited by Selby, p.236 [34]).

According to Selby [34], three types of gullies form. The first type forms when a rill enlarges and acquires gully dimensions or, when a break in slope of vegetation cover produces an abrupt change in erosion rates so that an abrupt change in elevations across the break occurs and a headcut develops. Often these headcuts develop when "the underlying soil of a hillslope is mechanically weak or unconsolidated" (Selby, p.236 [34]), and, when erosion reaches this layer, an abrupt change in erosion rates arises. Because of the weakness of the underlying materials, this type of gully is more common in "deep loess, volcanic ejecta, alluvium, colluvium, gravels, partly consolidated fans, and debris from mass movements" (Selby, p.236 [34]). The second class of gullies forms in weak argillic rocks, which are rocks formed from muds. They include mudrocks and shales. In the third class, gullies are initiated by subsurface flows or natural pipes. These include gullies formed by seepage and by the collapse

of pipes .

Gullies frequently result from changes in the environment, particularly environments where the equilibrium between the erosive and resistant forces is precarious. They are usually produced by an increase in the erosive power of the system (e.g., due to an increase in flood runoff or decrease in sediment load) or by a decrease in the resistance to erosion (e.g., due to the deterioration of vegetation)

Gullies may be continuous and form channels, or discontinuous and form erosion-deposition sequence patterns. Continuous gullies that form by the enlargement of a rill may have no headcut, and become deeper and wider toward their downstream end, but as they approach the base of the slope, "the gullies have zones of deposition which extend [and form fan deposits at their lowest end]" (Selby, p.239 [34]). This type of continuous channels usually form in non-cohesive material without a resistant capping and resemble a gravel or sand channel formed only by scouring. Gullies that form above underlying cohesive material, or where a resistant layer covers a non-cohesive layer, have the potential to develop and maintain headcuts [34].

Because new gully-enhancing mechanisms appear once gullying begins, it is easier to prevent it than to correct it. Some solutions used to solve the problem focus on reducing the flow such as: the building of check dams; the revegetation of the slopes to slow the flow down and increase infiltration; the channelization of flow away from the areas prone to gullying; and the bank sloping of gullied channels to reduce the flow velocities and thus the flow's erosive power [34]. Other solutions focus on increasing the resistance to erosion, through a good vegetation cover and through the use of rip rap [34].

Hillslope forms and orientation have been correlated with certain erosion processes. Headcuts are related to seepage erosion. Gradually sloping heads are usually related to saturation overland flow. Seepage and landsliding normally lead to steep slopes and overland flow processes to gentle slopes. It has been observed that pole-facing slopes experience less erosion due to slope instability than equator-facing slopes. An explanation for this is that these slopes receive less solar radiation and thus fewer cracks develop, less water infiltrates and lower pore pressures develop.

And so, pole-facing slopes are more stable and subject to more fluvial erosion and weathering than equator-facing slopes[34]. The effects of slope orientation are beyond the scope of this work.

2.5 Mass wasting

"Mass wasting of soil and rock is a major process in the development of hillslopes, [particularly in steep mountainous regions]" (Selby, p. 249 [34]). The term refers mostly to landslides. "Mass wasting is the downslope movement of soil or rock under the influence of gravity without the direct aid of ... water, air, or ice" (Selby, p. 249 [34]); water and ice generally reduce the strength of the slope materials "contributing to plastic and fluid behavior of soils" (Selby, p. 249 [34]).

Mass wasting includes landslides, falls, topples and creep. Headcut retreat produces falls, which "involve small amounts of material and are usually the result of undercutting of the toe or face of a slope by a river or by wave action... Falls are facilitated also by weathering and the opening of fissures near a cliff top as a result of freeze-thaw, wetting and drying, earthquake shocks, or tension" (Selby, p. 249 [34]).

Scarps of gully walls or heads may also mass waste through slumps. Slumps have a curved failure plane and fail with a rotational movement [34]. They are common in engineering works such as cuttings and "under entirely natural conditions, especially where the toe of a slope has been undercut by a river or wave action" (Selby, p. 260 [34]).

Water has a large effect in mass wasting. Some of the water effects on slopes are the hydration of clay (and thus its expansion and contraction), undercutting of slopes, increasing of the weight of soil, weathering of the soil, and spontaneous liquefaction. But most important are the water's buoyancy effects, the reduction in capillary tension, decrease in aggregation, and viscous drag on soil grains, that produce instabilities that often lead to the falling of a block of soil [34].

The drag of moving water on soil particles is small in well drained soils (e.g., gravels), where the grains are resistant to the drag. In clays, seepage is usually minor

because clays are impermeable. It is on silts and fine sands where seepage is most effective. Silts and fine sands are permeable and offer little resistance to the water drag. Rapid drawdowns in reservoirs and along riverbanks generate steep pressure gradients in the water table and thus strong seepage flows and high pore pressures that cause bank collapse. In a rapid drawdown, the walls of dams and riverbanks also lose the restraining pressure provided by the water body, further contributing to the wall collapse [34].

The effect of buoyancy and reduction of capillary tension, due to soil saturation and resulting increase in pore pressure, is larger in slopes where flow is not parallel to the slope and converges into the base of the slope, and the resulting pore pressure increase is even larger where an impermeable layer, such as that resulting from a debris flow, prevents the flow from emerging. Pore pressure effects are higher in hollows, where subsurface flow converges [34].

The effects of water in destabilizing a headcut as described in the above paragraphs are out of the scope of this thesis.

2.6 Retreating process

Mass wasting itself is a complex erosion mechanism because several mechanisms and influences of variable intensity are active it. An approach that simplifies the study of the mechanism is focusing on the retreat produced by the mass wasting mechanism, instead of analyzing the stability of the headcut through a factor of safety, as the problem has traditionally been approached. The retreat can be easily measured (a length in a given amount of time) and related to known and measurable factors (such as erosive and resistive forces acting on it).

Retreat can been defined as the parallel retreat of a slope. Parallel retreat is a type of slope evolution "characterized by the preservation of constant angles in the steepest part of the slope" (Selby, p.131 [28]), and it "is characterized by the retreat of a nearly-vertical ... face without a change in its inclination" (Ritter *et al.*, p.230 [28]). This type of slope evolution takes place where a step-change (i.e., a scarp)

in the slope occurs. For the process to take place, the face of the scarp most be uncovered, clear of debris or talus. This type of slope evolution is more common in semiarid lands than in more humid areas, where diffusion processes are more active and step-changes in the topography tend to diffuse away [28].

Top layer resistance to erosion, and cohesion in the soils, help in the development of parallel slope retreat [28]. These two factors contribute to the maintenance of scarps. Parallel retreat is common in layered soil profiles [28] where the top layer is more resistant to erosion. Step-changes in rocks and cohesive soils last longer [13] than in cohesionless sediments, where they will smooth quickly (Ritter, 1999, cited by Ritter *et al.*, p.230 [28]).

Some have related retreat to weathering of rocks (e.g., Howard [17], and the parallel retreat described in Ritter *et al.* p.131 [28]), to subsurface flow seeping through scarp faces [16], and plunge pool erosion at the base of a headcut [1, 10, 11, 39]. In modeling efforts, retreat has also resulted from the adjustment of slopes to a maximum slope gradient, when the such gradient increases due to the erosion of the bottom of the slope by wash processes [18].

The retreat processes described above creates landforms that evolve in ways that wash erosion and diffusion processes cannot reproduce, and make them distinct from the landforms created only by fluvial and diffusive erosion processes.

The fluvial and diffusion erosion processes, however, also act on these particular landforms. Diffusion processes tend to diffuse the sharp slope changes characteristic of these landforms, and wash erosion tends to diffuse headcuts. Wash erosion along channels, however, often contributes to the undermining of channel walls and thus contributes to the maintenance of scarps. In addition, vertical scarp faces frequently result from channel deepening due to wash erosion. Plunge pool erosion at the base of headcuts is a mechanism that undermines these land features as wash processes do along channel wall bases: through the entrainment of particles by the flow.

2.7 Work on which the headcut-retreat model is based

Gully erosion as a mass wasting process at the hillslope scale is a complex phenomenon that results from the interaction of several erosive mechanisms occurring at its head scarp, its walls and channel bed (e.g., sapping by seepage, piping, scouring, undermining of the scarps, instabilities of the slope due to changes in soil water content, etc.). Therefore studying each of these mechanisms individually first is a reasonable step toward the understanding or the gully erosion phenomenon. In the future, the interaction between these processes and the sum of their effects can be explored.

Headcut retreat through plunge pool, which may be one of the strongest erosive mechanisms in gully development, is studied in this thesis through field observations and modeling. The following findings from past experiments and modeling efforts are used as the basis for the development of this thesis' headcut-retreat model.

1. De Ploey (1989) [10] developed a mathematical model to describe the retreat of a headcut due to plunge pool erosion. This model estimates a retreat rate as a function of the height of a headcut (H), the flow velocity at the brink of the headcut (V_{brink}), and an *erosion coefficient.* The model assumes that the volume eroded from the scarp is proportional to the kinetic energy of the flow striking the pool, and inversely proportional to the stability of the headcut. The model's proportionality coefficient, the *erosion coefficient*, comprises the stability of the headcut, and is a *black box* factor meant to be found empirically on the field. The difficulty in estimating this value, and the uncertainty of what this value is for most cases, make De Ploey's model difficult to use as a predicting tool.

2. Dey *et al.* (2001) [11] carried out a set of laboratory flume experiments in a stratified soil. The top layer was fine poly vinyl chloride (PVC) grains that acted as a cohesive topping, while the lower layer was composed of coarse sand that acted as a non-cohesive bed material. The top surface of the PVC material was covered with and adhesive spray that made a surface resistant to erosion.

They studied the effects of changes in the height of the headcut (H) and in the flow per unit width (q) in the impinging jet's characteristics, the shape of the plunge pool, and the headcut's retreat rate. With the data collected, they fitted the parameters of a retreat rate model. In their model they use concepts developed by Stein *et al.* [37] regarding the the maximum shear stress produced at the bottom of the plunge pool. In their model the retreat rate is a function of that shear stress and of a sediment transport equation applied to the zone of maximum shear stress at the bottom of the pool. The equation is of the form

$$d = A(\tau - \tau_{cr})^m$$

where d is a deepening rate of the plunge pool, A an erodibility coefficient, τ and τ_{cr} the shear stress and the critical shear stress respectively, and m, an empirical exponent.

Dey *et al.*'s model is similar to the retreat rate model of this thesis because both of them estimate a retreat rate as a function of the maximum shear stress generated by an impinging jet at the bottom of the pool, following a procedure suggested by Stein *et al.* [37]. However, Dey *et al.*'s model represents headcut migration in a stratified soil, while this thesis' model focuses on homogeneous soils. In addition, Dey *et al.*'s model uses a measured depth of the plunge pool as an input, while, in this thesis, that depth is calculated within the model, as explained in Section 4.2.1)

3. Stein *et al.* (1993) [37] explored the mechanics of the scouring of a plunge pool by an impinging jet immediately downstream of a headcut. In their analysis the impinging jet characteristics (velocity (V_{pool}), thickness of the flow (y_{pool}), and angle of impingement (β)) and depth of the pool (D) are enough to estimate the maximum shear stress at the bottom of the pool. With the shear stress, they estimate the maximum possible depth of the pool (depth of equilibrium, D_e, for a given critical shear stress) and the pool's deepening rate following a sediment transport equation like the one used by Dey *et al.* (2001) [11].

4. Stein and Julien (1994) [36] studied the detachment of sediment from a plunge pool developing due to an impinging jet. They found a relationship between the scoured volume per unit width of a plunge pool and scour depth for a considerable variety of materials and of flows. This thesis uses the relationship between scoured volume per unit width and plunge pool depth to estimate the depth of the plunge pool (D) as a function of the geometry of the water jet impinging the pool (see the *Shape of the plunge pool assumption* in Section 4.2.1.

5. Bennett (1999) [2], Bennett *et al.* (2000) [3], and Bennett and Casali (2001) [4], carried out a series of flume experiments on homogeneous soils in which, in a narrow flume, a headcut retreats at a constant rate by plunge pool scouring at its base. These experiments are the basis of the constant headcut retreat rate assumption of this thesis (see *Homogeneous soil and constant retreat rate assumption* in Section 1). These experiments explore the effects of changes in: slope (S), flow (q), and the headcut height (H), in: the shape of the plunge pool, the headcut migration rate, and the sediment yield. In addition, in Bennett (1999) [2] and Bennett *et al.* (2000) [3], a constant ratio between the maximum depth of scour and the length from the headcut to the maximum depth of scour is observed as the dimensions of the pool change due to variations in flow (q) and slope (S). In this thesis, that ratio is assumed (see the *Shape of the plunge pool assumption* in Section 4.2.1).

6. Recently, Alonso *et al.* (2002) [1] created a model that predicts headcut retreat in homogeneous soils in zones of concentrated flow such as rills. In addition to the headcut retreat, their model predicts the sediment produced by the headcut retreat and the plunge pool depth (D). The inputs to their model are the overland flow rate (q), the initial headcut height (H), and the flow conditions upstream of the brink. Alonso *et al.* (2002) [1] based their model on and validated it with the experimental results published by Bennett (1999) [2], Bennett *et al.* (2000) [3], and Bennett and Casali (2001) [4]. The model calculates the retreat rate by combining two equations. First they solve for the power per

unit width lost by the flow at the plunge pool from a hydraulic point of view. Second they solve for the power lost by the flow due to the action of removal of sediment from the plunge pool, using a sediment detachment equation such as that employed by Dey *et al.* [11]. Then, equating the power loss of both approaches, a retreat rate equation is found. That equation relates the headcut migration rate to the impinging jet velocity (V_{pool}), the depth of the plunge pool (D), the flow per unit with (q), and a parameter μ that is a function of the soil erodibility and the jet entry angle (β). Alonso *et al.* (2002) [1] propose a correction factor for the angle of impingement, β (see Figure 4-5), when the water impinging the plunge pool is submerged, a case that occurs when the depth of the flow downstream of the headcut is similar to or higher than the height of the headcut. According to Alonso *et al.* (2002) [1], the angle of impingement increases when it is submerged. The submerged case is excluded from the current thesis' model because it would add complexity to a model already complicated, with many variables and intermediate calculations. In their model, the depth of the plunge pool (D) is a fraction of the depth of equilibrium (D_e, which is the maximum possible depth of the pool due to scouring for a given critical shear stress). The fraction is determined with an empirical coefficient particular for each material and each hydraulic condition.

Alonso *et al.* (2002) [1] model is appealing. The retreat rates it predicts are similar to those observed (they are within 40 percent from the observations, in the range of conditions of the experiments). But the need of an empirical factor to estimate the depth of the plunge pool limits its use to situations where the coefficient is known or can be calculated.

Chapter 3

Field exploration

3.1 Introduction

Fieldwork was carried out at two military training sites, Fort Carson and Piñon Canyon Maneuver Site (PCMS), with the objective of studying the dynamics of gully development in the region. These two sites are located in the semiarid region of southeastern Colorado (Figure 3-1). Fort Carson is located at the foot of the Colorado Front Range, just south of Colorado Springs, and PCMS is located in the High Plains grassland of southeastern Colorado (Las Animas County) north of the Purgatoire River. Fort Carson's physiography ranges from low-relief piedmont slopes to rugged foothills, and is underline primarily by Mesozoic and Cenozoic sedimentary rocks. The mean annual rainfall of neighboring Colorado Springs is $412mm$, over half of which falls between May and August. These months also see the most thunderstorm activity. The soils in the region are silty clay and clay loam in the plains, and gravelly sandy loam with scattered rocks on the hillslopes and steeper slopes. In this region, incising gullies are typically rectangular to U-shaped in cross-section, with distinct headcuts and steep side walls, along which mass wasting is evident.

The goals of this fieldwork were to gather evidence of the environment where gullies develop in terms of topography, vegetation, geology and soil type, and to gather evidence of the processes taking place in such development. In the beginning, the objective was to identify the main mechanisms of gullying in the region. Later

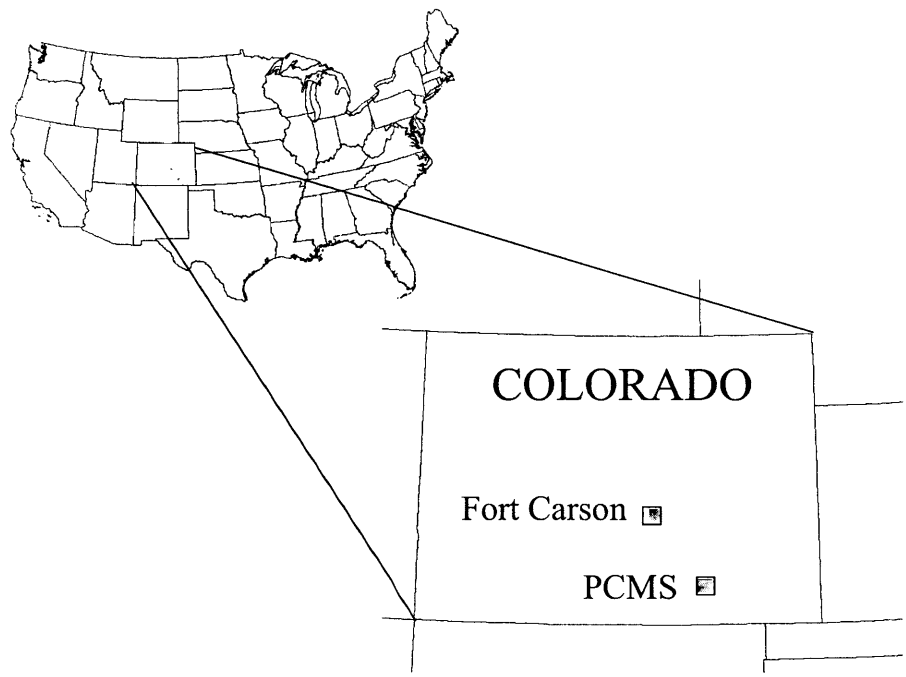

Figure 3-1: Fort Carson and PCMS training sites.

on, two of these, headcut retreat due to plunge pool erosion and headcut and gully wall retreat due to instability, were the main focus of the remainder of the fieldwork.

This fieldwork provided a sense of the processes contributing to gullying and headcut retreat, of the environment where these land features form, and of characteristics of this environment contributing to gully development and headcut retreat. The hypothesis of the thesis is largely due to the insight obtained from this fieldwork.

The fieldwork was carried out during the summers of 2002 and 2003. During the summer of 2002, measurements and observations consisted of visually documenting the site through photography, obtaining the soil's particle size distribution and field-saturated hydraulic conductivities from points in and around gullies, and mapping headcuts and other points of interest in the field with a global positioning system (GPS). It was planned to accurately record the location of selected headcuts every

year to keep track of these headcuts' retreat.

During the summer of 2003, measurements and observations consisted of visually documenting the sites through photography, obtaining cohesion of the soil at several headcuts and arroyo walls, measuring the geometry of headcuts and plunge pools, measuring upstream of the headcuts slopes, and mapping headcuts and other points in the field with a GPS. In the summer of 2003, most sites explored in the summer of 2002 were revisited (Little Grand Canyon, Big Valley and Big Arroyo in Figure 3-3), and a new site was explored (Taylor Arroyo, in Figure 3-3)

This chapter describes the field observations and measurements, the basis for the thesis' hypothesis and the thesis' headcut-retreat model.

3.2 Observations and measurements

This section describes the processes thought to shape gullies and arroyos based on observations of the landforms; environment where gullying takes place; field observations and measurements of headcut-plunge pool systems; and analysis of field factors thought to affect the stability of slopes. It is suggested that often gullies result from the combination of two processes: headcut retreat through plunge pool erosion and scarp retreat due to instability.

The observed characteristics of gullies, arroyos, and the region where they occur, suggest that plunge pool erosion is a dominant mechanism of headcut retreat. They also suggest that the stability of steep and vertical walls on gully channels is an essential element of the gullying process.

3.2.1 The processes

The evidence of the processes taking place in gully development collected in the field is primarily the morphology of the incised channel. The process itself is unlikely to be observed because it is episodic and of short duration. The development of a gully may consist of several stages that form part of a cycle of gully head retreat such as that proposed by Collison [7]. A gully may also be at different stages of evolution

along its lifetime, such as those proposed by Oostwoud *et al.* [25]. This variability in the stages of the process make the morphology of a gully difficult to interpret.

In addition, several processes may be contributing to the development of the gully, and the environmental factors that control the evolution of the gully may change in space (the land is heterogeneous) and in time (for instance, moisture, a property of the soil, varies due to water fluxes). This makes the process complex, and the gully morphology more difficult to interpret. Nevertheless, the following processes were evident in the field: seepage and runoff, rilling, plunge pool erosion and piping causing gully development, undermining of channel walls due to flow, retreat of slopes due to the incising of the base of their toe due to flow, and cracking, contributing to the widening and lengthening of gullies, and falling of gully walls.

The evidence of seepage were wet layers of sand at gully head faces. Traces of runoff converging into gully heads were evident because grass was bent in the downslope direction, some rills formed, and sediment had recently been deposited along the flow's path. Plunge pools at the bottom of headcuts, and pipes on gully sides and heads, indicated the occurrence of these processes. Undermining of the base of channels was common in arroyos and gullies. The retreat of slopes due to the incising of the base of their toe most occur along slopes of non-cohesive materials in gullies or arroyos whose base level decreases due to erosive flows. Cracks were common on top of gullies and arroyos's walls. These cracks tended to enlarge and produce falls of soil or soft bedrock. Blocks and debris of this material rested inside the channels.

3.2.2 Vegetation, soil and water fluxes in the areas where gullying occurs

This section offers a description of the environment where gullying occurs, and where headcut retreat and scarp retreat take place. The description focuses on the environmental conditions believed to be relevant to these processes: vegetation, soil moisture, soil type and its properties, and water flux conditions.

Vegetation and moisture. Vegetation is variable in space and in time. Such variations are linked to soil moisture variations. Larger amounts of vegetation and moisture were observed along topographic convergence zones, that is, along flow paths. These convergence zones, in addition, required a soil mantle cover in order to hold moisture and vegetation. Bed sections of arroyos where bedrock was exposed, even if they were convergent zones, did not hold moisture or vegetation.

Denser vegetation cover was observed in zones of larger contributing areas rather than in zones of smaller contributing areas, where terrain was broad and gentle in slope. Also, the vegetation cover was denser during seasons of larger rainfall amounts. Figure 3-2 shows the changes observed in Big Arroyo in PCMS, between the summer of 2002 and the summer of 2003, when more rainfall occurred. On August 8 of 2003 a large rainfall event occurred in the area, according to PCMS personnel. The field work and observations presented here took place on September 23 of that year.

The contributing areas of the zones surveyed were estimated using the field-obtained geographic location of headcuts and a $30m$ resolution digital elevation model (DEM) of the zone. The DEM used was obtained from the U.S. Geological Survey (USGS) National Seamless Data Distribution System (http://seamless.usgs.gov).

Location of headcuts, within the surveyed zones, with a submeter accuracy, was obtained with a Trimble Navigation Limited GPS Pathfinder ProXR receiver. The data was postprocessed through the GPS Pathfinder Office software and then exported as an *ARC/INFO Generate* to the ARC/INFO geographic interphase system (GIS). The exported files were in the Universal Transverse Mercator (UTM) Zone 13 reference system, with the WGS84 datum and the EGM96 (Global) Geoid.

In ARC/INFO the DEM was projected into the appropriate UTM coordinate system. The projected DEM was processed by filling local topographic depressions. The ARC/INFO function used was grid:fill [sink]. Then the flow directions of each DEM data point were found. The flow directions are the directions of the steepest descent for each DEM pixel, or data point. The ARC/INFO function used was grid:flowdirection. Last the drainage area of each data point was estimated. The ARC/INFO function used was grid:flowaccumulation.

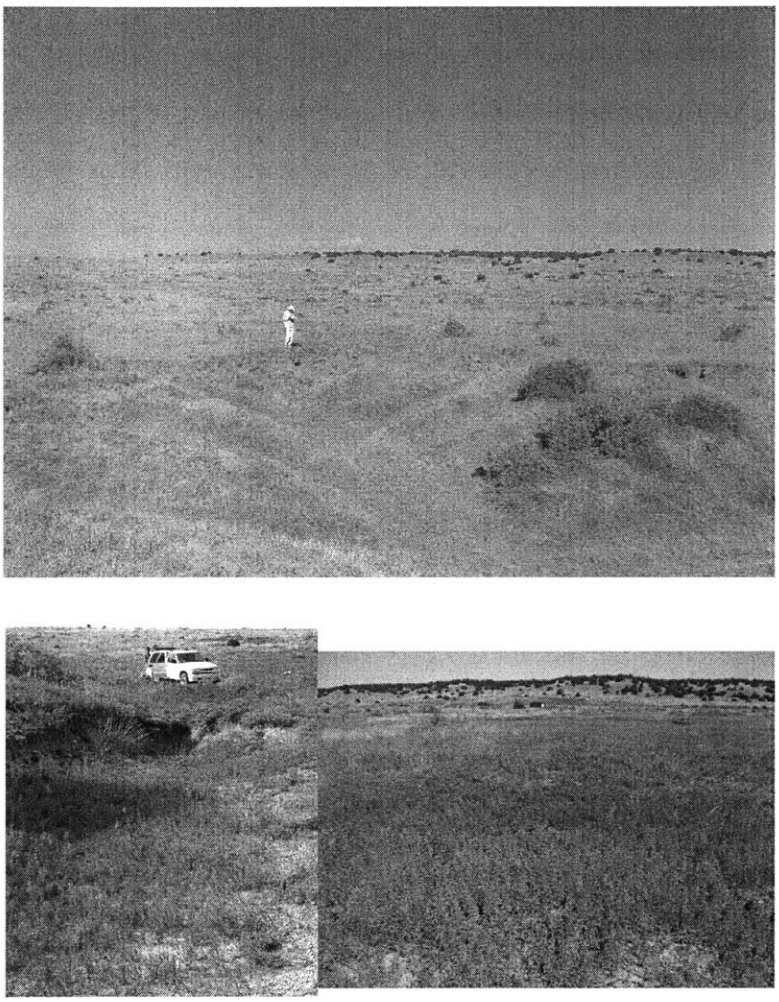

Figure 3-2: Big Arroyo in PCMS. The top photograph shows the site in the summer of 2002, while the lower photographs show the same site in the summer of 2003, when more rain occurred.

Table 3.1: Headcut field measured dimensions, slopes, cohesion, and drainage areas.

LOCATION	NAME	DATE	H [m]	L [m]	D [m]	S	D AREA [m^2]	C [kPa]
Big Valley -FC								
	BV 7a	19-Sep-03	2.3				14850	40.9
	BV 7b	19-Sep-03	3.4				14850	24.5
	BV 8	19-Sep-03	2.5				14850	27.8
Little Grand Canyon -FC								
	LGC 11	20-Sep-03	1.195				900	39.2
	LGC 12	20-Sep-03	2.1				23400	38.0
	LGC 12 b	20-Sep-03	0.6				23400	38.0
	LGC 12 c	20-Sep-03	1.4				23400	38.0
	LGC 13	20-Sep-03	1.6				2700	32.7
Taylor Arroyo -PCMS								
	TA 4 PP	22-Sep-03	0.9	2.1	0.9		1800	32.7
	TA 7	22-Sep-03	0.9	0.8	0.2		3600	
	TA 9A	22-Sep-03	0.75	0.6	0.2		9000	
	TA 10 a	22-Sep-03	0.7	0.7	0.15		1800	31.1
	TA 10 b	22-Sep-03	0.5	0.4	0.01		1800	31.1
Big Arroyo								
	BAC 1	23-Sep-03				0.05		28.4
	BAC 2	23-Sep-03	0.65	1.3	0.4	0.04	3600	94.0
	BAC 2b	23-Sep-03	0.4	1.1	0.2	0.03	3600	102.2
	BAC 3	23-Sep-03	1	4.3	0.7	0.03	14766300	69.5
	BAC 4 small ones	23-Sep-03	0.4	0.5	0.2	0.02	21600	57.2
	BA03-4	23-Sep-03	0.45	0.8	0.15	0.05	14766300	18.0

The drainage area assigned to each headcut was that calculated for the DEM pixel that corresponded to the headcut location. Table 3.1 summarizes the drainage areas estimated.

Soils. The soil is a complex domain to study. Several physical properties are attributed to it, and they vary widely, in time and space: "The physical properties of soils are strongly influenced by their mineralogy, texture, and fabric [or structure]. The properties are not constant over time, with water-content and void space capable of changing very quickly and other properties changing more slowly. Nor are properties constant in space with major variations in structure, fabric, and mineralogy being identifiable over distances of a 'few meters'" (Selby [34] p.106). One way to begin understanding how the soil behaves is through knowing its texture.

"The relative proportions of gravel, sand, silt and clay define the texture of a soil" (Selby [34] p.11). These proportions were obtained for 42 samples from 5 different gully systems in Fort Carson and PCMS: Horton Gully, Big Valley, Little Grand Canyon, Big Arroyo and Lockwood Arroyo. The locations of the extraction of the

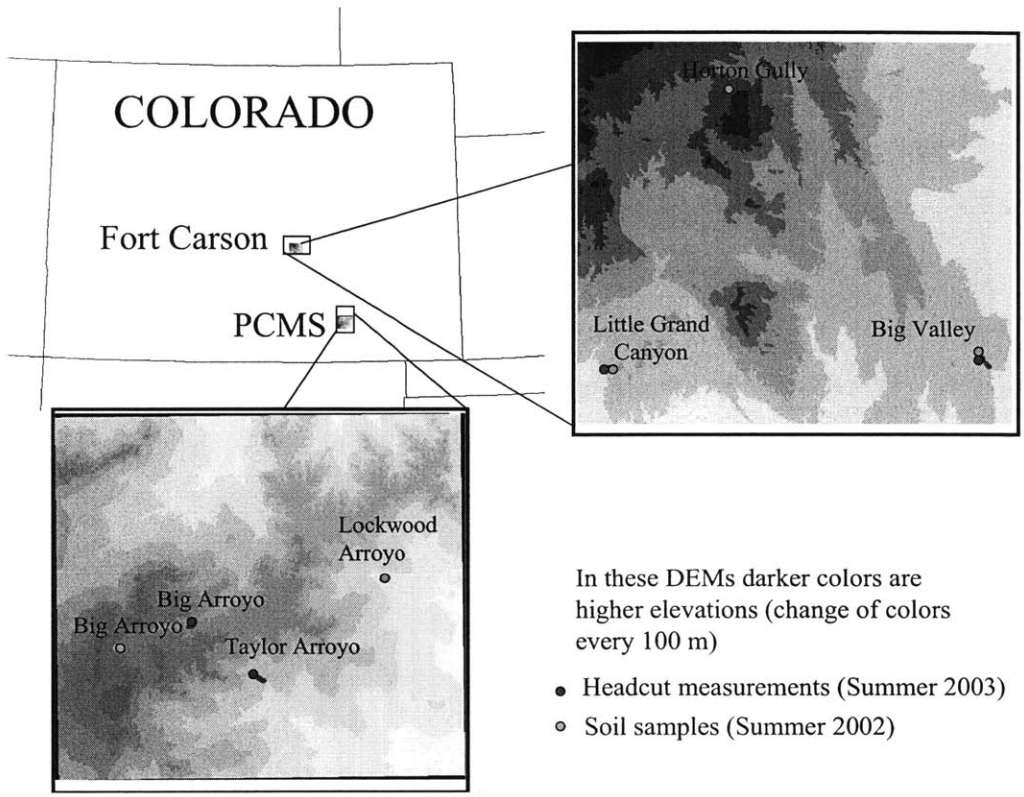

Figure 3-3: Location of the soil sampling and of the headcut measurements.

samples are shown in Figure 3-3. Samples were taken from the bed of the gully channels, their walls, and the surrounding of the gully.

The grain size analyses, or granulometric tests, were carried out in accordance with the American Society for Testing and Materials (ASTM) Standard D422 and resulted in a series of granulometric curves corresponding to each sample. From these curves, the parameter d_{50}, representative of the grain size of a soil, the percentages of sand, silt, and clay, and the sample's texture classification, were obtained. The results are reported in Table 3.2.

Particle size is useful as an indication of soil properties such as water storage capacity, drainage and nutrient availability [34] p.11. Table 3.3, produced by Selby [34], shows the properties of the soils that may be inferred from the soil's particle size.

Table 3.2: Soil samples characteristics.

Sample Name	d50 (mm)	% sand	% silt	% clay	texture	Field -saturated hydraulic conductivity,Ks (cm/sec)	mean Ks, per site (cm/sec)
Horton 1	0.075	55	23	22	sandy clay loam	0.00248	0.00286
Horton 2	0.048	48	34	18	loam		
Horton 3	0.022	41	31	28	clay loam	0.0028	
Horton 4	0.019	31	29	30	clay loam		
Horton 5	0.007	31	33	36	clay loam	0.00098	
Horton 6	0.007	34	30	36	clay loam	0.00505	
Horton 7	0.014	32	35	33	clay loam		
Horton 8	0.058	51	26	23	sandy clay loam	0.00298	
Horton 9	0.0058	24	40	36	clay loam		
Big Valley 1	0.005	27	39	33	clay loam		0.00115
Big Valley 2	0.0095	27	64	9	silt loam		
Big Valley 3	0.06	54	26	20	sandy clay loam/sandy loam		
Big Valley 4	0.0095	16	56	28	silty clay loam		
Big Valley 6	0.013	28	43	29	clay loam	0.0008	
Big Valley 7	0.18	50	23	17	sandy loam/loam	0.00174	
Little Grand Canyon 1	0.025	38	35	27	loam	0.0007	0.0006
Little Grand Canyon 2	0.03	43	33	24	loam	0.0015	
Little Grand Canyon 3	0.004	15	43	42	silty clay	0.00042	
Little Grand Canyon 4	0.0032	23	35	42	clay	0.00019	
Little Grand Canyon 5	0.0035	17	36	42	silty clay	0.00014	
Little Grand Canyon 7	0.006	31	31	38	clay loam		
Big Arroyo 1	0.0015	13	35	52	clay	4.2E-05	0.00177
Big Arroyo 2	0.0028	10	45	45	silty clay	0.00091	
Big Arroyo 3	0.06	58	29	13	sandy loam	0.00115	
Big Arroyo 4	0.0041	18	33	44	clay	0.00084	
Big Arroyo 5	0.008	28	37	35	clay loam	0.0007	
Big Arroyo 6	0.0051	33	27	40	clay/clay loam	0.00853	
Big Arroyo 7	0.033	39	37	23	loam	0.0002	
Lockwood 1	0.0092	19	45	36	silty clay loam	3.6E-06	0.00326
Lockwood 2	0.054	51	26	23	sandy clay loam	0.00298	
Lockwood 3	0.22	63	21	14	sandy loam	0.00133	
Lockwood 4	0.03	36	36	28	clay loam	0.00223	
Lockwood 5	0.032	40	35	25	loam	0.00827	
Lockwood 6	0.049	50	28	22	sandy clay loam	0.00476	
Lockwood 7	0.013	27	38	35	clay loam		
Lockwood 8	0.025	50	27	23	sandy clay loam		
Big Arroyo b1	0.024	33	44	23	loam	0.00099	0.00126
Big Arroyo b2	0.0032	21	35	44	clay	0.00066	
Big Arroyo b3	0.054	53	29	18	sandy loam	0.00224	
Big Arroyo b4	0.07	55	31	14	sandy loam	0.00114	
Big Arroyo b5	0.069	55	31	14	sandy loam		

Table 3.3: Physical properties of the major size fractions in soil [34].

Property	Gravel	Sand	Silt	Clay
Volume change				
from dry to wet conditions	None	None	Slight	Large (marked swelling)
Tensile strength				
when wet	Low	Low	Intermediate	High
when dry	Low	Lower than when wet	Higher than when wet	Very high
Compressibility				
when wet	Very low	Very low unless particles separated by water when change is high	Intermediate unless saturated with water when change is high	Very high
when dry	Very low	Very low	Low	Intermediate to low when very dry
Plasticity				
when wet	None	Slight	Intermediate	Very high
when dry	None	None	None	None, partial cementation
Porosity	Very high	High	High	Very high
Permeability	Very high	High	Intermediate to low	Very low
Size of voids	Large	Intermediate	Capillary	Subcapillary
Shape of particles	Rounded	Round to angular	Angular	Thin tabular
Water retention	Very low	Low	High	Very high

The variability of soil properties in the vertical and horizontal planes make the gully and headcut retreat processes more intricate. Often, layers of different types of soil occur, and layers of more permeable materials (e.g., sands) underlie layers of less permeable materials (e.g., silts and clays). Then, when water flows into the permeable layers, for instance, because they are in contact with the surface at a higher point in the hillslope, or because water infiltrates through cracks and macropores to them, and these layers outcrop (e.g., in a gully head), seepage faces develop. Moist layers of coarse material were observed at headcuts and gully and arroyo walls.

The amount of clay and silt in a soil explains in large part the behavior of several of the gully walls observed (see Figure 3-4). These walls have large cracks due to the shrinking of the soil, and are "too hard to be broken readily in the fingers" (Selby [34] p.11). In addition, the material supports vertical and hanging walls (see Figure 3-4), revealing its tensile strength. And the material, when wet, becomes soft and malleable. These properties resemble Selby's description of clays: "Clay soils (usually having more than 20 per cent clay size particles), when moist, have a smooth greasy feel ... and can be molded into threads ... [that] support [their] own weight if held at one end and thus [exhibit the soil's] tensile strength caused by its own cohesion (a silt would not do this). On drying, a thread of clay will crack and break into flakes, the thread may shrink and residual lumps may be too hard to be broken readily in the fingers" (Selby [34] p.11).

"Silty soils (usually more than 50 per cent silt) ... can be rolled into threads ... [that] tend to crumble as they dry." Silts exhibit properties unexpected by those not familiar with them: "If a wet sample is shaken in the hands its surface becomes wet and shiny. If it is then compressed between the fingers the water disappears into the sample and the surface becomes dull and dry, [and] at the same time the soil becomes firmer and gives increasing resistance to compression. This change, as pressure causes rearrangement of grains into a larger volume, with greater void space into which water is drawn, is called dilatancy" (Selby [34] p.11).

Cohesion and moisture are soil properties of particular relevance in the maintenance of vertical scarps observed on gully sides and heads, as further discussed in

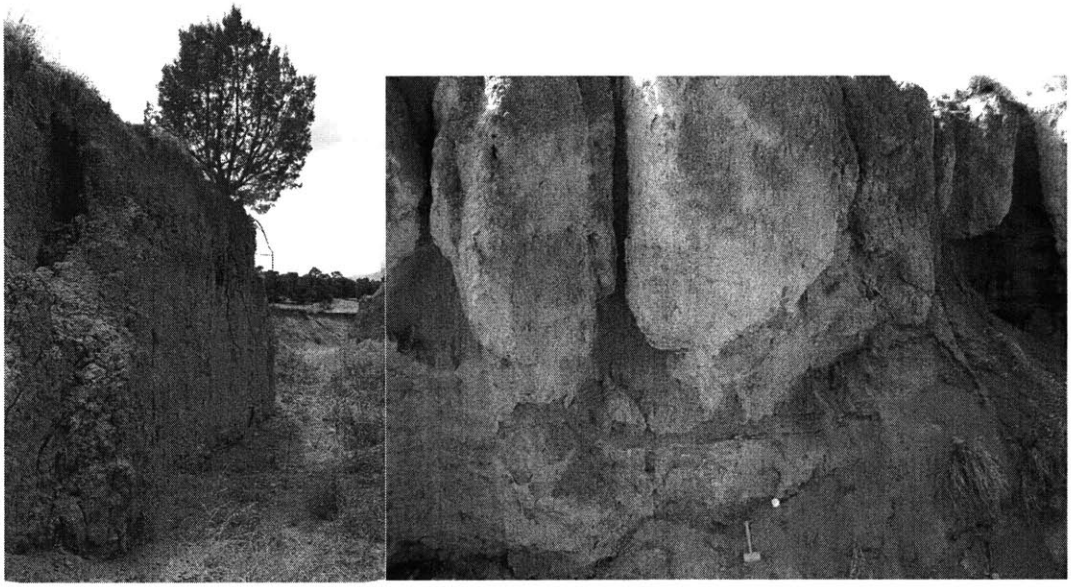

Figure 3-4: Vertical walls of gullies. On the left, "Horton Gully", a gully formed on the east of Fort Carson's Route 11 and whose location is shown in Figure 3-3. On the right, a hanging wall in Big Valley, Fort Carson, formed in a soft cohesive bedrock.

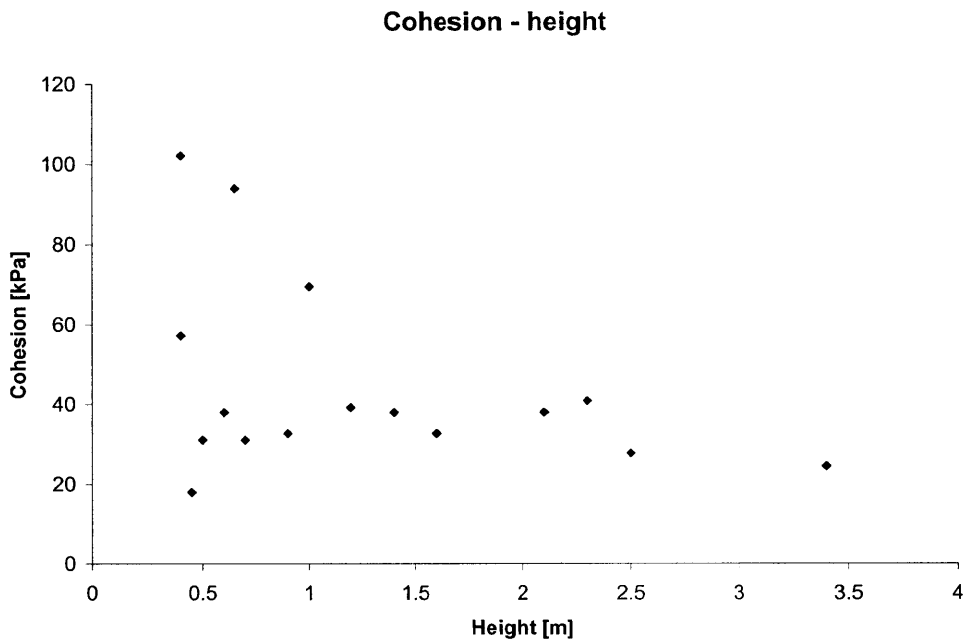

Figure 3-5: Cohesion and headcut height H of several headcuts, reported in Table 3.1.

Section 3.2.4. In the field, cohesion of the walls and tops of several headcuts were measured. Three measurements were made at each instance and the average of these measurements is reported in Table 3.1. Cohesion varied between 20 and $100kPa$, with most values being around $35kPa$, as seen in Figure 3-5. The height of the selected headcuts varied between 0.5 and $3.5m$.

Other properties of the soil relevant to its scouring are its erodibility (κ) and critical shear stress (τ_{cr}), parameters of the headcut-retreat model. The values of these parameters were not measured in the field. They were selected based on values proposed by others for soils of similar textures, as described in Chapters 6 and 7.

Dispersion of a soil is a characteristic that can say much about the type of erosion occurring at one place. Arid and semiarid regions commonly present dispersive soils as exchangeable sodium accumulates in them due to the climate. Dispersion occurs

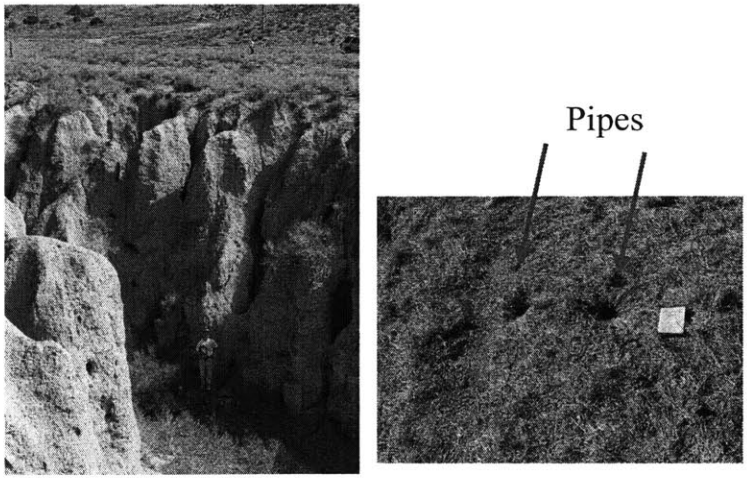

Figure 3-6: Pipes observed in Big Valley (left) and in the Big Arroyo headwaters (right) in Fort Carson. Dispersion of soils is a major cause of the formation of natural pipes in soils. A notebook serves as scale on the photograph on the right.

naturally in soils containing a high exchangeable sodium percentage. "Dispersion is a process which separates clay particles by breaking the bounds between them ... and is a major cause of the formation of natural pipes in soils" (Selby [34] p. 118). During this fieldwork, areas with abundant pipes were observed, in particular in Big Valley (at Fort Carson) and in some areas of Big Arroyo (in PCMS) (see Figures 3-1 and 3-6). The dispersion of the soils was not measured in this study, nor were piping or dispersion considered in the modeling.

Runoff. Gullies and retreating headcuts were observed along zones of topographic convergence. There was evidence of surface flow upstream of the headcuts such as bent stems, rills, and recent deposits of runoff. To learn about the mechanisms of

runoff production and of subsurface flow production, point estimates of the soils' field-saturated hydraulic conductivity, K_s, were obtained using a Guelph Permeameter. This was done following a standard procedure [9] that required two steady rates of water infiltrating the soil. The results of those measurements, shown in Table 3.2, highlight the high variability among measurements within a few meters, and the difficulty in obtaining infiltration rates representative of the area that would allow us to estimate the runoff production and the contribution to any subsurface flow. The existence of cracks, macropores, and pipes, particularly in the surroundings of a gully, makes the quantification of fluxes into and within the ground complex.

The measurements of K_s obtained reflect the fine sand composition of the soils (the values are between $1x10^{-7}$ and $1x10^{-5}m/sec$). These values suggest that considerable infiltration excess runoff (Hortonian flow) will occur unless plenty of cracks, macropores and pipes, exist in the areas contributing to runoff. The runoff flowing towards a gully will flow through a headcut, or into the cracks, pipes and macropores that frequently surround gullies and scarps.

Other environmental aspects observed and measured, which affect the runoff flow, are conditions such as the vegetation, slope, and contributing area upstream of gullies and headcuts. Vegetation influences the amount of flow and the flow's velocity. The former because it increases infiltration and evaporation thus reducing runoff. The latter because vegetation increases the roughness of the surface over which flow occurs. An increasing slope increases the flow's velocity, and the amount of flow is proportional to contributing area.

The areas upstream of the surveyed gullies, corresponding to small contributing areas, were sparsely vegetated with shrubs and grasses. In addition, these areas had vehicle tracks. The sparse vegetation, in combination with the vehicle tracks, which are known to concentrate flow [23, 19], must lead to flow volumes larger than in neighboring areas with denser vegetation and without vehicle tracks. These conditions must favor gullying. The areas upstream of all observed gullies had gentle slopes. It is believed that in steeper slopes, headcuts diffuse due to the high shear stresses produced by the flow.

Drainage areas and erodibility properties. From the field observations and calculation of the drainage areas corresponding to several of the measured headcuts, it was noted that these areas varied between $1,000$ and $1,000,000m^2$ and that the material's resistance to sheetwash and to plunge pool erosion varied as well between headcuts with different drainage areas. In zones where the drainage areas are large, headcuts incised in strong bedrock or in well vegetated areas, both of which make the upstream section of the headcut resistant to wash erosion. In zones of smaller contributing areas (or drainage areas) headcuts incised soils with little resistance to erosion and with little vegetation cover. The above reinforces the notion that headcuts can only exist where sheetwash, or wash processes, are weak enough not to diffuse the headcuts: only areas very resistant to wash erosion can support headcuts where large drainage areas exist, and material with little resistance to wash erosion can only support headcuts where the drainage areas are small.

The environmental conditions described in the preceding paragraphs: a vegetation mat that protects the top of a headcut from fluvial erosion, a cohesive material that is strong enough to support vertical slopes, and large amounts of flow converging in a zone with gentle slopes, are conditions believed to be favorable to the headcut retreat through plunge pool erosion mechanism. The above observation led to the formulation of the hypothesis of this thesis, and motivated the study in greater detail of the role of headcut retreat through plunge pool erosion in the development of gullies. The above observations also motivated the design of the experiments carried out with the headcut-retreat model in CHILD.

3.2.3 Plunge pool erosion and headcut retreat

During the fieldwork several headcuts were surveyed. Some of these headcuts lengthen channels that drain into larger incising channels (in some cases a larger gully, in others an arroyo). Other headcuts were channel heads belonging to a discontinuous channel system. Figures 3-7 and 3-8 show a sketch and photographs of the headcut-plunge pool systems observed. The top image of Figure 3-8 shows the upstream section of a headcut-plunge pool system such as the one represented in Figure 3-7; the bottom

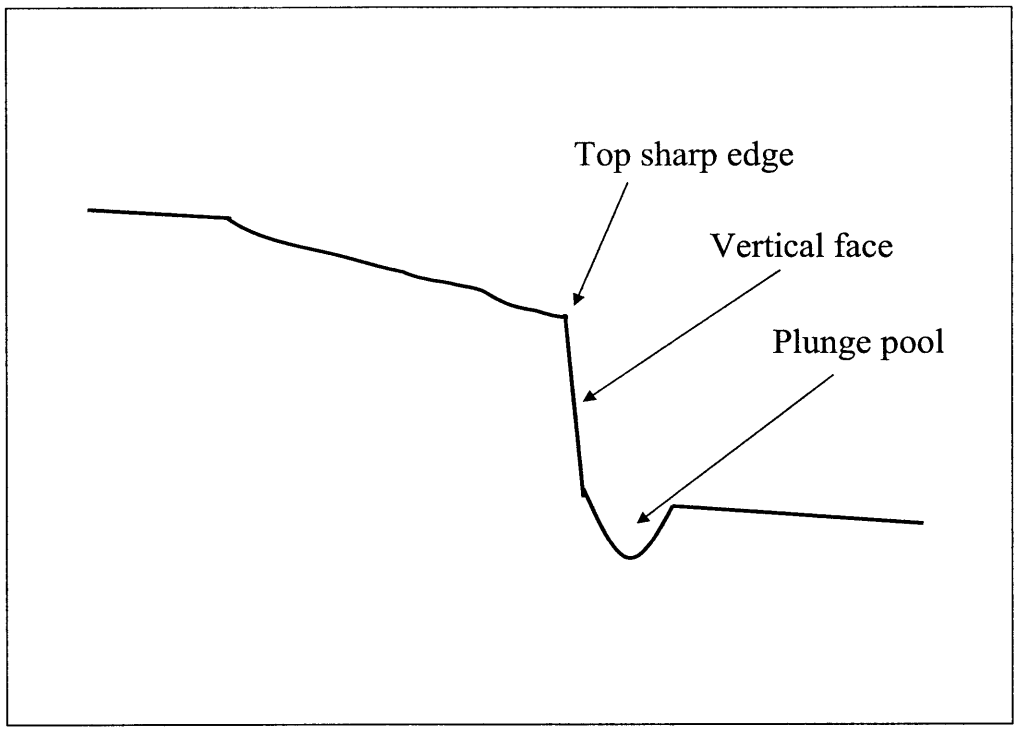

Figure 3-7: Sketch of a field plunge pool. This is the general plunge pools' profile observed at the Little Grand Canyon, in Fort Carson.

image shows a scarp along which a series of small plunge pools occur. A notebook serves as scale in the last photograph. The plunge pools are shallow, and thus are difficult to appreciate in the photograph.

Several headcut heights, and the depth and length of the plunge pools at the bottom of these headcuts, were measured in the field. With the dimensions of the plunge pool, the shape factor (S_f) was estimated. The S_f is the ratio between the pool depth and the pool's mid length. It will be further discussed in Chapter 4. The S_f is a parameter of the headcut-retreat model. The theory developed in this thesis assumes a constant S_f for a given soil. The value of the S_f obtained in the field, however, varies as shown in Figure 3-9. Such variability can be attributed to heterogeneities in the soil properties, to the fact that the flow is not constant in space

Figure 3-8: Plunge pools observed at the Little Grand Canyon in Fort Carson (top) and Big Arroyo in PCMS. The top gully drains into a larger incising channel. The channel formed by the retreating headcut shown at the bottom disappears a few meters downstream.

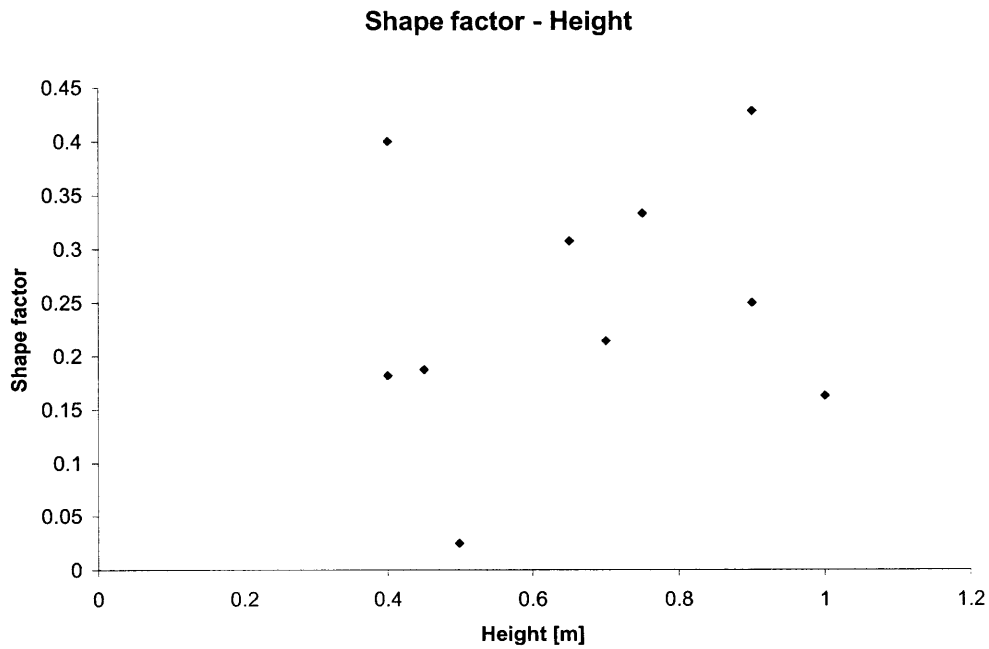

Figure 3-9: Shape factor S_f of the last ten headcuts described in Table 3.1 and their corresponding headcut height H.

and time, and to the fact that the plunge pool shape is really not constant. Table 3.1 summarizes the values measured and estimated for selected headcuts.

The field-obtained S_f varied between 0.025 and 0.425, with a mean of 0.25. Based on this field evidence, the CHILD simulations described in Chapter 7 used an $S_f = 0.2$ (the value most frequently observed).

In addition to these dimension measurements, five headcut-plunge pool systems were further characterized by measuring their upstream slope gradient, S. This value is considered in the headcut-retreat model, as discussed in Chapter 4. The measured gradients, summarized in Table 3.1, belong to gentle slopes covered with a vegetation mat. Along zones where a channel had incised, and vegetation was nonexistent, headcuts did not maintain the sharp top edges characteristic of headcuts.

At this stage a link can be made between the headcut-plunge pool system observed in the field and the modeling outcomes. The profiles observed in these scenarios are similar (see Figures 3-7 and 7-8). In the profiles, the sharp step-change in topography takes place, and then upstream of this change, a fluvially eroded section follows until it reaches a point where a second change in slope is evident. This second change in slope occurs because upstream of such point the flow is not enough to erode the land surface ($\tau < \tau_{cr}$).

In the field, the sharp edge on top of headcuts is maintained due to the protection of a mat of vegetation; otherwise it would be diffused away by processes such as rainsplash diffusion. In the model, the sharp edge is maintained because diffusion is neglected for simplicity of the modeling, not because vegetation on top of the slope is considered.

Incision and incision history. Retreating headcuts often begin where the convergence of flow intersects a channel that incises and thus creates a step-change in the profile of the flow path intersecting it. Among the reasons for such incising are first, change in land cover. An example is a change from forest to grazing land, change that promotes the decrease of infiltration and roughness of the land surface, and a decrease of the surface resistance to erosion, thus providing larger flow velocities that incise with smaller resistance to erosion. Second, the creation of roads can result in the concentration of flow at certain flow venues that will be more likely to incise. Third, the propagation of the base level lowering of a channel through knick point migration causes channel incision. Fourth, channels incise due to variations in the sediment supply across the basin. These variations may result from changes in the land use of the basin, road construction, base lowering, or climate changes. Other causes of channel incision are seepage erosion and landsliding [20].

Thorne [40] argues that large amounts of sediment were produced in the Mississippi Valley due to the "over-extensive and intensive agriculture since hardwood forest clearance by European settlers starting in the 1830s." And later, between 1950 and 1960, after a reduction of the sediment amounts produced in these areas and the

channelization of streams, the streams' transport capacity increased by 50 fold, and resulted in channel incision.

Ritter *et al.* [28] describe the increase in sediment yield of southern Illinois since the late 1800s due to clearing of upland forests and intensive agriculture in steep slopes that resulted in aggradation of valley floors. Later on in 1986, these valley floors began to experience large amounts of scour after the upland areas were reforested and thus provided a water flow with less sediment and larger sediment transport capacity.

A third example of channel incision due to changes in sediment supply across the basin is that provided by Tucker [41]. Through a modeling exercise, he shows how cyclic fluctuations in climate, and their effects on the sediment production of the basin's hillslopes, result in "waves" of propagating sediment in the downstream direction. Such waves, to a local observer, would appear to be an aggradation and scouring cycle of the channels.

Headcuts of different heights retreating along the same flow path were observed in the field. They were separated by a few meters as illustrated in Figure 3-10. Also, series of step-changes in the slope along hillslopes where arroyos cut through were observed, such as the one shown in Figure 3-11. These series of retreating fronts suggest incising events of different magnitudes whose incising depth and frequency is recorded in these land features.

The effects of various periods of incision on the evolution of a hillslope due to headcut retreat through plunge pool erosion can be explored in the future with the model developed in this thesis.

3.2.4 Stability and stabilization of slopes

To be stable, a vertical face in the landscape, characteristic of a headcut and of a channel wall along gullies and arroyos in the southwest of the U.S., requires that the material that forms it is strong enough to support it (i.e., it is cohesive enough), and that mechanisms that maintain it exist. These mechanisms must remove debris from the vertical face's base, and produce the face's retreat (otherwise, with time, the vertical face would diffuse and it would no longer be vertical). The strength of the

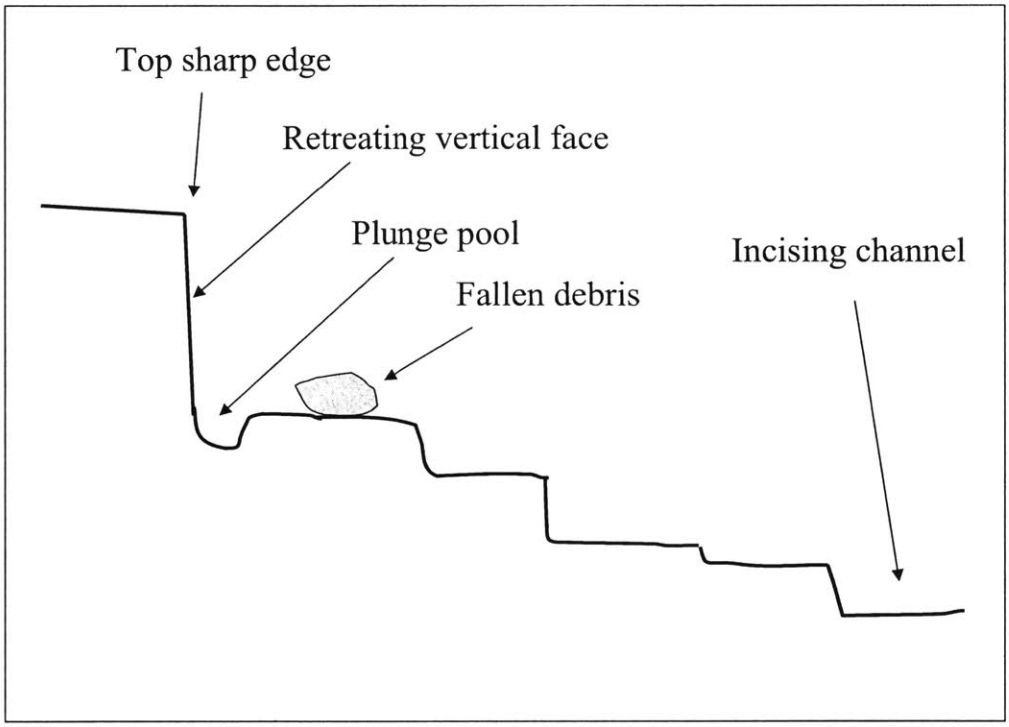

Figure 3-10: Scheme of a series of plunge pool observed in the Little Grand Canyon, in Fort Carson.

Figure 3-11: Series of retreating scarps along an incising channel shown by the white arrows, in Big Arroyo (PCMS).

material required to support a vertical face increases as the height (and consequently weight) of the scarp increases. Such strength is generally correlated to the cohesion of the material (e.g., in the Coulumb equation).

Gentle slopes require as well certain stability to allow them to remain and not be eroded away. In the field, along arroyos, several gentle slopes were stable and covered with vegetation (see Figure 3-12), while vertical scarps were not covered with vegetation. The stability of these gentle slopes depends on the vegetation cover, cohesion and other elements that provide resistance to movement such as friction among soil particles. The stability also depends on the magnitude of the forces that tend to move the soil of the slope, which are gravity and the shear stress produced by water flow.

Usually soils with little cohesion form gentle slopes of gradients equal to the maximum gradient they can stand (e.g., their friction angle), and any decrease or increase in the resisting or moving forces will destabilize such slope. If the gradient of such a slope is increased, for example, due to the slope's undermining by water flow, it will become unstable. Then soil from the top of this slope will move downwards until a stable gradient is achieved. Such soil movement causes the retreat of the slope. This type of retreat takes place at several locations along arroyos studied in this work, for example, see Figure 3-13. Howard [18] modeled this type of retreat. Because vegetation increases the soil's resistance to erosion, and thus to undermining, vegetation greatly increases the stability of the slopes and decreases drastically the retreat rate of these slopes, often stopping retreat completely.

Cohesion measurements of the surroundings of the studied headcuts show that cohesion is high (see Figure 3-5), at least in the dry state in which it was tested, and it allows for large vertical wall heights. However, because a large portion of the measured cohesion corresponds to an apparent cohesion that disappears as the soil saturates with water, smaller values of cohesion are expected under wet conditions.

Because cohesion is dependent on soil moisture, the stability of a vertical face is then dependent on soil moisture. Vertical walls are favored in equator-facing walls because soil moisture is smaller in walls facing the equator. Equator-facing walls

Figure 3-12: A section of Taylor Arroyo (PCMS) showing a gentle slope covered with vegetation in the foreground, and vertical slopes with no vegetation at all in the background.

Figure 3-13: A section of Taylor Arroyo (PCMS). The slope retreats when its toe is incised and made unstable.

Figure 3-14: A branch of "Horton Gully" in Fort Carson. One side has vertical scarps, while the other has gentle slopes and vegetation.

receive larger amounts of solar radiation than pole-facing walls. The stability of the vertical face will also depend on the flow converging to a gully wall as more water availability will decrease cohesion. Zones where flow converges will be less stable. The above two reasons may explain why some walls of a gully (or of an arroyo) are kept vertical (see Figure 3-14) and neighboring walls are not. The role of moisture in slope stability has been considered in modeling and field studies, for example [21, 8], but it is not considered in this work for simplicity, as stated in Section 2.5.

In gentle slopes, opposite to what happens in steep slopes, the effect of moisture is generally stabilizing given that large cohesion strengths are not important in their stability, and that it promotes establishment of vegetation. Debris forming gentle slopes, when moist, is more likely to be colonized by vegetation and acquire a higher

resistance to erosion than drier debris, and thus, flow paths move towards the less vegetated zones, generally below the vertical walls. Such change in the flow path accentuates the undermining of the vertical wall faces, contributes to the stability of gentle slopes, and enlarges the contrast between vertical walls and gentle sloping walls.

3.2.5 Combination of mechanisms

Both, the stability of slopes and the headcut retreat through plunge pool erosion are relevant in the gullying process. Further work combining the effects of headcut retreat through plunge pool erosion with the effects of retreat of gully walls due to instability is expected to yield a better representation of the gully phenomenon than the headcut-retreat model alone.

The reasons discussed above highlight the relevance of the study of vegetation in the stability of slopes in the development of gullies, arroyos, and, in the semiarid landscape in general. Revegetation of fallen debris, which provides the fallen material with a high resistance to erosion, similar to that of the original protective cover (vegetation mat) may be extrapolated to explain the striking difference between rolling hills in humid environments and mesas and U shaped channels in semiarid lands. In semiarid lands, vegetation recolonization is very slow and weak, and erosion events are rare but extreme in intensity, so that debris is easily removed and the vertical faces are exposed and maintained. In more humid environments, the debris remains, because revegetation is faster, and extreme erosion events are not common, so that a more gentle, less abrupt topography, forms. In addition, in humid environments incision rates are smaller.

Vegetation may play an additional role in both types of environments. Vegetation differential growth in the landscape, as observed on several occasions in the field (see Figure 3-13), where the channels were much more vegetated than the surrounding areas, may make the base of channels much more resistant to erosion than the surrounding landscape. As a result those surrounding areas will erode at a higher rate than the base of the channel, and the walls of the channel will tend to disappear.

Whether this occurs or not will depend on the magnitude and frequency of the eroding events, and the magnitude of the resistance to erosion of the different zones of the landscape during the eroding events. This topic could be further discussed but is out of the scope of this work.

Chapter 4

Headcut Retreat Model through Plunge Pool Erosion

4.1 Introduction

4.1.1 The novelty of the plunge pool approach

The main novelty of the present plunge pool approach is that it is a physically based retreat model applied in a 3D landscape evolution model. It estimates plunge pool retreat for the given hydraulic characteristics of height of the gully head (H), slope (S), manning's roughness (n), and flow (q); and the given soil properties of erodibility (κ) and critical shear stress (τ_{cr}), shown in Figure 4-1. The geometry of the pool is a rather important piece of information within the model. It is described through H, the depth of the plunge pool (D), and the length of the plunge pool (L) (see Figure 4-1). Of these, the depth of the pool is particularly relevant because a deep pool will dissipate the plunge pool erosive energy, while a shallow pool will not. In this model the depth is estimated from the hydraulic characteristics; most previous plunge pool modeling attempts use an experimentally measured plunge pool depth.

This chapter presents the headcut-retreat model developed for this thesis and implemented into CHILD, a 3D landscape evolution framework.

The headcut-retreat model consists of two parts; the first part estimates a linear

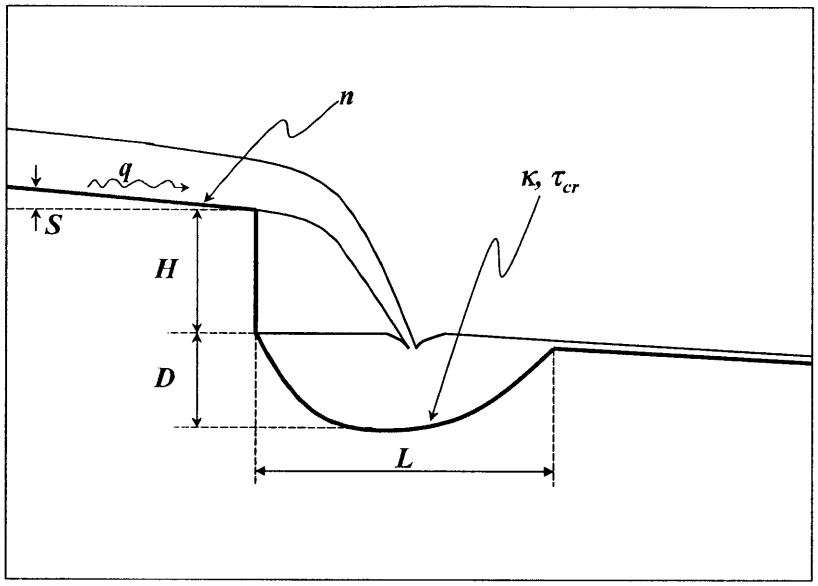

Figure 4-1: Hydraulic characteristics considered in the headcut-retreat model.

retreat rate at a point in a land surface for given flow and physical environment conditions; the second part produces the actual retreat in the landscape represented by CHILD according to the retreat rate previously calculated. In CHILD the headcut retreat interacts in the shaping of the landscape with other erosion processes such as diffusion (i.e., soil creep) and fluvial scouring.

The last section of this chapter describes some limits of the model.

4.2 Description of the retreat rate model

The section is divided into four parts: an overview of the model; a description of the flow characterization before it enters the plunge pool; a description of the flow inside the plunge pool and the calculation of the shear stress produced at the bottom of the pool; and a description of the calculations of the scouring of the plunge pool and of the retreat rate.

4.2.1 Overview

Plunge pool erosion is the scouring of a hole resulting from falling water. Sometimes plunge pool erosion occurs beneath a nearly vertical scarp, and causes the retreat of the scarp. This scarp is referred to as a headcut if it occurs at the head of a channel, or as a knickpoint if it occurs within a channel. The retreat rate model is applicable to both, headcuts and knickpoints; however in CHILD, the retreat is only considered for headcuts. Frequently these types of scarps happen along ephemeral water courses, and their initiation and evolution is tightly linked to the flow through the plunge pool erosion. Therefore the consideration of the flow characteristics is an essential part of the retreat rate model.

In the model, the flow characteristics as the water approaches the scarp and then falls into the pool are determined from the flow per unit width (q), the upstream slope (S), the upstream surface roughness (Manning's n), and the scarp height (H). Then, the shape of the pool is estimated from the impinging jet geometric characteristics. Next, with the impinging jet and plunge pool shape characteristics, the maximum shear stress at the bottom of the pool is assessed. With the shear stress, in combination with the soil erodibility (k) and the critical shear stress (τ_{cr}) parameters, the scouring of the plunge pool and retreat rate of the scarp are finally calculated.

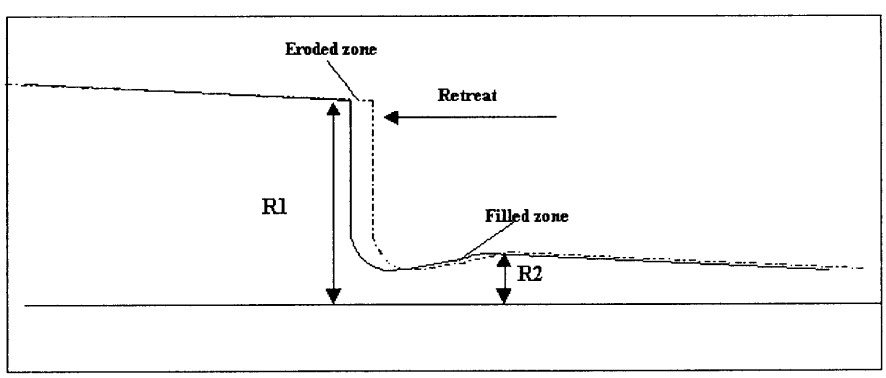

Figure 4-2: Plunge pool retreat schematic.

Several assumptions are made in the development of this model. Some assumptions concern the flow's characterization (Sections 4.2.2 and 4.2.3); one concerns the

form of the detachment limited equation (Section 4.2.4); other four justify the constant retreat rate model proposed in this thesis. These last four assumptions are:

1. *Homogeneous soil and constant plunge pool retreat rate assumption.* The plunge pool occurs in a homogeneous soil, making a constant retreat possible. The flow characteristics are assumed to remain constant in time. Then, because the shape of the pool is a function of the flow, the shape remains constant, as Figure 4-2 shows. As the scarp retreats, the plunge pool location and the jet's impinging point also migrate. The result is that the shear stress at the bottom of the pool, the scouring of the pool and the retreat rate remain constant. Constant retreat in homogeneous soils has been observed in laboratory flumes by Bennett and coworkers [2] [3] [4]. Figure 4-2 shows which zones of the system erode and fill in during a small increment of time (Δt).

2. *Instantaneous state of equilibrium for a constant retreat rate assumption.* In [2, 3, 4], the constant retreat rates were achieved soon after the beginning of a flow (a few seconds). Assuming a similar behavior, in this model an instantaneous steady state of retreat is achieved at the beginning of the flow. This assumption is a limitation to the model because in soils resistant to erosion, or during flows that cause little erosion, the time to reach a steady state of retreat may be large. The time to equilibrium is not considered in this thesis.

3. *Shape of the plunge pool assumption.* This assumption consists of a constant relationship between the horizontal distance between the scarp and the jet's impinging point, X_p, and the depth of the pool D (see Figure 4-3). This relationship is given by the shape factor, S_f, as

$$S_f = D/X_p.$$

This assumption is useful to estimate D. In previous plunge pool retreat models, D was obtained from observations [11] because it is a parameter difficult to predict. It depends on several conditions such as soil properties, water jet

structure and transport capacity of the flow.

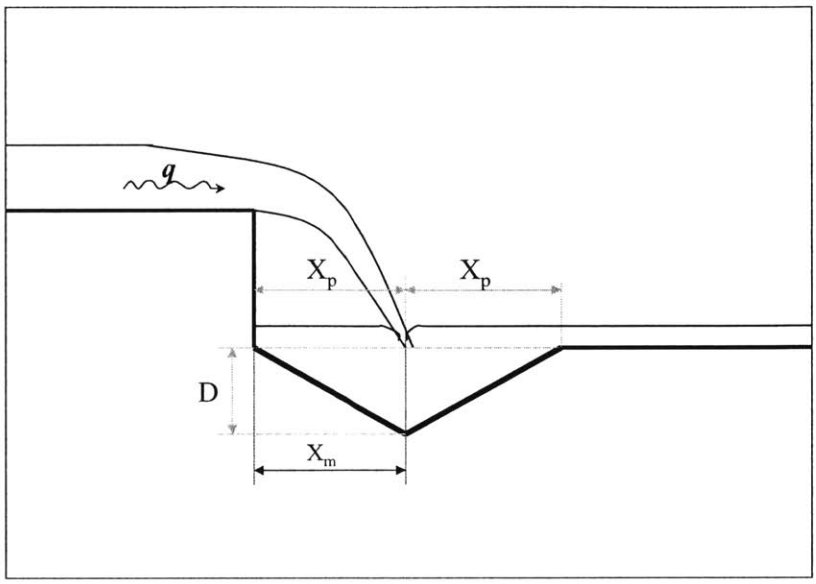

Figure 4-3: Shape of an idealized plunge pool.

It has been observed, however, that a ratio between the depth of the pool (D) and the pool's mid length (X_m) is maintained for given materials throughout a significant range of flow conditions [3, 36, 39]. This observation is used here to estimate an approximate D.

Stein and Julien [36] observed that for three materials (coarse sand ($d_{50} = 1.5mm$), fine sand ($d_{50} = 0.15mm$) and cohesive soil ($d_{50} = 0.045mm$)), for flows between 0.001 and 0.005 m^2/sec, a relationship between the eroded volume per unit width (q) and the depth of the plunge pool (D) exists. This relationship is shown in Figure 4 of their paper (see Figure 4-4). In this figure the volume is normalized by D_e^2, and the depth by D_e, where D_e is depth to equilibrium, to yield V^* and D^* respectively.

D_e corresponds to the maximum possible depth achieved in a plunge pool under given physical environment conditions and flow. When D_e is achieved, scouring of the plunge pool stops. This happens when the shear stress τ, at the bottom of the pool, equals the critical shear stress τ_{cr}.

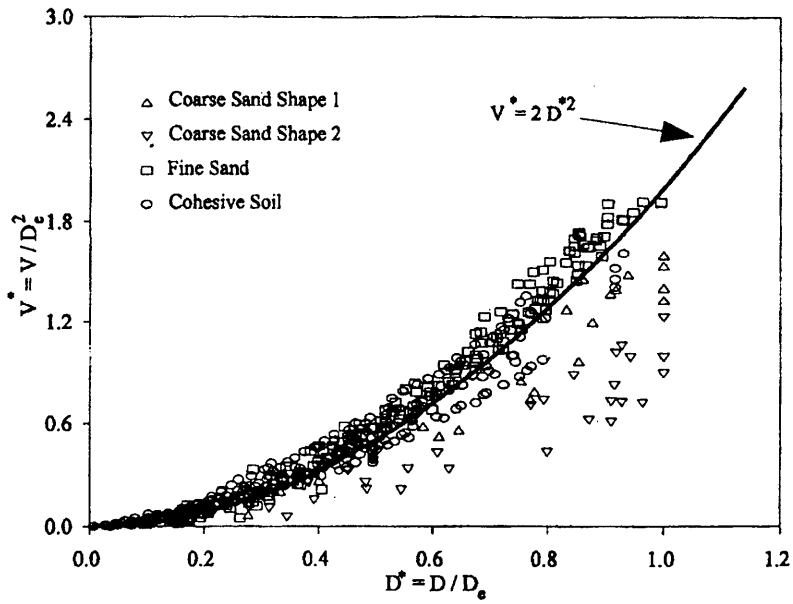

FIG. 4. Measured-Scour-Hole Volume versus Measured Depth

Figure 4-4: Relationship between the volume and shape of a plunge pool, from Stein and Julien, 1993 [36].

Stein and Julien [36] found that

$$V^* = 2D^{*2}. \tag{4.1}$$

Then if

$$V^* = V/D_e^2$$

and

$$D^* = D/D_e$$

are substituted into (4.1), solving for V yields

$$V = 2D^2. \tag{4.2}$$

If we further assume that the plunge pool approximately resembles an isosceles triangle, as shown in Figure 4-3, and that the horizontal distance between the scarp and the point of maximum depth of the plunge pool (X_m) is the same

as the distance from the scarp to the impinging point, that is, X_p (given by equation (4.10)) (see Figure 4-3), then the volume of the pool per unit width is

$$V = X_p D. \tag{4.3}$$

Finally, substituting (4.3) into (4.2), and solving for D yields

$$D = \frac{X_p}{2} = S_f X_p. \tag{4.4}$$

The shape factor corresponding to Stein and Julien's [36] observations is $S_f = 1/2$.

Stein and La Trey [39] observed a relationship between the dimensionless scour hole half width (X_m^*) and the dimensionless sour depth (D^*), in Ottawa sand, constant and equal to 1.8. This relationship is equivalent to a S_f of 1/1.8, very close to the value derived from Stein and Julien's [36] observations.

4. *2D assumption.* This part of the model produces a retreat rate that is a 1D value. Also, it assumes a 2D space that represents a 3D space per unit width, in which the side effects are neglected. Because a 3D approach is more complex, and because flume experiments to which we can compare this model are of a 2D nature [2] [3] [4], this simplification seems reasonable.

4.2.2 Flow characteristics

Normal and free overfall flow assumptions. The characterization of the flow begins upstream of the scarp where the flow is assumed normal with depth h_n and velocity V_n obtained using Manning's equation as

$$h_n = n^{0.6} q^{0.6} S^{-0.3} \tag{4.5}$$

and

$$V_n = \frac{q}{h_n}. \tag{4.6}$$

Once the normal flow characteristics upstream are estimated, the Froud Number (Fr) for the upstream flow is calculated to determine the flow regime: if it is supercritical, the flow at the brink depends on the normal flow conditions (and so on n, q and S); if it is subcritical, it only depends on q. Fr is calculated as

$$Fr = \frac{V_n}{\sqrt{h_n g}}. \tag{4.7}$$

Ventilated jet assumption. The water is assumed to fall freely through the scarp forming a ventilated jet, that is a jet surrounded by an atmospheric pressure above and below, as shown in Figure 4-5. As the water approximates the brink of the head cut, it accelerates. The flow at the brink (see Figure 4-5) is assumed to be 1/0.715 as fast as the critical flow when an upstream subcritical flow regime occurs ($Fr \leq 1$). Then,

$$V_{brink} = \frac{\sqrt[3]{qg}}{0.715}. \tag{4.8}$$

When a supercritical flow regime occurs($Fr \geq 1$), V_{brink} is given by

$$V_{brink} = V_n \frac{Fr^2 + 0.4}{Fr^2}. \tag{4.9}$$

The above equation was proposed by Hager [14].

Once the flow characteristics at the brink and the jet's drop height (H) are known, four parameters to characterize the water jet are calculated through the equations provided in [1] for a ventilated jet profile. These parameters, shown in Figure 4-5, are the horizontal distance from the brink to the impinging point

$$X_p = V_{brink}\sqrt{\frac{2H}{g}}, \tag{4.10}$$

the angle of the jet impinging the plunge pool relative to a horizontal plane

$$\beta = \arctan\sqrt{\frac{2gH}{V_{brink}}}, \tag{4.11}$$

the thickness of the jet impinging the plunge pool

$$y_{pool} = h_{brink} cos\beta, \tag{4.12}$$

and the velocity of the water at the jet impinging the plunge pool

$$V_{pool} = \frac{q}{y_{pool}}. \tag{4.13}$$

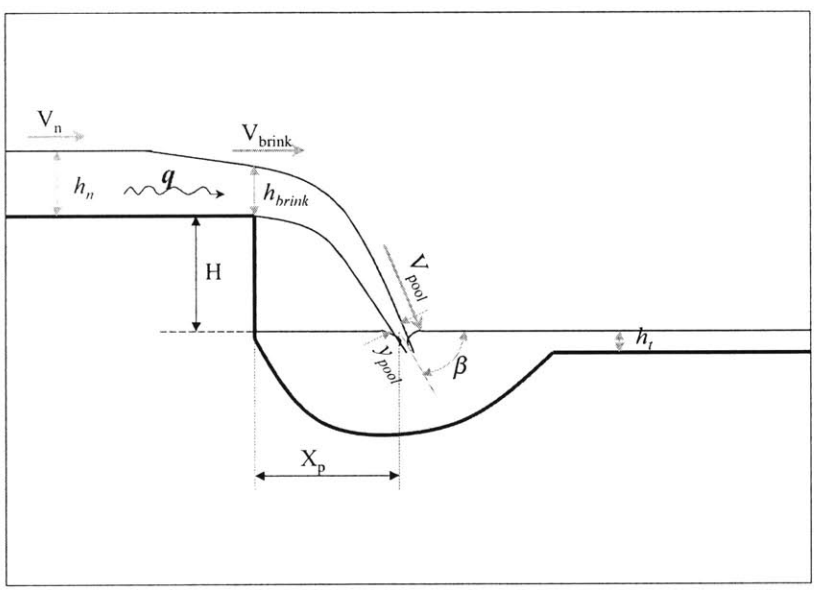

Figure 4-5: Flow characteristics before it penetrates the plunge pool.

Once the characteristics of the jet impinging the pool are known, the shape of the pool is estimated using equation (4.4). With the D known, the shear stress at the bottom of the pool and the retreat rate of the scarp are calculated.

4.2.3 Impingement region

The flow diagram of a jet entering a plunge pool is shown in Figure 4-6. At the impact with the water surface, the jet has an initial thickness y_{pool}, an average velocity V_{pool}, and an impact angle β.

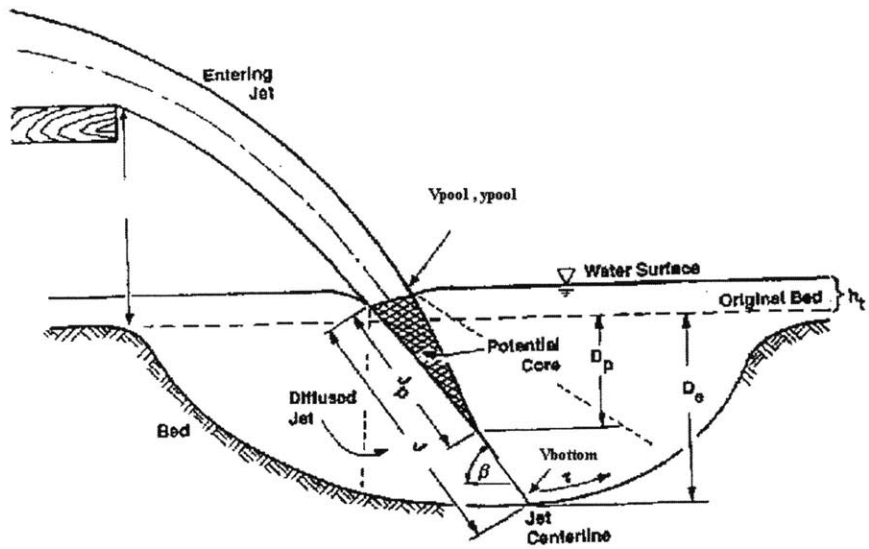

Figure 4-6: Jet impinging a plunge pool, modified from Stein *et al.*, 1993 [36].

As the jet penetrates the plunge pool, it diffuses throughout the surrounding fluid, decreasing its average velocity except at its potential core [36]. The zone along the jet where the flow velocity at the centerline of the jet trajectory remains constant and equal to V_{pool} is defined as the potential core, of length J_p (see Figure 4-6). Beyond J_p, the flow velocity remains maximum along the jet centerline but the entire flow velocity field is reduced by diffusion. It is generally accepted [36] that the centerline velocity at a given centerline distance J, outside of the potential core, is given by the thickness of the jet impinging the pool, y_{pool} (see equation (4.12) and Figure 4-5), and by an empirical constant C_d, as shown by the following equation

$$\frac{V}{V_{pool}} = C_d\sqrt{\frac{y_{pool}}{J}}, J > J_p. \tag{4.14}$$

In equation (4.14), when $V = V_{pool}$, $J = J_p$. Therefore

$$J_p = C_d^2 y_{pool}. \tag{4.15}$$

The value used for C_d in work is 2.6. Values for C_d vary between 2.5 and 2.72, according to Beltaos and Beltaos and Rajartham's experiments, cited by Stein and Julien [36].

Negligible downstream flow depth assumption. The geometry of the pool (D and X_p) is linked to J through

$$D = J \sin\beta - h_t, \tag{4.16}$$

where h_t is the tail water depth or depth of the flow downstream of the pool. The value of h_t is assumed small in comparison to H and D, as shown in Figure 4-5, and hence it is neglected in the model.

The maximum shear stress acting close to the bed of the pool is responsible for the scouring of the plunge pool. This maximum shear stress happens in the vicinity of the intersection between the jet centerline and the pool's bed, and is a function of the maximum velocity near the bed [35]. The shear stress can be expressed as

$$\tau = C_f \rho {V_{bottom}}^2, \tag{4.17}$$

where C_f is a coefficient of friction, g is gravity, and V_{bottom} (see Figure 4-6) is the jet's centerline velocity at the bottom of the pool. Because V_{bottom} is constant and equal to V_{pool} within the potential core, the shear stress is given by an equation identical to equation (4.17) when $J < J_p$. In this case the plunge pool is said to be in a non-diffusion state. When $J > J_p$, then the plunge pool is said to be in a diffusion state and V_{bottom} is given by equation (4.14). The shear stress is then given by

$$\tau = \frac{C_d^2 C_f \rho {V_{pool}}^2 y_{pool} sin\beta}{D}. \tag{4.18}$$

Blasius flow assumption. Making a Blasius flow assumption [36], the friction

coefficient (C_f) is a function of q and the kinematic viscosity of the water ν:

$$C_f = \frac{0.22}{8}\left(\frac{\nu}{q}\right)^{0.25}. \tag{4.19}$$

But because C_f does not vary much for a wide range of water flows, C_f is assumed constant. For small flows, between 0.0001 and 0.01 m^3/sec, C_f is assumed 0.009. For larger flows, between 0.001 to 0.7 m^3/sec, C_f is assumed 0.004.

4.2.4 Erosion and retreat

Following a detachment limited equation, a function of the shear stress and the soil's erodibility characteristics, the scouring rate of the pool is calculated by

$$\frac{dD}{dt} = E = \kappa(\tau - \tau_{cr})^p. \tag{4.20}$$

In order to keep the constant shape of the plunge pool, the relationship between D and X_p must be maintained. Therefore X_p must change in time as follows:

$$\frac{dX_p}{dt} = \frac{1}{S_f}\frac{dD}{dt}. \tag{4.21}$$

As a result, the scarp migration rate, equal to the rate at which the pool as a whole moves in the upstream direction, C_x, is

$$C_x = \frac{dX_p}{dt} = \frac{\kappa(\tau - \tau_{cr})^p}{S_f}. \tag{4.22}$$

p = 1 assumption. Usually in the plunge pool scouring literature, p is assumed 1 for cohesive soils [36, 37, 1], so here that same value is assumed.

4.3 Implementation of the headcut retreat through plunge pool erosion model into CHILD

The retreat rate computed in the previous section is the input of an *eroding* model that in CHILD causes the retreat at a given point in the landscape during a simulated Δt. The following description of CHILD is extracted from Tucker *et al.* [42].

4.3.1 CHILD as a framework

CHILD is a computational framework that "simulates the evolution of a topographic surface" driven by a number of eroding and sedimentation processes, given a set of initial and boundary conditions. It is "designed...for investigating...problems of catchment geomorphology." It "is both a model, in the sense that it comprises a set of hypotheses about how nature works, and a software tool in the sense that it provides a dynamic simulation environment for exploring the consequences of different hypotheses, parameters, and boundary conditions." Here the word model is used to describe "collectively...the software and the assumptions and hypotheses embedded within it."

The spatial framework of CHILD that represents the land surface is discretized as a set of points connected to form a triangulated irregular mesh. "The mesh is constructed using a Delaunay triangulation" which "lends itself to numerical solution of the continuity equation using finite-volume methods.... Each node (vortex) in the triangulation, N_i, is associated with a Voronoi (or Thiessen) polygon of surface area A_i [(see Figure 4-7)], in which the polygon edges are perpendicular bisectors of the edges connecting the node to its neighbors" (see Figure 4-7). This way "the Delaunay triangulation defines the connectivity between adjacent nodes...", while the associated Voronoi [polygon] defines the surface area associated with each node..." "In CHILD each Voronoi polygon is treated as a finite-volume cell."

The temporal framework of CHILD is discretized as a series of time increments Δt that correspond to the length of a storm or of an inter storm. For each storm,

surface runoff collected at each node on the mesh is routed downslope toward one of its adjacent neighbor nodes, following the edge that has the steepest slope. This way a runoff network is created in the landscape for a given topographic configuration. The flow of water and sediment running through it drive the fluvial erosion and sedimentation processes. At each Voronoi cell, each process uses information provided by the framework regarding inflows and outflows of water and sediments, and regarding the physical characteristics of the environment such as slopes and soil parameters. Next, each cell has an information output that may be needed by another part of the model. The Voronoi cells can also produce a change in the land surface by an increment or decrease in their elevation.

In the case of the plunge pool model, a retreat rate is calculated with the input values of H, S, n, q, k and τ_{cr} values for each cell. This rate is then the input value to an *erosion* model that produces the corresponding changes in the topographical surface during a given time increment Δt. The erosion model is explained below.

4.3.2 The eroding model for retreat

The retreat of a headcut produces changes in the landscape that are considered erosion. The retreat is assumed to occur along the flow path established by the runoff network. An example of these flow paths is shown in Figure 4-7.

Once the retreat *rate* is know, a retreat *length* for a given Δt is calculated and assigned to each cell. First, this length is accumulated in each cell. Second, if the accumulated retreat length extends further than the length of the cell, the excess length is transmitted to neighboring upstream cells proportionally to their contributing area. In the model, the length of the cells is assumed to be the distance between mesh points. Third, when the accumulated retreat length in a cell equals or exceeds the cell's size, the cell is lowered to match the elevation of the cell downstream. Figure 4-8 schematically shows the retreating of a Voronoi cell.

At the current state of the modeling efforts, the material produced by the retreat is assumed to be transported out of the system by the flow, and so, the headcut retreat through plunge pool erosion is a detachment limited process.

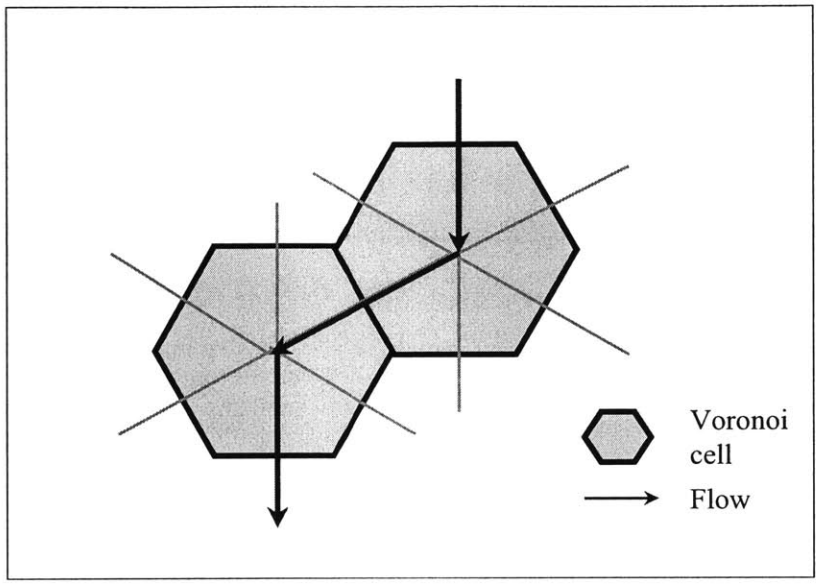

Figure 4-7: Schematic of a section of the flow network created by CHILD.

4.3.3 Defining a headcut in CHILD.

In CHILD, H is obtained from the difference in elevation between cells, assuming that the surface of each Voronoi cell representing the landscape is horizontal and that the change in elevations along their edges is abrupt and forms *steps*. A more realistic smooth landscape is obtained if the Voronoi cell's size decreases. But, because small cells would require a large number of nodes to represent the landscape, and because the cell's size determines the width of the water course in this particular CHILD framework (where sheet flow is considered), the Voronoi cell's are not small enough to represent a detailed topography. Therefore, a criterion to decide whether a large H is a headcut or a steep slope is required. In the thesis, a cell is considered a headcut when its slope (in the downstream direction) is steeper than 40°, and the value of the slope of its downstream neighboring cell (also in its downstream direction) is at the most half (i.e., if the first value is 42°, the second value should be at the most 21°).

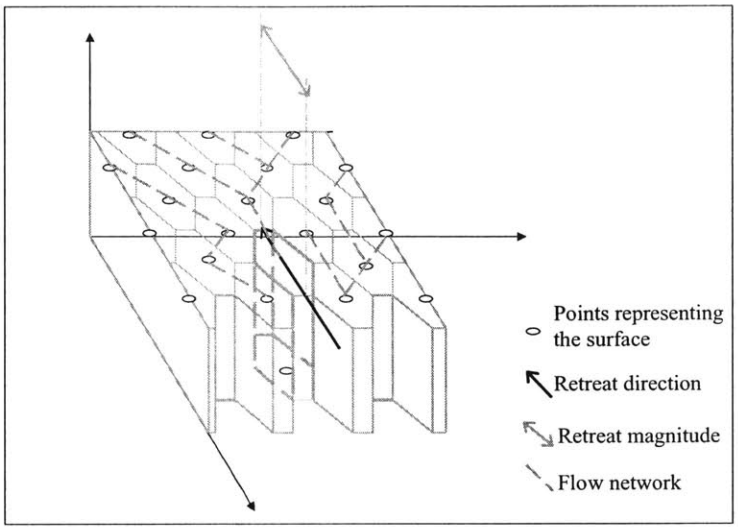

Figure 4-8: Example of the retreat of a cell.

4.4 Limits of the retreat rate model

Several assumptions of the retreat rate model have been discussed in Section 4.2. This section presents some of the retreat rate model's limitations regarding the range of flow conditions under which it is applicable. The retreat rate model is constructed in such a way that the geometry describing the plunge pool could acquire unrealistic dimensions such as having a shallow headcut and an extremely large pool. Such unrealistic dimensions could occur if Manning's n were very small, close to zero, or S tended to infinity. In such an extreme case the velocity at the brink would become infinitely high and the flow thickness infinitely thin. However, the above scenario is not possible because a lower boundary for the value of n and an upper boundary for the value of S exist.

According to Chow [6], the value of n may be composed of the addition of the roughness due to different components. For bare soil n is about 0.02, and the contribution to n of vegetation varies from 0.005 to 0.01, 0.01 to 0.025, 0.025 to 0.05 or 0.05 to 0.1 depending on whether the vegetation cover is low, medium, high or very high,

respectively. Then an n within a range of 0.02 to 0.1 is reasonable. Flow variations within this range of values are explored below, but the model is not limited to it. The values given by Chow [6] correspond to channelized flow. Here those values are assumed for overland flow. The range of 0.02 to 0.1 is within the range of overland flow values given by Engman in [12] for overland flow in rangeland conditions. In the current model, the roughness (n) is set by the user.

The values of S according to our field data observations vary between 3 and 9 percent. An S within this range seems a reasonable input into the model. Flow variations within this range of values are explored below, but the model is not limited to it. In the current model the slopes are constantly changing throughout the simulation as the topography is modified by erosional processes, and therefore no control a-priori exists over S.

The model should not consider unrealistic shallow flows. Figure 4-9 shows the normal flow and the flow at the brink depths, for the deepest and shallowest flow depth cases within the ranges of n and S defined above, for flows between 0.005 and $0.25m^2/sec$.

The above condition was inspected for flows as small as $0.005m^2/sec$ only. Flows smaller than $0.005m^2/sec$ produce little shear stress at the pool's bottom and thus, little retreat, in comparison to larger flows (for an example of shear stress values as function of flow, see Figure 4-10).

The model assumes that h_t, the flow depth downstream of the plunge pool, is negligible. However often it is not. The h_t/D ratio may be adopted as a criteria to determine whether h_t is significant or not. Next, if h_t is assumed similar to h_n, the normal flow upstream of the headcut, then the ratio h_n/D must be much smaller than 1 if h_t is insignificant. Under a slow flow scenario, that is, when S is small and n is large, h_n/D is rarely that small(see Figure 4-11). It is then acknowledged that the retreat rate calculation for small heights H, under slow flow conditions, is out of the range of calculation of the model.

To satisfy the ventilated jet condition (see the *Ventilated jet assumption* in Section 4.2.2), h_t must be smaller than H (see Figure 4-12), therefore, assuming $h_t = h_n$,

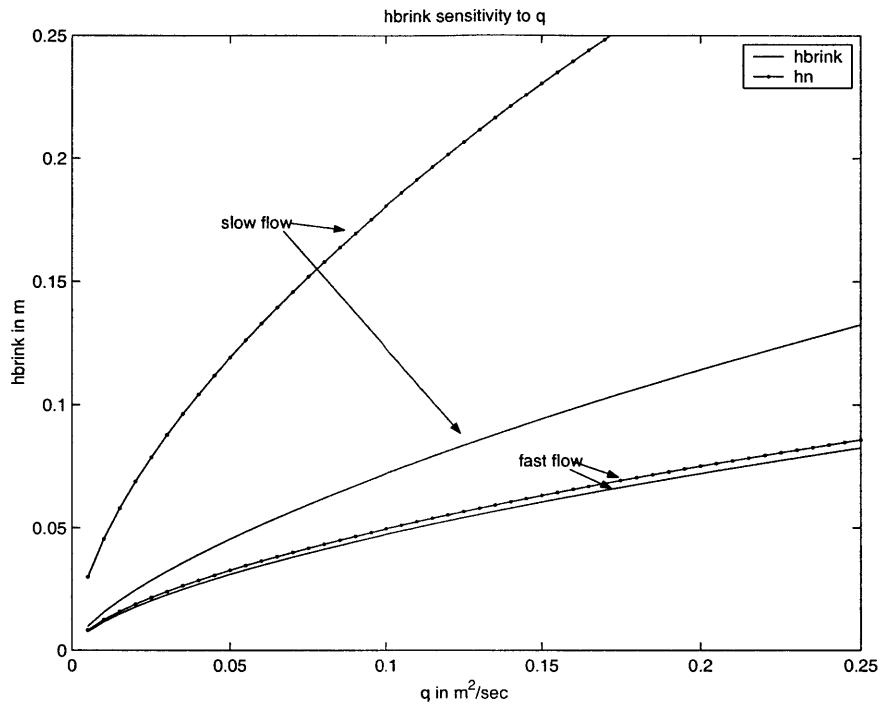

Figure 4-9: Flow at the brink under fast flow conditions. The figure shows the flow at the brink (h_{brink}) and the upstream normal flow (h_n), for the fast (a small flow depth) and slow (a large flow depth) flow conditions. These flow conditions delimit the possible depths at the brink for the specified ranges of n and S.

the ratio h_n/H should be at the most 1. Figure 4-13 shows the values h_t for different flows (q). When the condition h_n/H is not met, the calculation of plunge pool erosion should include the correction factor for the jet's angle of impingement suggested by Alonso *et al.* [1]. This thesis neglects the correction factor to reduce complexity.

The headcut retreat model and its incorporation into CHILD have been described in this chapter. The next chapter explores a sensitivity analysis of the headcut retreat rate model and the critical condition, or threshold, for plunge pool erosion under the model's setting.

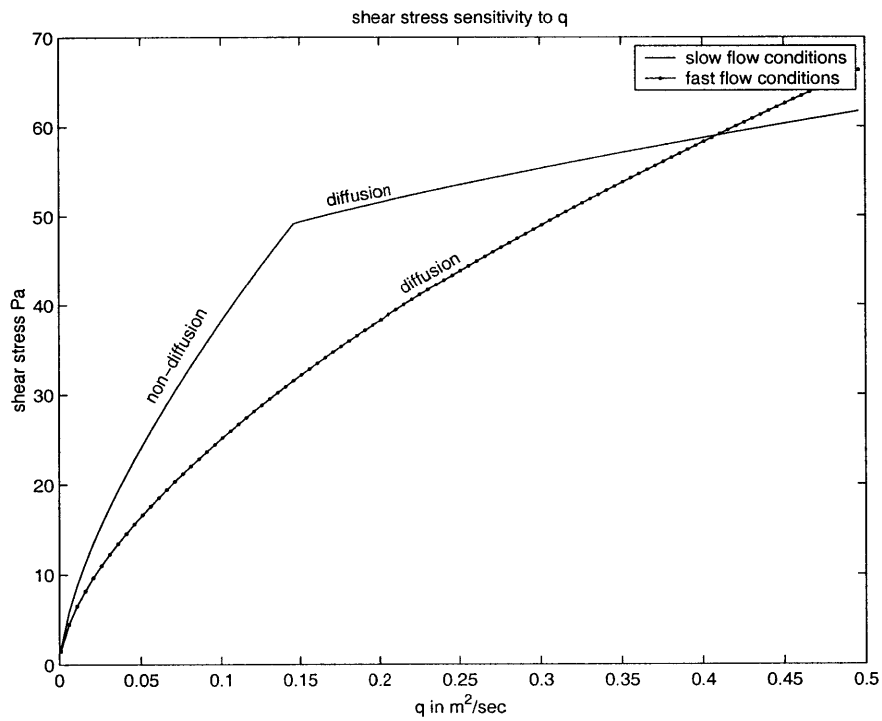

Figure 4-10: Shear stress at the bottom of the pool for $H = 0.5m$ as q increases. Two flow conditions are shown: the slow flow conditions correspond to the maximum roughness n and minimum slope S of the previously specified range for these parameters; the fast flow conditions correspond to the minimum roughness and maximum slope within the previously specified range. The break in the slope of the line corresponding to the slow flow conditions marks a transition from a diffusion to a non-diffusion state. This transition is further explored in Chapter 5.

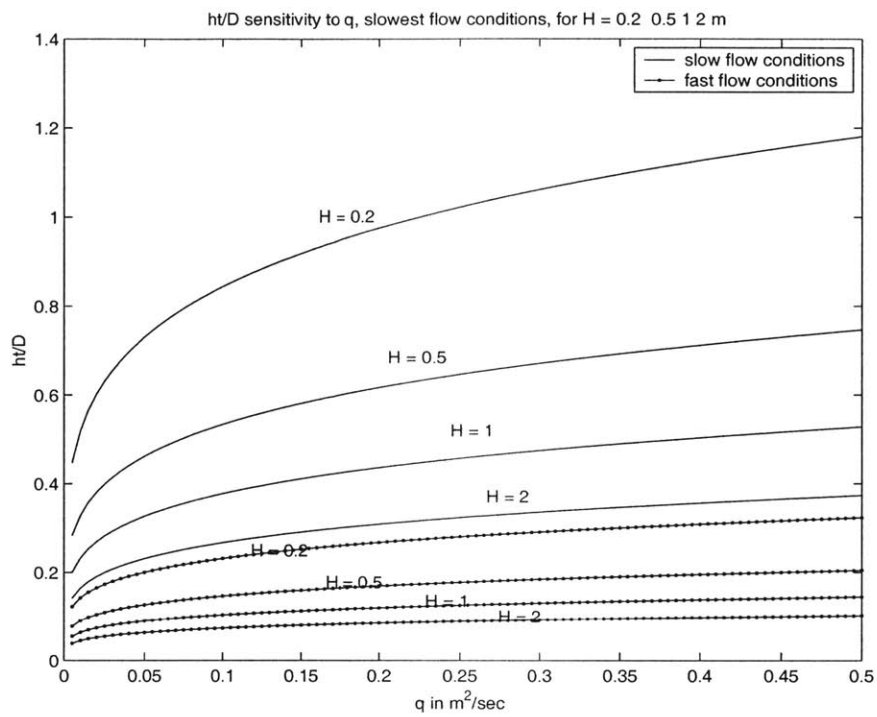

Figure 4-11: h_t/D ratio, calculated with $h_t = h_n$. This figure illustrates how negligible or significant h_t is. Fast(small depths) and slow (large depths) flow conditions are shown. As H becomes smaller, the ratio h_t/D increases and h_t becomes more significant. In this example the shape factor, Sf, is 0.2.

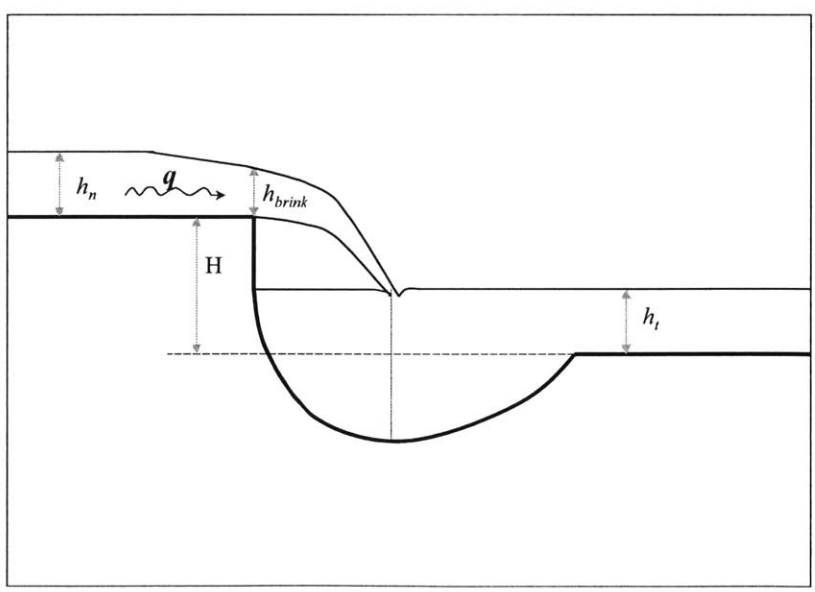

Figure 4-12: Flow depth at different points along the headcut-plunge pool system.

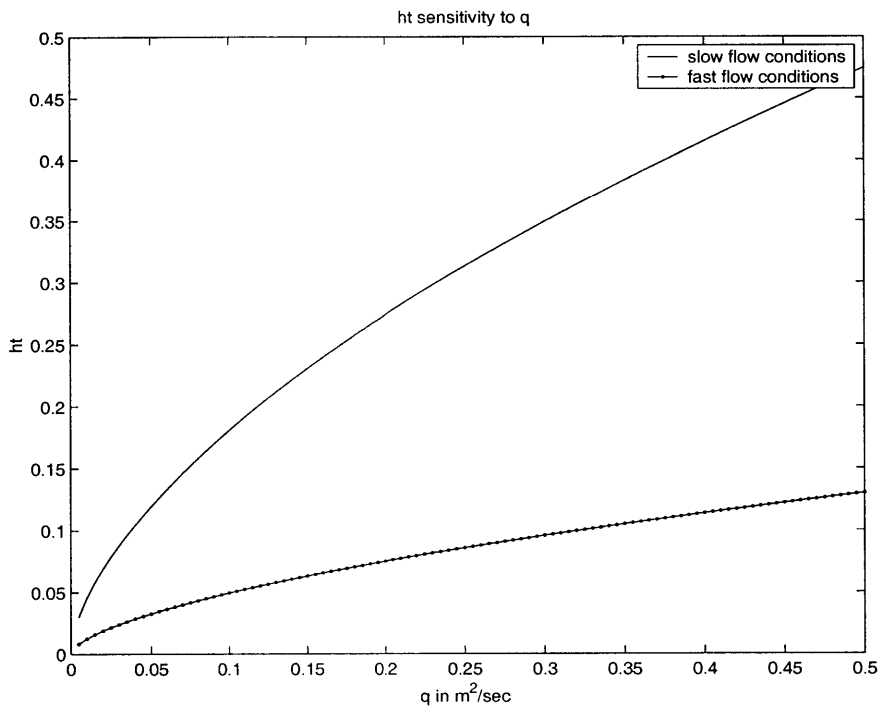

Figure 4-13: Depth of the flow downstream of the plunge pool, h_t, that should be smaller than $H_{original}$ in order to satisfy the ventilated jet condition (that is, a non-submerged jet). Fast(small depths) and slow (large depths) flow conditions are shown.

Chapter 5

Model sensitivity and conditions for plunge pool erosion

5.1 Introduction

This chapter explores the sensitivity of the retreat rate model to the topographic and flow input values H, S, n, and q. A diffusion and a non-diffusion state are distinguished in the analysis. The difference of the sensitivity of the model, corresponding to each of these states, is highlighted through diagrams that show the boundary between these two states as a function of H and q, for given n, S and S_f. This chapter also describes the values of q and H that define the critical condition or threshold for plunge pool erosion, given a certain τ_{cr}, n, S, and S_f.

5.2 Sensitivity of the retreat to q, H, n, and S

The sensitivity of the retreat model is explored through the shear stress, τ, since the retreat is proportional to τ when $\tau_{cr} << \tau$ and p=1 (see equation 4.22).

In this analysis four conditions, shown in Table 5.1, are distinguished. Most of the experimental data available in the literature reviewed correspond to the supercritical condition [2, 3, 4].

The first part of the analysis examines the diffusion and non-diffusion states in

terms of V_{brink} and H. Later V_{brink} is decomposed into a function of q, or of q, S, and n, according to the upstream flow regime. This yields four different equations that correspond to the four conditions shown in Table 5.1. The shear stresses, according to these equations, may increase, decrease, or stay constant as n or S change.

5.2.1 The diffusion/non-diffusion boundary

To describe the behavior of the model when the jet is diffusing and when it is not, the diffusion and non-diffusion zones are defined in a flow per unit width versus height of the scarp (q *vs* H) space (shown in Figure 5-1, for a subcritical flow regime) assuming a given Manning's roughness (n) and slope (S). This diagram is independent of n and S in a subcritical flow regime, but it is sensitive to these parameters under supercritical conditions, as described below. The variables involved in the diagram are show in Figure 5-2.

The boundary between the distinct zones is set by the height corresponding to the diffusion/non-diffusion boundary, H_p, a function of q and V_{brink}. H_p is the height of the headcut at which $J = J_p$, where J is the distance between the impingement point and the point where the jet's trajectory centerline intersects the bottom of the pool, and J_p is the length of the potential core, as shown in Figure 5-3. The depth of the pool at the diffusion/non-diffusion boundary, D_p, is used to obtain H_p and is given by substituting equation (4.15) into (4.16), with h_t negligible, yielding

$$D_p = C_d^2 y_{pool} \sin\beta \tag{5.1}$$

To obtain H_p as a function of q and V_{brink}, other expressions are required. First, D, the depth of the pool, is expressed in terms of V_{brink} and H by combining equations (4.10) and (4.4), which yields

$$D = S_f V_{brink} \sqrt{\frac{2H}{g}} \tag{5.2}$$

Next, the following two expressions are obtained through the trigonometric relationship between the V_{pool} and its component vectors (see Figure 5-4):

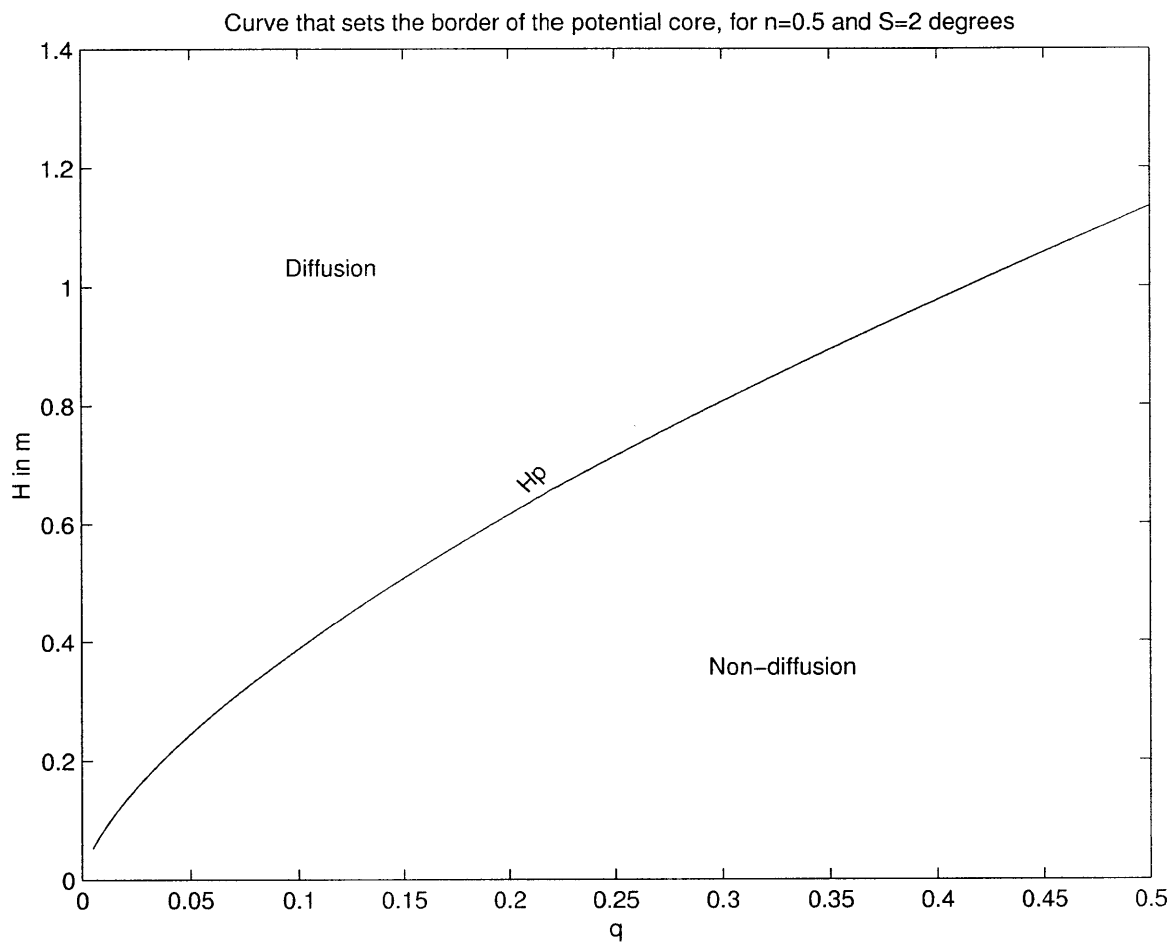

Figure 5-1: Boundary between the diffusion and non-diffusion zones. This example corresponds to a subcritical flow regime. In this example $S_f = 0.5$.

$$sin\beta = \frac{\sqrt{2Hg}}{V_{pool}} \tag{5.3}$$

and

$$V_{pool}^2 = V_{brink}^2 + 2Hg. \tag{5.4}$$

Then, y_{pool} is defined as

$$y_{pool} = \frac{q}{V_{pool}}, \tag{5.5}$$

and substituting equations (5.3) and (5.5) into (5.1) results in

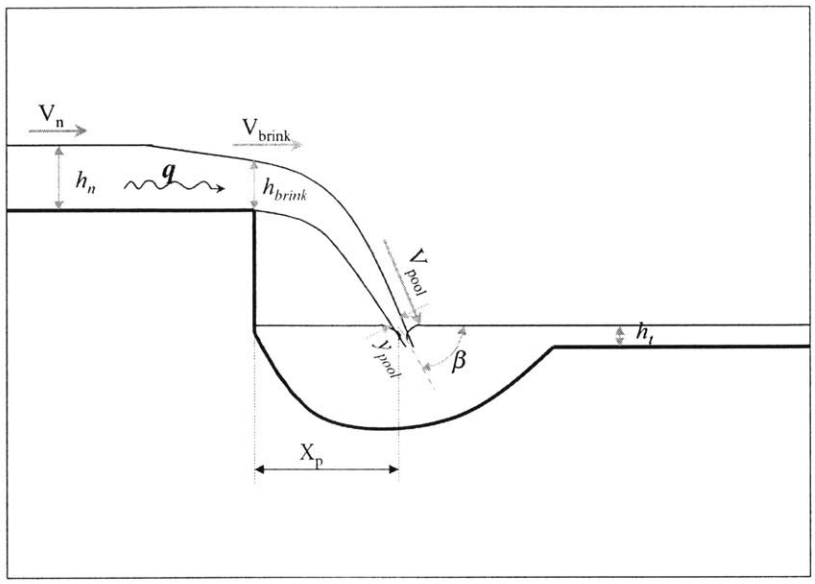

Figure 5-2: Flow characteristics before it penetrates the plunge pool.

$$D_p = C_d^2 \frac{q\sqrt{2gH}}{{V_{pool}}^2}. \tag{5.6}$$

Finally, inserting (5.2) and (5.4) into (5.6), and solving for H, results in

$$H_p = \frac{C_d^2 q}{2S_f V_{brink}} - \frac{{V_{brink}}^2}{2g}. \tag{5.7}$$

The above equation describes an increase in H_p as V_{brink} increases. H_p will thus vary with n and S according to the way V_{brink} varies with those parameters. Figures 5-5 and 5-6 show how the boundary between the two zones varies as n or S increase.

5.2.2 Diffusion state

In diffusion, as D increases and the length of the impinging jet centerline J (see Figure 5-3) becomes greater than the length of the impinging jet's potential core, J_p (see Figure 5-3), the shear stress produced at the bottom of the pool, τ, decreases. A relationship that describes the variations of τ as a function of V_{brink} and H under diffusion is derived below.

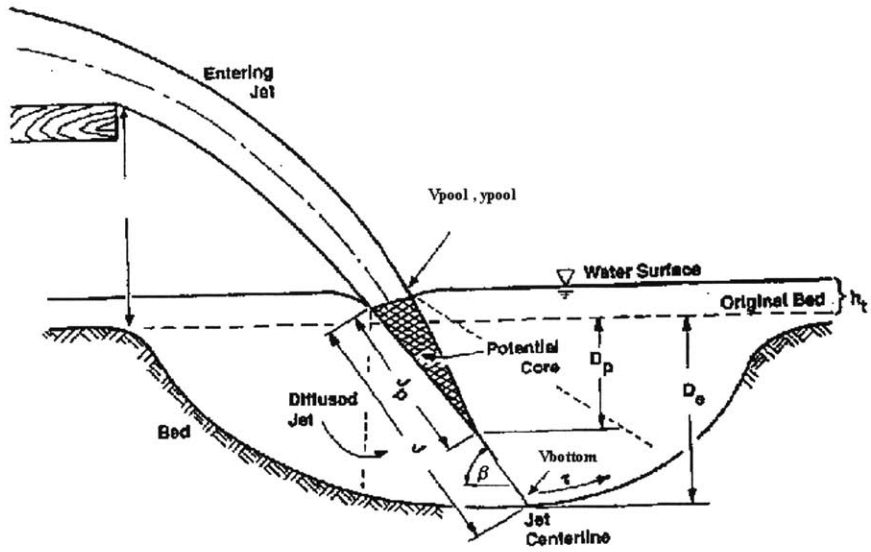

Figure 5-3: Jet impinging a plunge pool, modified from Stein *et al*, 1993 [37].

From equation (5.3) multiplied by q, and noting that $q = V_{pool}y_{pool}$, the following relationship is obtained

$$V_{pool}^2 y_{pool} sin\beta = q\sqrt{2Hg}. \tag{5.8}$$

Then, by substituting equations (5.8) and (5.2) into (4.18), the shear stress equation for a diffusing jet, the following is obtained:

$$\tau = \frac{C_d^2 C_f \rho q g}{2S_f V_{brink}}. \tag{5.9}$$

Note that τ is insensitive to H, directly proportional to q, and inversely proportional to V_{brink} (see Table 5.1). Figure 5-7 shows how the shear stress varies in the diffusion zone in a subcritical flow regime ($n = 0.05$, $S = 0.035$). The vertical lines are lines of constant shear stress. The lines are in $10Pa$ intervals.

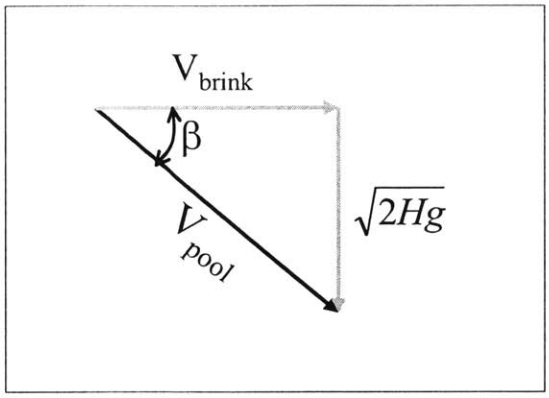

Figure 5-4: Velocity component vectors of the water jet impinging into the plunge pool.

5.2.3 Non-diffusion state

In the non-diffusion state ($J \leq J_p$)the potential core of the jet reaches the bottom of the pool, so that $V_{bottom} = V_{pool}$. This implies that equation (5.4) may be substituted into equation (4.17), yielding

$$\tau = C_f \rho (2Hg + V_{brink}^2), \tag{5.10}$$

where τ is a function of H and V_{brink} only. Note that V_{brink} is a function of q. Figure 5-8 shows how the shear stress varies in the non-diffusion zone in a subcritical flow regime ($n = 0.05$, $S = 0.035$). Curves of constant shear stress are shown, increasing upwards in $10Pa$ intervals.

5.2.4 Shear stress in terms of q, n, and S

In the following paragraphs the equations describing the shear stress are expressed in terms of q, n, and S instead of q and V_{brink}. This is to improve the understanding of the behavior of the shear stress as S and n vary.

In the subcritical flow regime, V_{brink} is $\frac{1}{0.715}$ that of the critical flow and it is given by equation (4.8), a function of q only. Substituting equation (4.8) into (5.9), for a diffusion state, results in

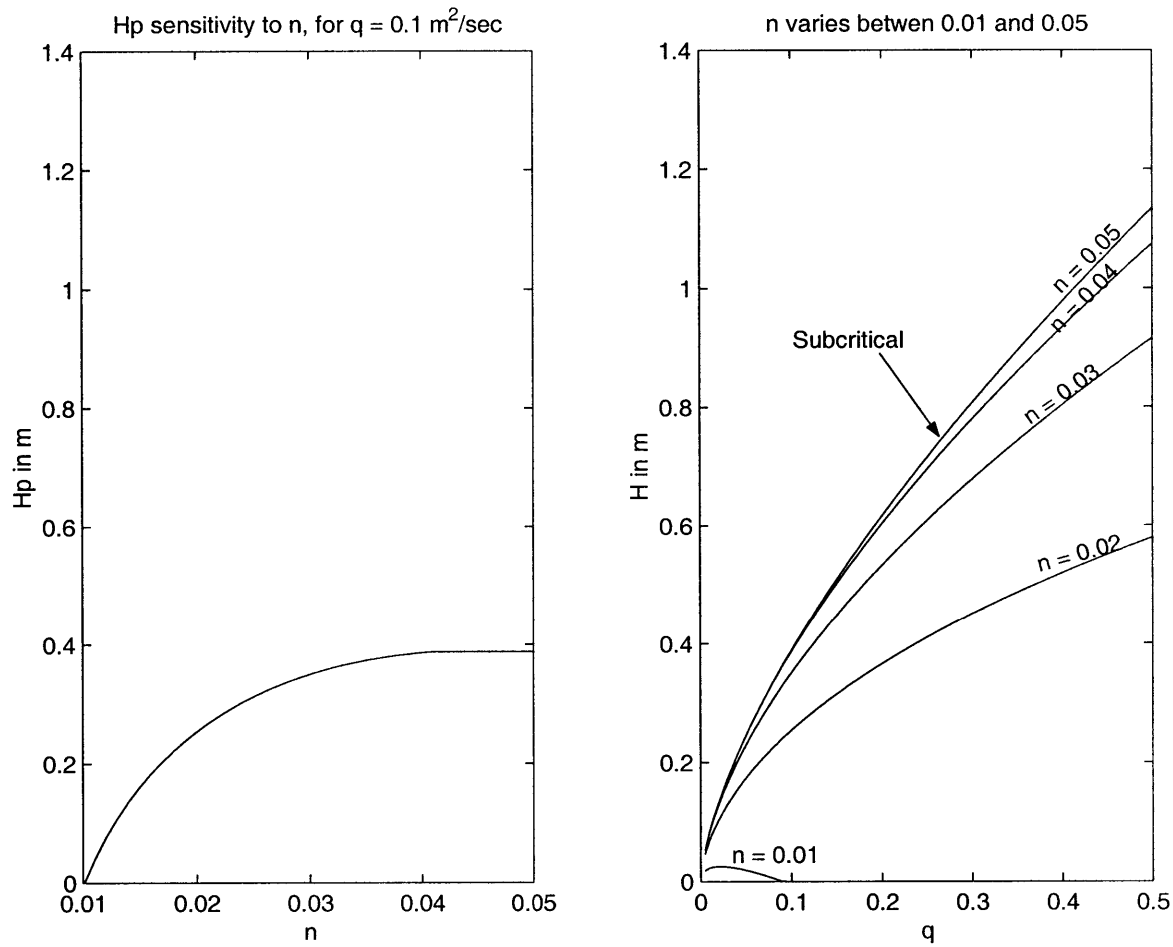

Figure 5-5: Variation of the boundary between the diffusion and non-diffusion zones as n varies. The boundary moves upward as n increases. A constant H_p is observed in the subcritical regime, where the boundary between the diffusion and non-diffusion zones is independent of n. In this example $S_f = 0.5$.

$$\tau = \frac{0.358 C_d^2 C_f \rho q^{2/3} g^{2/3}}{S_f}, \tag{5.11}$$

function of $q^{2/3}$ only. Substituting equation (4.8) into (5.10) for a non-diffusion state results in

$$\tau = C_f \rho (2Hg + q^{2/3} g^{2/3}), \tag{5.12}$$

a function of $q^{2/3}$ and H.

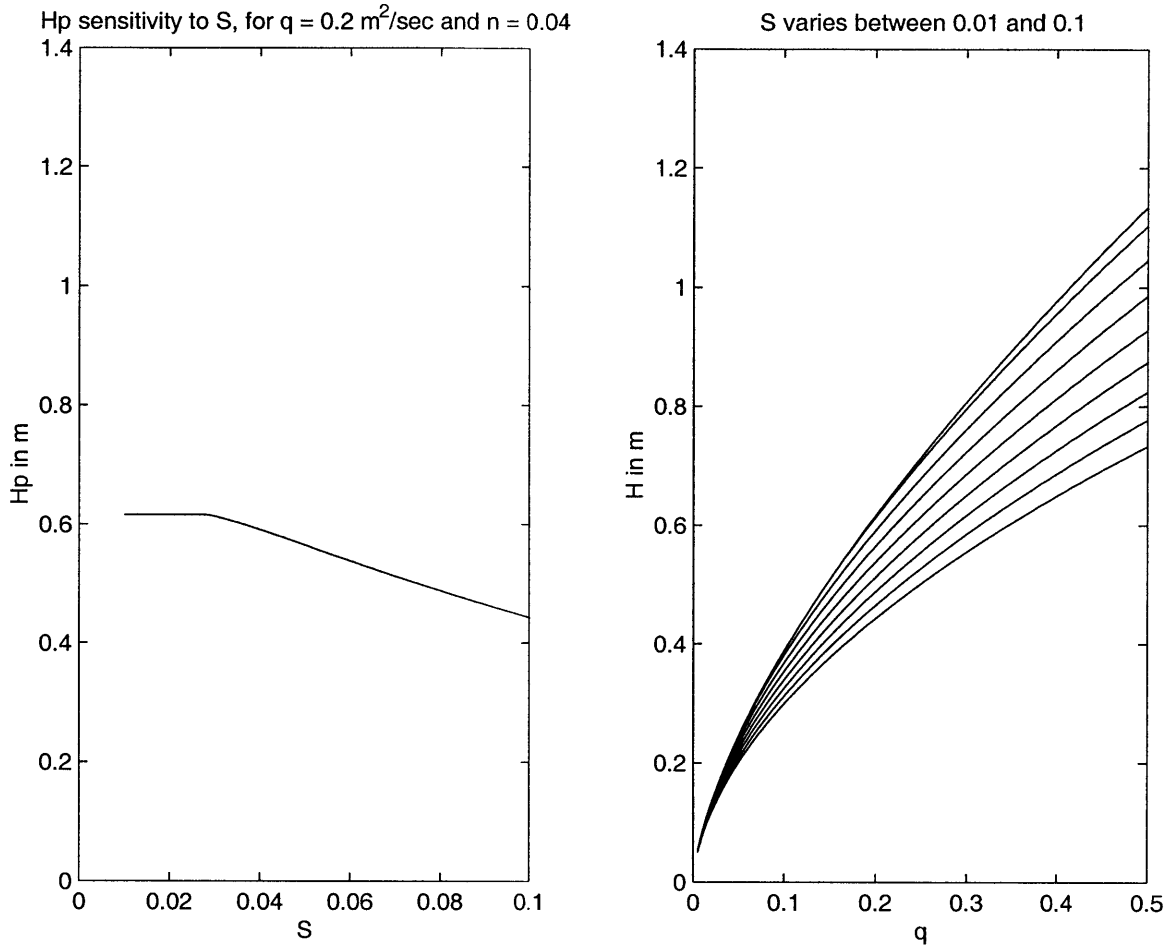

Figure 5-6: Variation of the boundary between the diffusion and non-diffusion zones as S varies.The boundary moves downward as S increases. A constant H_p is observed in the subcritical regime, where the boundary between the diffusion and non-diffusion zones is independent of S. In this example $S_f = 0.5$.

In the supercritical regime the flow becomes faster as it approximates the brink. Hager [14] has proposed equation (4.9), which describes the flow at the brink for a ventilated free overfall as a function of V_n. Because in the supercritical regime $Fr^2 > 1$, then $\frac{0.4}{Fr^2} < 0.4$, and therefore the fraction $\frac{0.4}{Fr^2}$ of the right hand side of equation (4.9) may be considered a small number. Then, the velocity at the brink, from equation (4.9), may be expressed as

$$V_{brink} = V_n(1 + smallnumber). \tag{5.13}$$

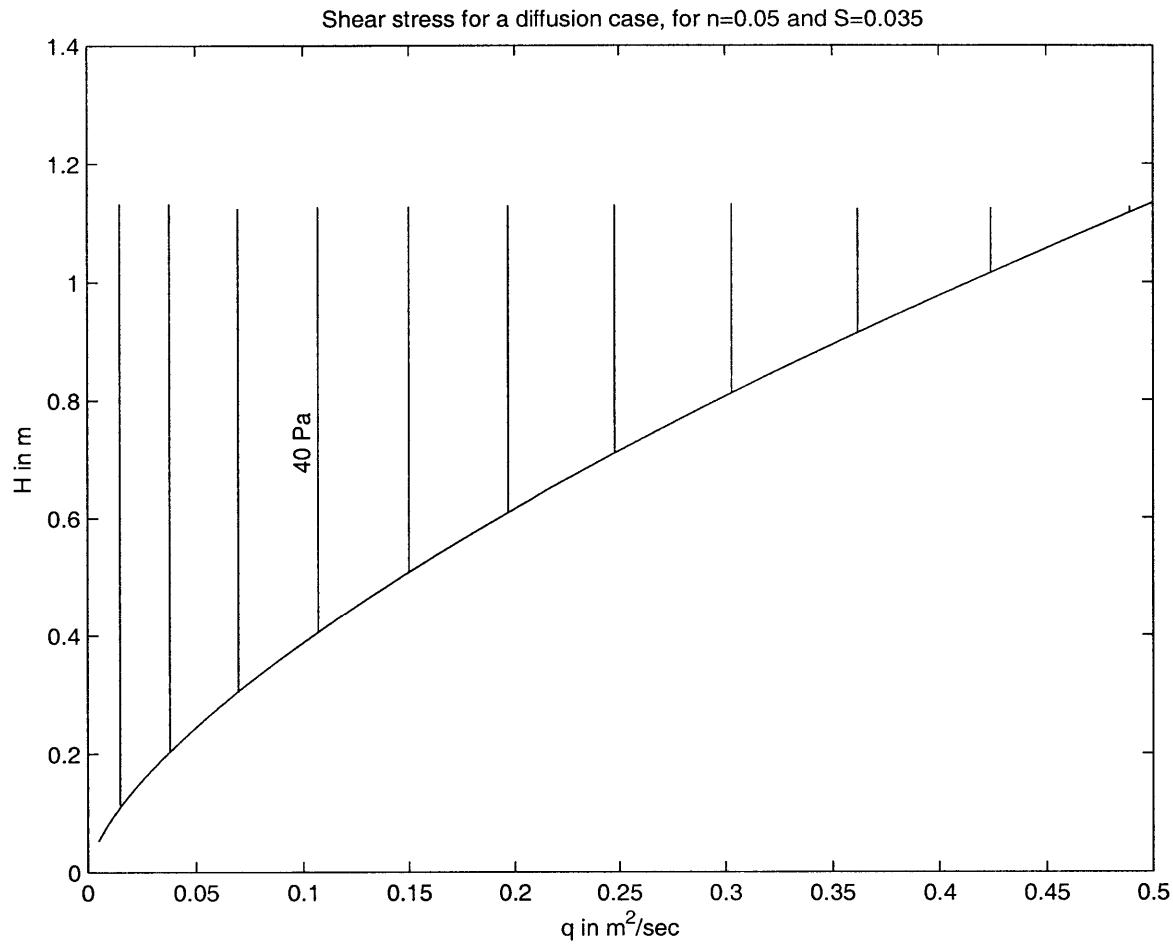

Figure 5-7: Variation of the shear stress in the diffusion zone. Each vertical line represents shear stress in intervals of $10Pa$, increasing as flow increases. In this example $S_f = 0.5$.

Because of the above, and inserting equation (4.5) into (4.6), and then its result into equation (5.13) (and assuming the small number to be insignificant), V_{brink} may be expressed as

$$V_{brink} = \frac{q^{0.4} S^{0.3}}{n^{0.6}}. \tag{5.14}$$

Substituting the above equation into (5.9) yields

$$\tau = \frac{C_d^2 C_f \rho g n^{0.6} q^{0.6} S^{-0.3}}{2S_f}, \tag{5.15}$$

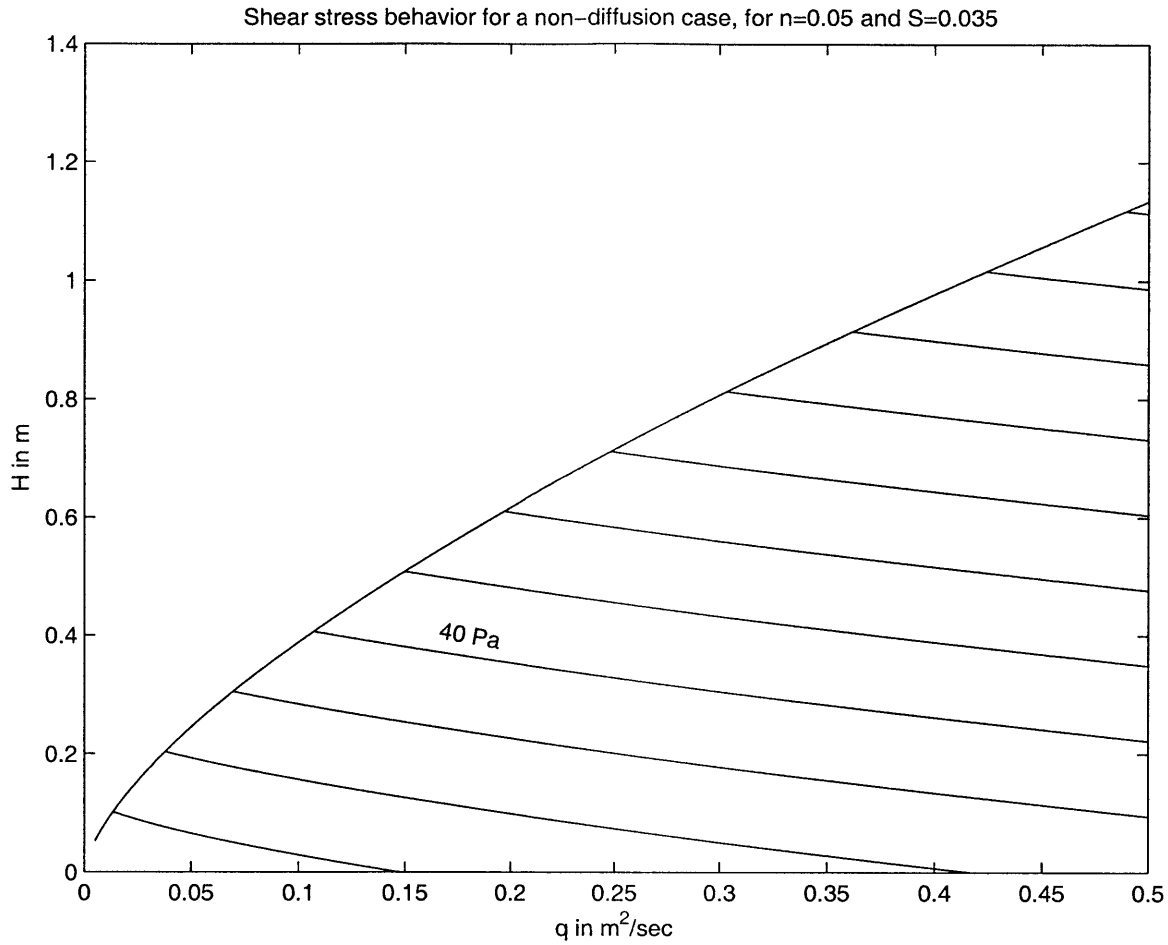

Figure 5-8: Variation of the shear stress in the diffusion zone. Each line represents shear stress in intervals of $10Pa$, increasing in the upward direction. In this example $S_f = 0.5$.

where τ, for the diffusion state, is proportional to $q^{0.6}$ and $n^{0.6}$, and inversely proportional to $S^{0.3}$.

Now, if we substitute equation (5.14) into equation (5.10), corresponding to the non-diffusion situation, the shear stress is

$$\tau = C_f \rho (2Hg + n^{-1.2} q^{0.8} S^{0.6}), \tag{5.16}$$

where τ increases with H, $q^{0.8}$, $S^{0.6}$, and decreases with $n^{1.2}$.

It is in diffusion that as V_{brink} increases, the pool becomes larger and deeper, and so diffusion increases, reducing the shear stress (in this state $\tau \alpha \frac{1}{V_{brink}}$). In non-

Table 5.1: How retreat varies with n and S, depending on the diffusion state.

	Diffusion	Non-Diffusion
Subcritical	$\tau(q)$ $(q^{2/3})$	$\tau(q, H)$ $(H,\ q^{2/3})$
Supercritical	$\tau(q, n, S)$ $(q^{0.6},\ n^{0.6},\ S^{-0.3})$	$\tau(q, n, S, H)$ $(q^{0.8},\ n^{-1.2},\ S^{0.6},\ H)$

diffusion, a high V_{brink} produces more erosion independently of the variations of the pool depth because the maximum velocity acting on the bed is independent of depth (in this state $\tau \alpha V_{brink}^2$).

The process can move back and forth from the diffusion zone as H, q, S, and n change. The behavior of the shear stress across the four different conditions is shown in Figures 5-9 (increase in q, in a subcritical regime), 5-10 (increase in H, in a subcritical regime), 5-11 (increase in n, that begins in a supercritical regime and transitions to a subcritical regime), and 5-12 (increase in S, that begins in a subcritical regime and transitions to a supercritical regime) as the four different parameters change. From Table 5.1 it may be stated that the retreat rate is most sensitive to H in a non-diffusion state, and largely sensitive to q in every other case.

Note that the behavior described above results from the constant pool shape assumption. If D were defined differently, the results from this analysis would be different.

5.3 Conditions for plunge pool erosion

Plunge pool erosion will occur when q, H, n, and S combine to produce enough shear stress at the bottom of a plunge pool to overcome the shear stress threshold (τ_{cr}). At this point a slight increase in shear stress would result in migration of the head cut.

Figure 5-13 illustrates the conditions for plunge pool erosion, and thus for headcut

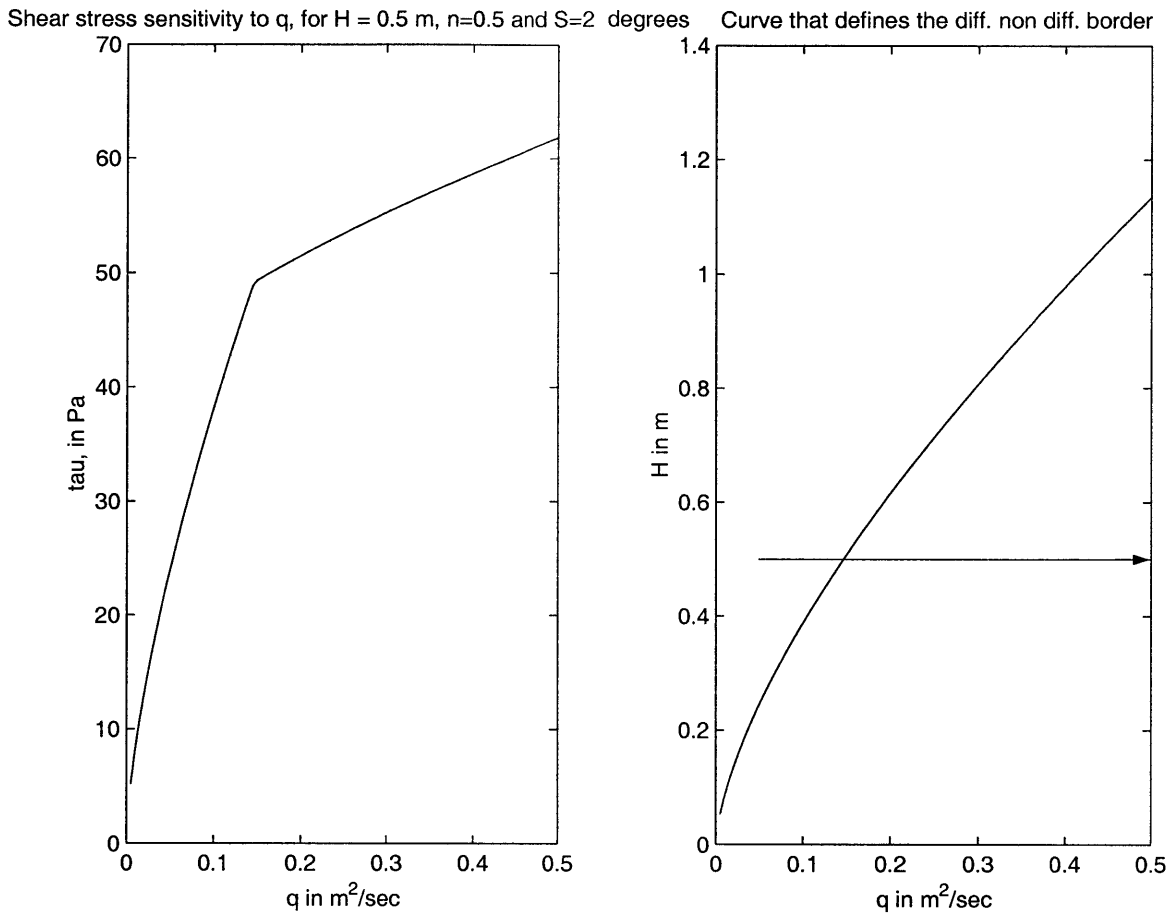

Figure 5-9: Behavior of the shear stress as q increases and the diffusion/non-diffusion conditions change. In this example the flow regime is subcritical and $S_f = 0.5$.

retreat, in a q vs H space. Assuming that $\tau_{cr} = 40Pa$, the solid line corresponding to a shear stress at the bottom of the plunge pool (τ) of $40Pa$ represents the threshold for erosion. Any larger τ (to the right of the solid line) will result in erosion, while any smaller τ will not (to the left of the thick solid line). The area on the right of the solid line is the zone of erosion; the area on the left of the solid line is the zone of no erosion. The transition from the diffusion state to the non-diffusion state along the line defining the threshold for plunge pool erosion (solid line) is a sharp break exactly where this line intersects the diffusion/non-diffusion boundary. The diffusion/non-diffusion boundary is represented by a dashed curve on the zone of erosion, and by a solid thin line on the zone of no erosion. Figure 5-13 corresponds to subcritical conditions, $S = 0.035$, $n = 0.05$ and $S_f = 0.2$.

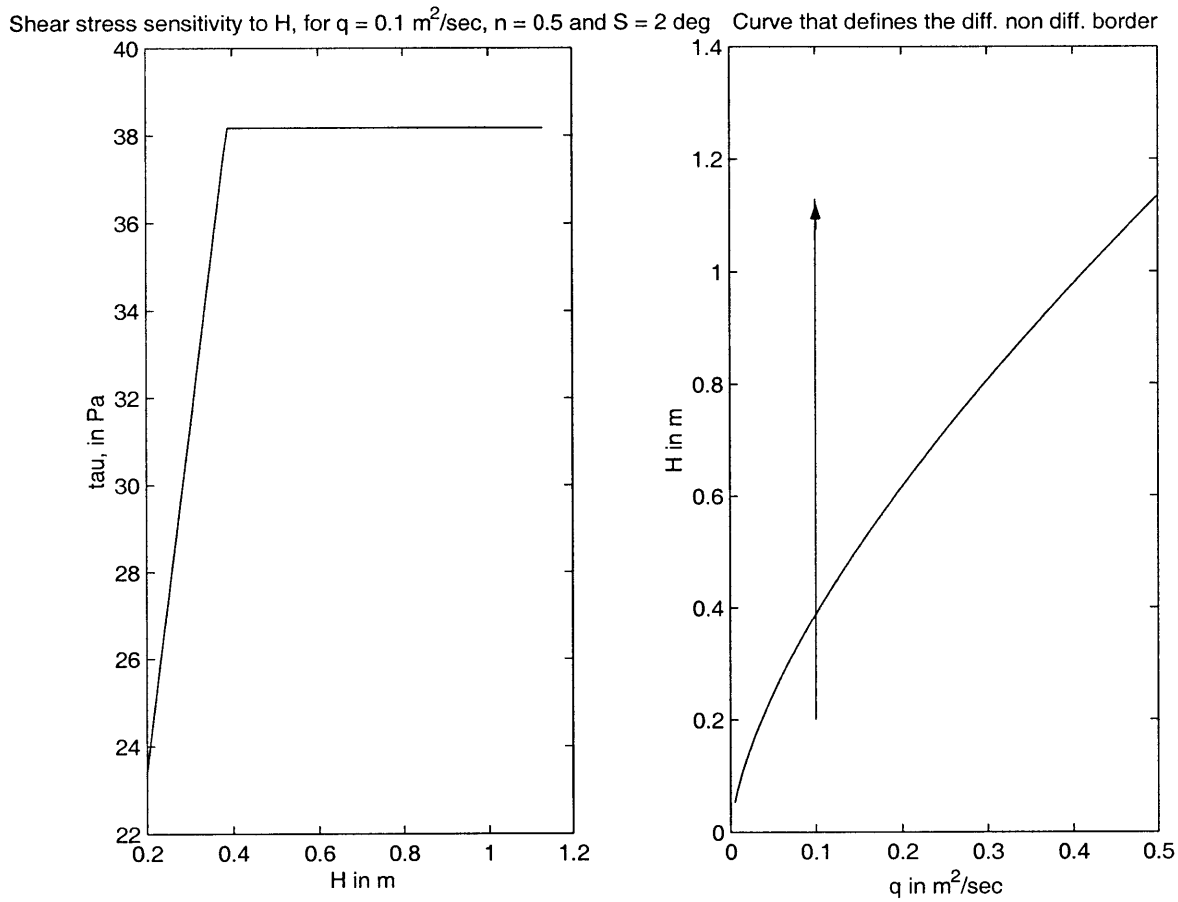

Figure 5-10: Behavior of the shear stress as H increases and the diffusion/non-diffusion conditions change. In this example the flow regime is subcritical and $S_f = 0.5$.

The threshold for plunge pool erosion is estimated differently in the diffusion and in the non-diffusion states. In the non-diffusion state, the threshold is derived by solving equation (5.10) for H, with $\tau = \tau_{cr}$. The value of this headcut height is referred to as the threshold height, H_t, and is given by

$$H_t = \frac{2\tau_{cr}}{2g\rho C_f} - \frac{V_{brink}^2}{2g}, \tag{5.17}$$

for the non-diffusion state.

In the diffusion state the threshold is independent of H, so it is represented by a vertical line parallel to the H axis (see Figure 5-13). In order to locate this line along

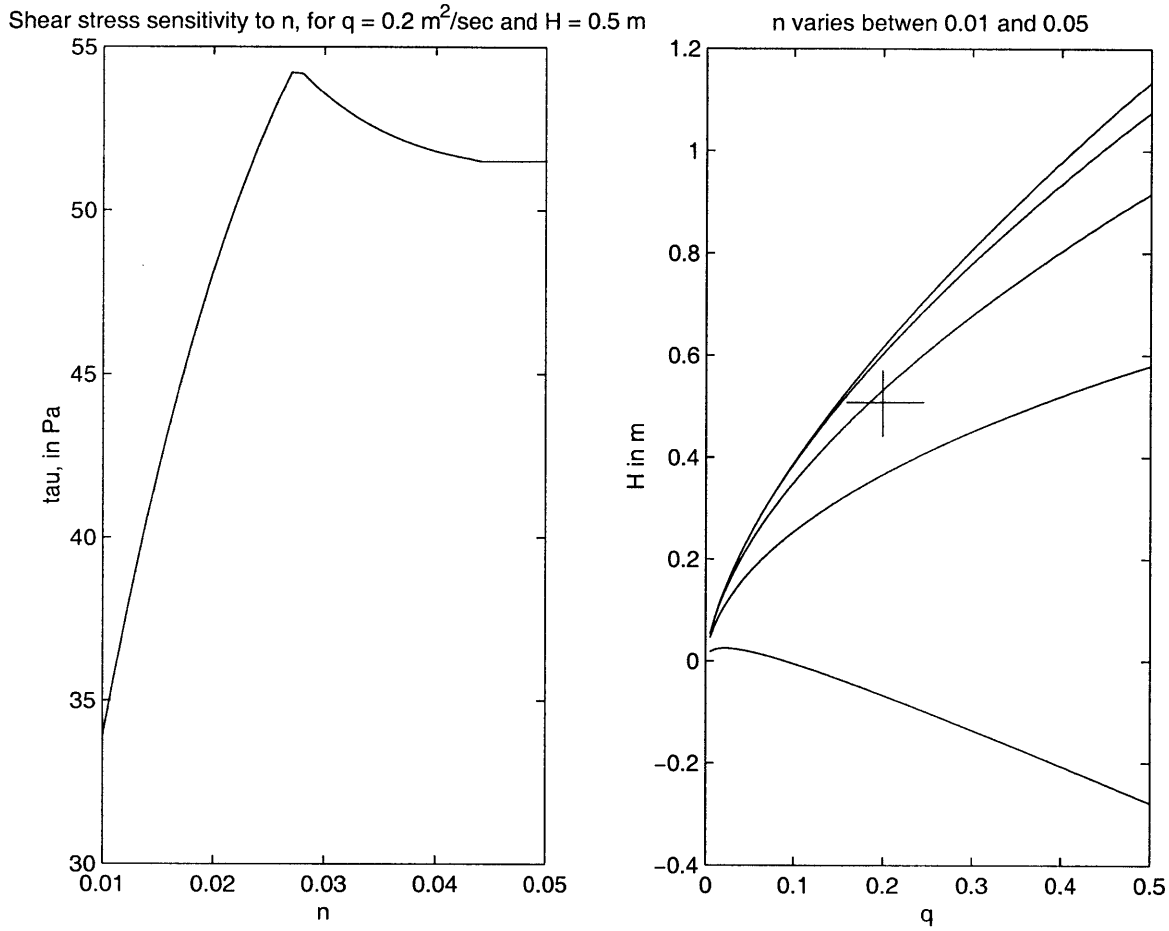

Figure 5-11: Behavior of the shear stress as n increases and the diffusion/non-diffusion conditions change. In this example, the flow regime is supercritical for small values of n, and subcritical for larger values. The horizontal line on the left plot corresponds to the subcritical regime. In this example $S_f = 0.5$.

the q *axis*, the intersection between the H_p and H_t curves is used as a reference. This is because, at the diffusion/non-diffusion boundary (given by H_p, equation (5.7) for any q), the shear stress value (threshold or not) is the same for both diffusion and non-diffusion.

The analysis shows two distinct zones in the H vs q graph of the threshold condition. In the diffusion zone on Figure 5-13, changes in H have no effect on the shear stress, while the changes in q have a large effect. In the non-diffusion zone the opposite is true. Thus, if nature behaves this way, the approach to prevent gullying should be to decrease q in a diffusion situation (e.g, by building a dam upstream) and

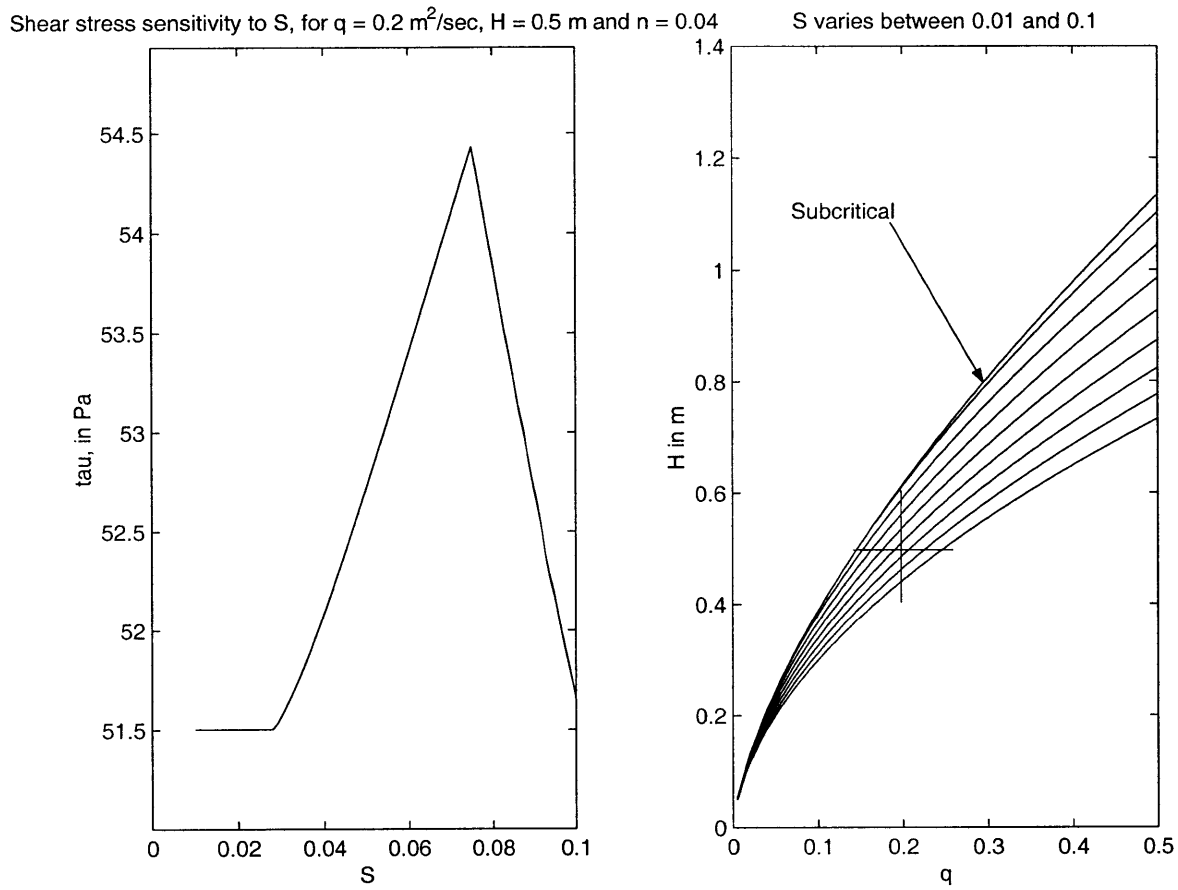

Figure 5-12: Behavior of the shear stress as S increases and the diffusion/non-diffusion conditions change. In this example, the flow regime is subcritical for small values of S and supercritical for larger values. The horizontal line on the left plot corresponds to the subcritical regime. In this example $S_f = 0.5$.

to decrease H in a non-diffusion state (e.g, to reduce the slopes of headcuts).

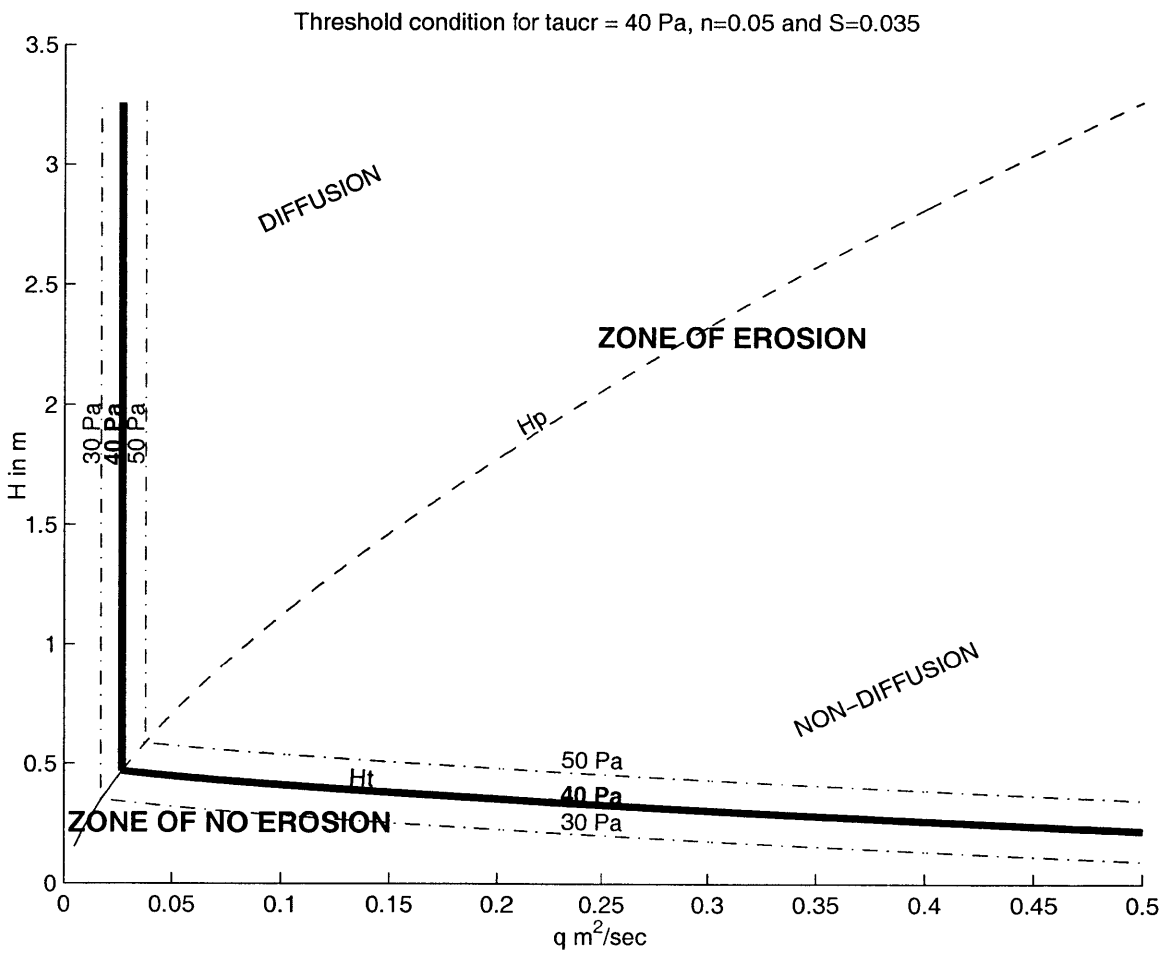

Figure 5-13: Headcut height (H) and flow (q) threshold conditions for plunge pool erosion with $\tau_{cr} = 40Pa$, $S = 0.035$, $n = 0.05$ and $S_f = 0.2$. The flow regime under these flow conditions is subcritical for the range of flows (q) shown.

Chapter 6

Comparison of the model output with observations from flume experiments

6.1 Introduction

In this chapter, the headcut-retreat rate model is compared to results of three flume experiments by Bennett and coworkers [2, 3, 4]. In the first experiment, the effect of the change in slope (S) in the headcut retreat is studied. In the second, the effect of the change in the initial headcut height (initial H) is explored. In the third, the effect of the change in the flow per unit width (q) is explored.

The data sets derived from these experiments were selected for this comparison because: a) they have been accepted and used by others in the field [1, 39]; b) they provide an excellent framework to test the behavior of the retreat rate model as three of its input variables change; c) they provide useful information on the flow and on the geometry of the retreating headcut and corresponding plunge pool; and d) the experiments fulfill most of the assumptions made in the development of the retreat rate model (homogeneous soil, constant retreat rate, achievement of steady headcut retreat soon after the flow begins, maintenance of the shape of the plunge pool in

time, and maintenance of a constant flow q throughout the simulations).

The experiments were carried out in a small flume, $0.167m$ wide, for a small H range (0.05 - $0.005m$) and q between 0.002 and $0.008m^2/sec$. Similar overfall jets and headcut retreat behavior have been observed in larger experimental flumes. Robinson studied in detail the shear stresses and velocities produced by a jet resulting from an overfall of up to $0.76m$ impinging into water under different hydraulic conditions [31, 32, 29]. The jet structure and diffusion of the jet impinging the body of water observed by Robinson and those observed by Bennett and coworkers are in agreement.

Headcuts retreating at a constant rate in homogeneous materials at large scales (width = $1.8m$, flume length = $29m$, H of up to $1.55m$, and flows up to $2.42m^3/sec$ that translate to flows per unit width (q) of $1.3m^2/sec$) have been observed by Robinson and Hanson [30]. Robinson and Hanson intended to test the effect of the variability of H and q in the retreat of a headcut, but only concluded that the variability of soil conditions (soil moisture and density) appeared to have as much influence on headcut retreat as did the overfall height and discharge variations. In their tests, the overfall jet was in ventilated conditions, and the soil was supposed to be homogeneous. Nevertheless, the degree of soil homogeneousness they attained was insufficient to eliminate the variabilities in the headcut advance due to soil heterogeneities.

A drawback in using these data sets is that some of the headcut-retreat model assumptions are violated by all the data points of the second two sets of experiments (when the initial H and q are explored). In these experiments the overfall jet is non-ventilated (instead of ventilated, as assumed) and the depth of the flow downstream of the headcut (h_t) is significant (instead of being insignificant). These violations, however, do not seem to be detrimental to model behavior as long as an appropriate shape factor (S_f) is selected.

These comparisons show that the experimental and modeled retreat rate follow the same trend of change when the parameters S, H and q are increased and an S_f representative of the experiments is used in the modeling. The comparative analysis also suggests that the model is largely sensitive to the depth of the pool (D). D has a large influence on the retreat rate in a diffusion state (see Section 5.2.2).

6.2 The trends of the headcut retreat rates as the parameters S, initial H and q change

The comparison is between the experiment and the trends in the retreat rate (E) produced by the model as S, H and q increase. In the model, the retreat rate was obtained for a range of q between 0.0001 and $0.01 m^2/sec$. The rest of the model's geometric input parameters (the Manning's roughness (n), H, S, and S_f) were values representative of each experiment. Table 6.1 shows the values of S, H and q used in each experiment. Other input values of the model are the friction factor (C_f) and the soil erodibility parameters, critical shear stress (τ_{cr}) and erodibility (κ). In this comparison the values used for each of these three parameters were 0.009, $1.75 kPa$, and $2520 \frac{m}{Pa\ yr}$, respectively.

κ. The value of $\kappa = 2520 \frac{m}{Pa\ yr}$ was selected because it provides an acceptable fit of the modeled erosion trends to the data. This value falls within the range of κ obtained by Stain and Nett [38] for sandy loams, clays, and clay loam textured soils native to Montana, in a laboratory flume. The values were obtained using a mathematical description of the impinging jet scour process to calibrate an excess shear detachment relation. Their mathematical description of the impinging jet scour process is similar to the one used in the headcut-retreat rate model.

Table 6.1: Conditions of flow q, headcut height H, and upstream of the headcut slope S corresponding to the experiments carried out by Bennett and coworkers. * See Section 6.2.1.

Experiment	S	H $[m]$	q $[m^2/sec]$
Changes in slope S	0.01-0.1	0.02-0.1 *	0.0055
Changes in headcut height H	0.01	0.005-0.05	0.007
Changes in flow q	0.01	0.025	0.002-0.008

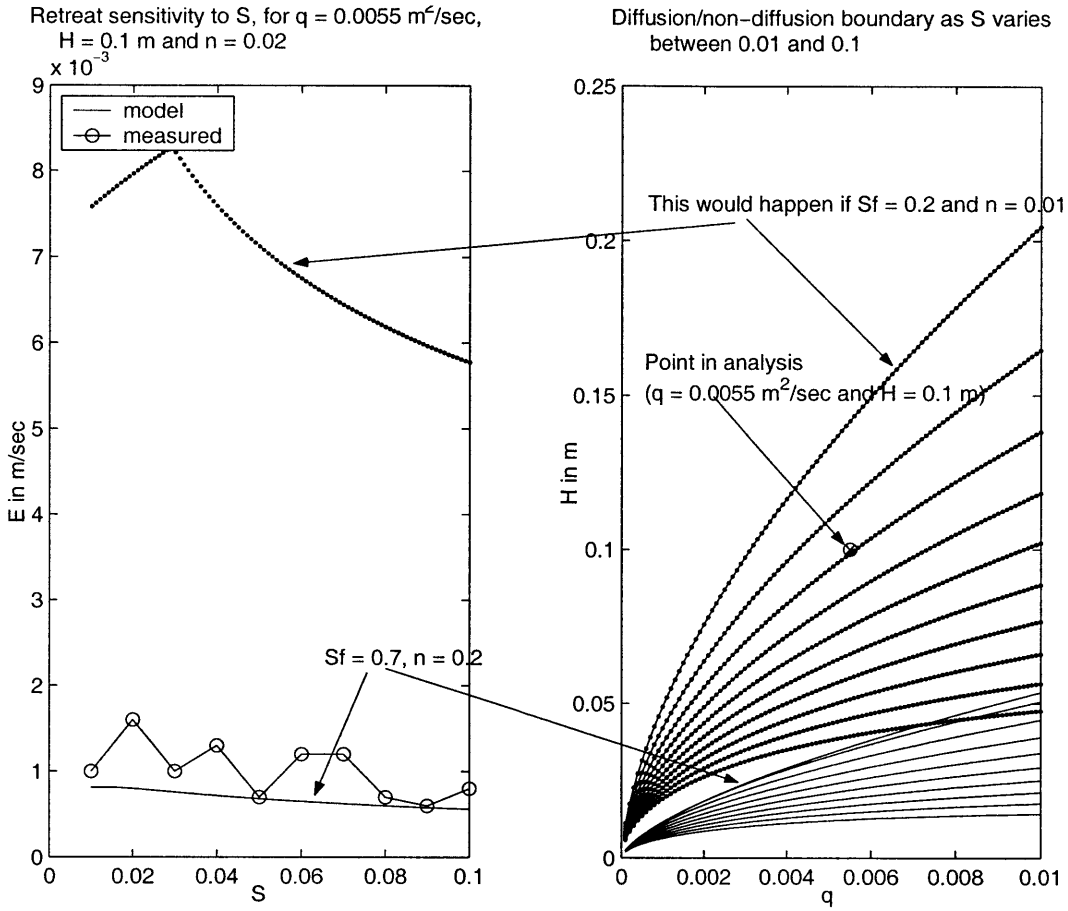

Figure 6-1: Observed and calculated retreat rates as S increases.

6.2.1 Variations in S

In the first experiment, the effect of the change in S was analyzed. In each experimental run, the flume was set to a different slope, between 0.01 and 0.1. As S increased, the retreat rate slowly decreased, in both the experiment and the model, as the left panel of Figure 6-1 shows. In this case, the plunge pool was in a diffusion state (the diffusion/non-diffusion states are explained in Chapter 4). The panel on the right side of the figure shows, in a q *vs* H space, that the point corresponding to the q and H of this experiment is above the diffusion/non-diffusion boundary, and thus, it is in the zone that corresponds to the diffusion state. The set of solid lines on this panel represent the diffusion/non-diffusion boundary corresponding to the S of each experimental run (from 0.01 to 0.1). The top line corresponds to $S = 0.01$.

Figure 6-1 also shows the large sensitivity of the model to the S_f and the difference in the model behavior between the diffusion and the non-diffusion states. The dotted lines show the model output corresponding to an $S_f = 0.2$, smaller than that representative of the experiment ($S_f = 0.7$), and a Manning's roughness $n = 0.01$. The smaller S_f results in higher retreat rates, and in combination with $n = 0.01$, in a transition from a non-diffusion state to a diffusion state as S increases.

The panel on the right side of Figure 6-1 shows how the diffusion/non-diffusion boundary moves downwards as S increases from 0.01 to 0.1. In the beginning, when $S = 0.01$, the plunge pool is in a non-diffusion state (for $S_f = 0.2$), because the point corresponding to the q and H of this experiment is below the boundary, in the non-diffusion zone. Later, when $S = 0.03$ and higher, the point corresponding to the q and H of this experiment is above the diffusion/non-diffusion boundary and thus the plunge pool has switched to a diffusion state. The left panel of the figure shows an increasing trend in the retreat rate as S increases while it is in a non-diffusion state, and then, a decreasing trend when it switches to a diffusion state, again for the $S_f = 0.2$ case.

The experimental E, S, q and H were direct observations. In this experiment, H increased in each run as the headcut retreated because the upstream slope was larger than the slope of the channel resulting from the headcut retreat. $H = 0.1m$ was a value representative of H for the experiment (it varied between 0.02 and 0.12, Table 6.2 shows the final H of each run).

The value of $n = 0.02$ used in the model was representative of the experiment. The experimental values of n varied between 0.0088 and 0.0268 as Table 6.2 shows. n was not directly measured. It was back calculated with the measured flow depth upstream of the headcut (h_n), q and S. A normal flow that followed Manning's flow velocity equation was assumed, and so n was back calculated as $n = (h_n S^{0.3} q^{-0.6})^{1/0.6}$.

The value of S_f used is representative of the experimental values, which varied between 0.42 and 0.87 as Figure 6-2 shows. The S_f was not directly measured, but the distance from the headcut to the point of maximum depth at the pool (X_m) was measured, and D was obtained as described in the following paragraph, so that S_f

Table 6.2: Values of H and n of the experiment when S increases. The values of n were back calculated from the experimental upstream flow conditions.

Run	1	2	3	4	5	6	7	8	9	10
H	0.02	0.02	0.05	0.05	0.075	0.08	0.1	0.1	0.12	0.12
n	0.0088	0.0103	0.0104	0.0132	0.0234	0.0182	0.02	0.0249	0.0268	0.0197

could be estimated as $S_f = D/X_m$.

D was not directly measured. Instead, a parameter S_d, the maximum scour depth, equal to the sum of H and D, was measured, and so D was obtained as $D = S_d - H$. Figure 6-3 shows how the D predicted by the model compares with the D observed. The trends of change of both the experimental and observed D, as S increases, are in agreement.

6.2.2 Variations in H

In the second experiment, the effects of the changes of H were analyzed. In each experimental run, a different initial H, between 0.005 and $0.05m$ was set. Each initial H remained constant during each run. As H increased, the retreat rate slowly increased in both the experiment and the model, as Figure 6-4 shows. In this case, at least in the model, the plunge pool is in a non-diffusion state at the beginning ($H = [0.005 - 0.03]$), and then switches to a diffusion state, where retreat is independent of H. Whether the experiment is also insensitive to H or not for $H > 0.3m$ (and thus in a diffusion state) is not clear from the experimental observations. More data would be needed to clarify this.

The panel on the right side of Figure 6-4 shows the vertical line that represents the change in H in the experiments with q constant. The line begins below the diffusion/non-diffusion boundary (as indicated by the H_p *vs* q curve), in the zone corresponding to the non-diffusion state, and ends above the boundary, in the zone corresponding to the diffusion state.

The values of the parameters used in the figures corresponding to this experiment

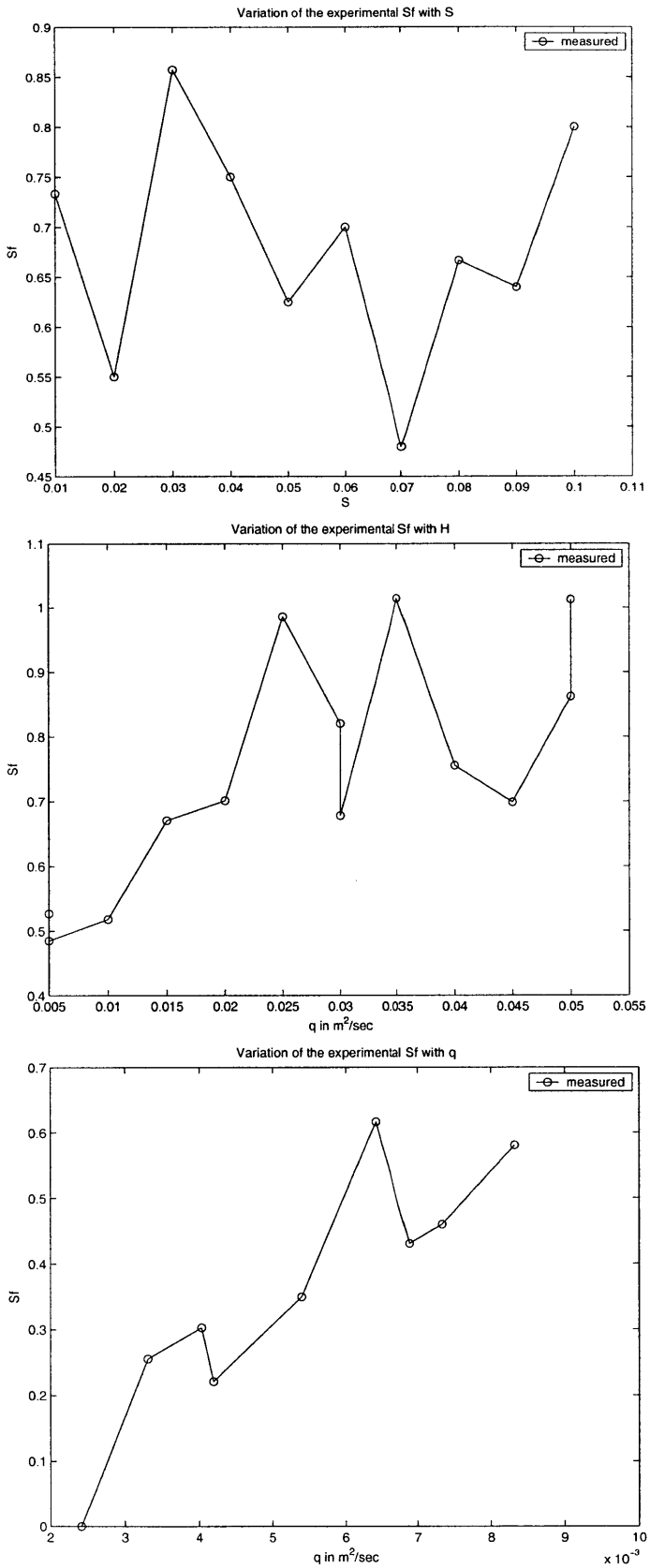

Figure 6-2: Values of S_f as S, H and q change.

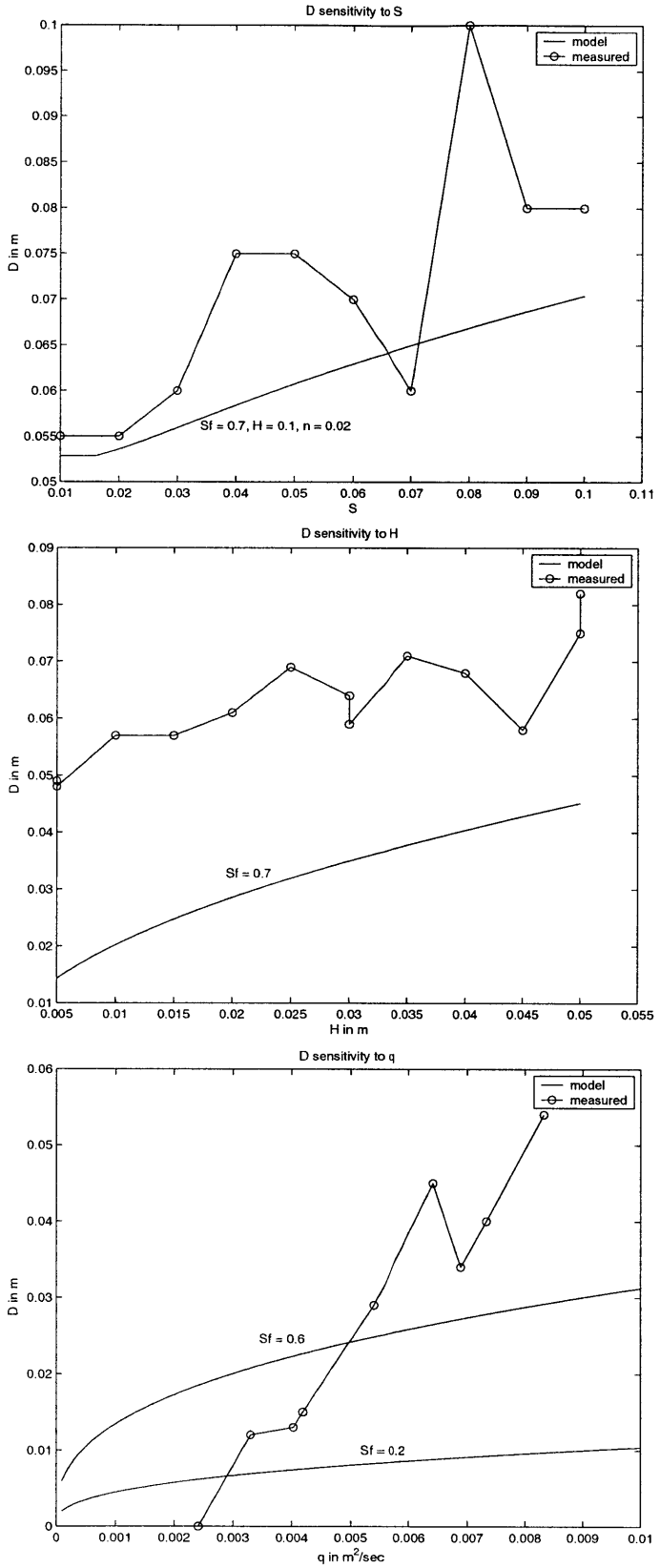

Figure 6-3: Values of D as S, H and q change.

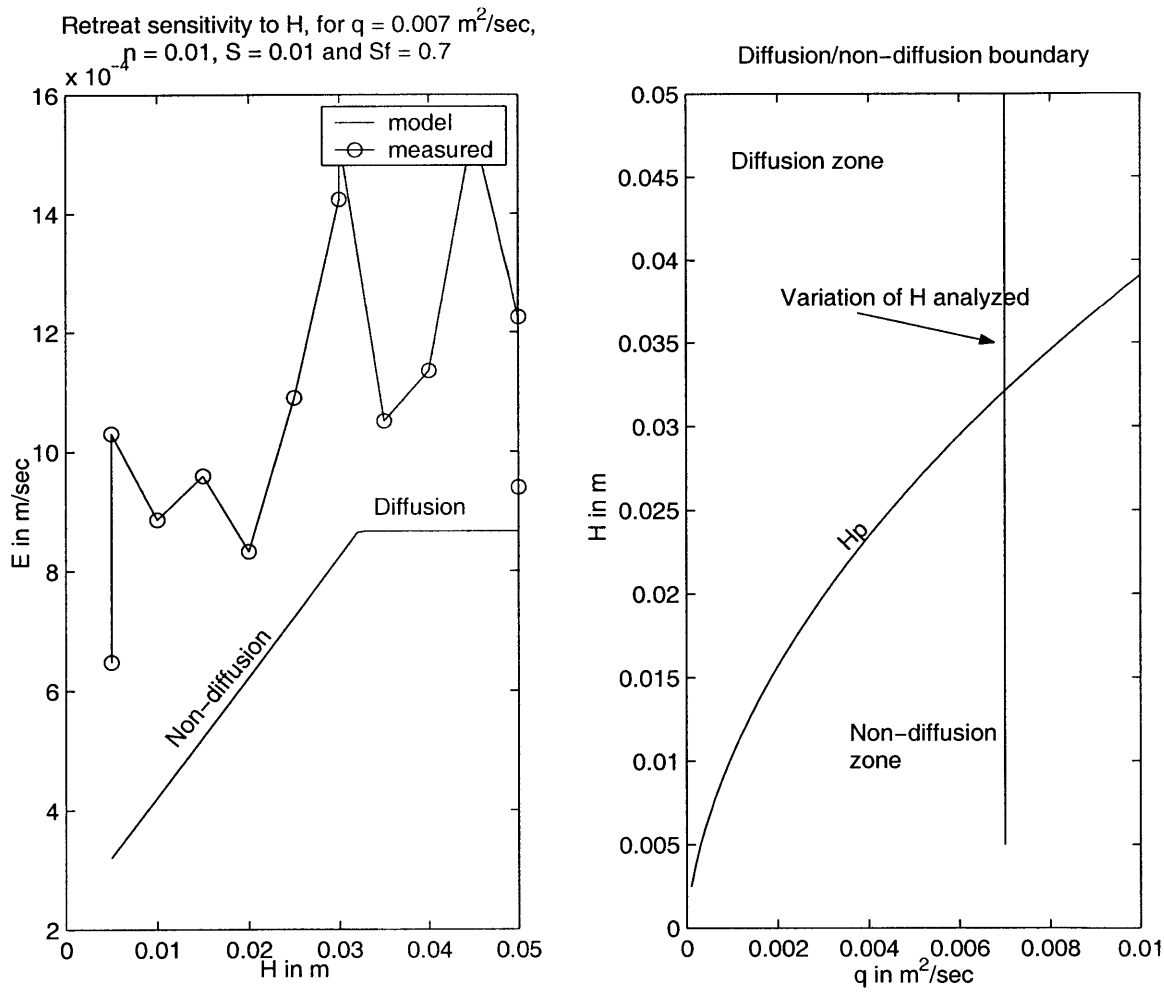

Figure 6-4: Observed and calculated retreat rates as H increases.

were obtained in the same ways as in the case of the first experiment. The values used as inputs to the model representative of the experiment were $n = 0.01$, $S = 0.01$, $q = 0.007m^3/sec$ and $S_f = 0.7$. In this experiment, the value of S_f varied between 0.48 and 1.02, as Figure 6-2 shows.

Figure 6-3 shows how the D predicted by the model compares with the observed D. The trends of change of both the experimental and observed D, as H increases, are in agreement.

6.2.3 Variations in q

In the third experiment the effects of changes in q were explored. In each experimental run, a different q between 0.0024 and $0.0083m^2/sec$ was set. In the experiment, as q increased, the retreat rate slowly decreased as shown in the left panel of Figure 6-5. In addition, in this experiment, unlike in the previous two, the experimental S_f steadily increased. This increase is shown in the third panel of Figure 6-2.

Because the model is greatly sensitive to S_f, as shown above in Section 6.2.1, it cannot represent this experiment's observations with a constant S_f. As q increases, S_f should be increased in the model as well. If this is done, the trend of decreasing E observed in the experiment is also obtained in the model. In Figure 6-5, on the left panel, curves showing the model output for $S_f = 0.2$ and $S_f = 0.7$ are shown. The top curve corresponds to $S_f = 0.2$ and thus to smaller values of q. The bottom curve corresponds to $S_f = 0.6$ and thus to larger values of q. The arrow on this panel represents the trend of E that the model experiences as q and S_f increase, all else remaining constant. This way, the experiment and model trends of change in E as q increases agree.

The decrease in the retreat rate as S_f increases is due to the fact that the retreat rate becomes a smaller fraction of the deepening rate, because $E = \frac{dD}{dt}\frac{1}{S_f}$. A larger S_f means that more material needs to be eroded from the plunge pool shape to produce retreat and thus retreat is slower. The change of S_f as q increases is not understood yet.

The values of the parameters used in the figures corresponding to this experiment

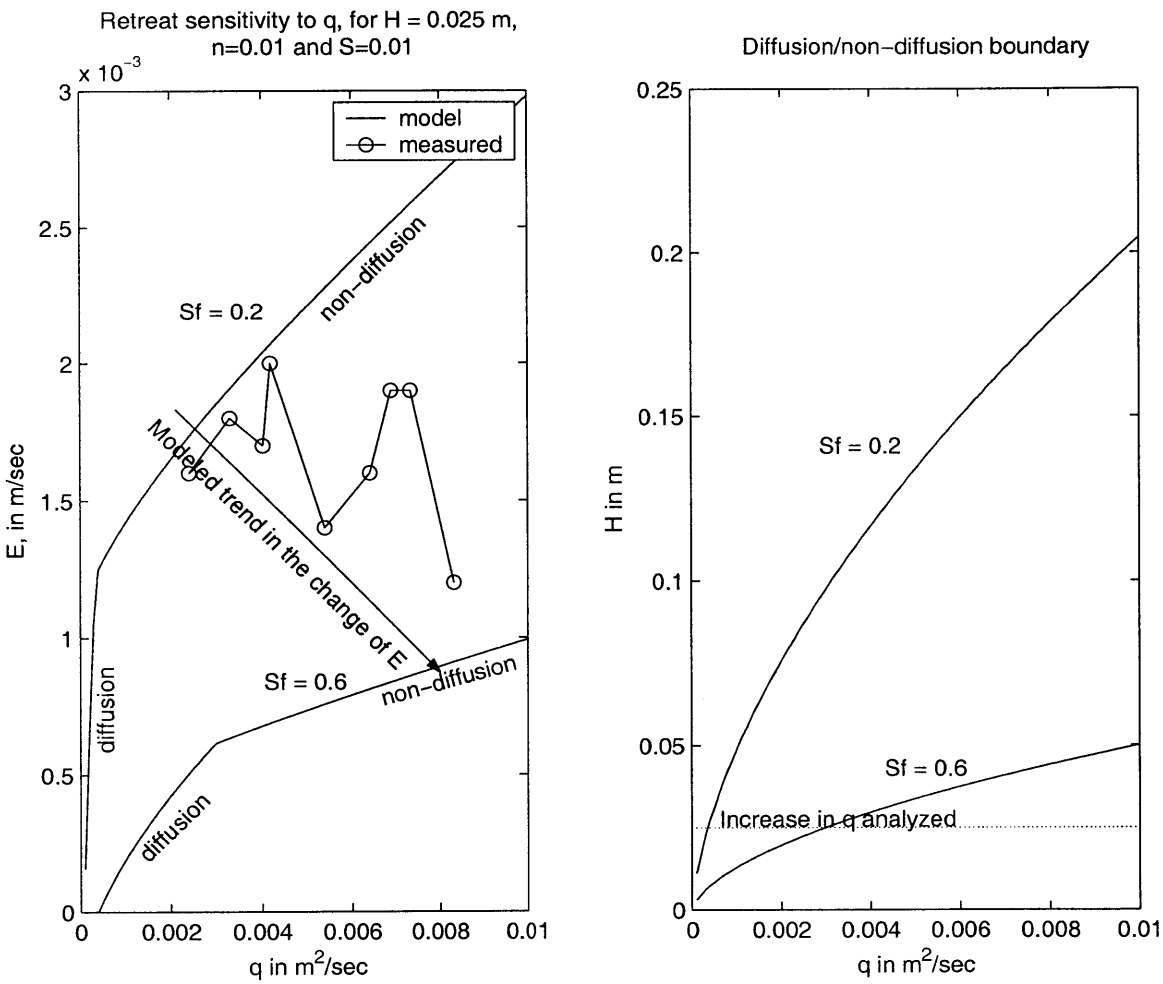

Figure 6-5: Observed and calculated retreat rates as q increases.

were obtained in the same ways as in the previous two experiments. The values used as inputs to the model representative of the experiment were $n = 0.01$, $S = 0.01$, $H = 0.025m$ and $S_f = 0.2$ and 0.6. In this experiment, the value of S_f varied between 0.0 and 0.6, as Figure 6-2 shows. Figure 6-3 shows how the D predicted by the model compares with the observed D. The trends of change of both the experimental and observed D, as q increases, for both $S_f = 0.2$ and $S_f = 0.6$, are in agreement.

6.3 Summary

Bennett and coworkers' data sets are detailed data sets that show the sensitivity of a headcut retreat rate to variations in S, H and q and that are useful in the understanding of the constant headcut retreat process in a homogeneous soil. The E and D reported in these data sets were compared against the E and D calculated with the retreat rate model presented in this thesis. The trends of change in E and D of the experiments were well represented by the model when a representative value of the S_f observed in the experiments was used as an input to the model. Different values of S_f were observed within each data set. The S_f observed in the first two experiments were similar and varied around 0.7. In the third experiment, the S_f observed steadily increased as q was increased. Such increase in S_f is not understood yet.

The model results of D had a better agreement with the experimental observations for a case of an overfall jet in ventilated conditions (i.e., in the first experiment) than for a non-ventilated case (i.e., in the second two experiments).

Chapter 7

Results of CHILD runs

7.1 Introduction

This chapter presents the results of the experiment carried out in CHILD to test the implementation of the headcut-retreat model. This experiment aims to show under what conditions headcut retreat through plunge pool erosion is more or less effective, in comparison to sheetwash erosion. It is hypothesized that for headcut retreat to take place, a headcut must exist, and the retreat of the headcut must be faster than other processes that may diffuse the headcut, such as sheetwash.

The experiment consists of the simulation of the evolution of a region $50m$ by $50m$. Several initial surface elevation configurations are tested under a constant rainfall event that produces $30mm/hr$ of runoff during $1hr$ intervals simulating an intense storm of short duration, such as those occurring in semiarid regions of southwestern USA. The inter-storm periods are neglected because diffusion processes, which generally are the only erosion processes considered during inter-storms, are not active in this modeling experiment. One thousand storm events are simulated.

The initial surface elevation configurations have slopes of 3 and 9 percent. A nearly vertical scarp 0.5 or $2m$ high is created along one of the sides of each plot. The different initial conditions simulated are summarized in Table 7.3. The left image of Figure 7-7 shows the simulated plot as if viewed from the top. In this image the lighter tones represent higher elevations. At the bottom of the image, a black stripe

represents an elevation 0.5 or $2m$ below the rest of the neighboring upper region. The border between the black stripe and the rest of the region represents the nearly vertical scarp. Such scarps in the field may result from channel incisions. Retreating headcuts can develop along these scarps. The soil is assumed to be strong enough to support the steep scarps. Such strength is observed in cohesive soils found in the southeastern region of Colorado. The soil erodibility parameters used in this experiment are $\tau_{cr} = 1.75Pa$ and $\kappa = 2.52\frac{m^3}{Nyr}$. This value is within the range of values of κ estimated for soils in the field. For example, Laften (1991), cited by [22], and Nearing *et al.* [22] estimated κ of the order of 10^{-7} and $10^{-6}m^2s/kg$ for a coarse loamy soil in a deep loess region of the Midwestern USA, and Hanson and Simon [15] found κ between $3x10^{-6}$ and $9^{-9}m^2s/kg$ for silts of low densities in stream beds of Midwestern USA loess.

Because "in general, rill erodibility ... on relatively undisturbed rangelands is an order of magnitude or more[,] less than for disturbed cropland soils" (Laften (1991), cited by [22]), the κ of flume experiments should be larger than the κ of the field. Thus, the value of κ used in the previous chapter's comparison between the model and flume experiments, seems reasonable for the altered soil used in a flume, while the value used in this chapter fits field values well.

7.2 Design of the experiments

Before doing the experiments in CHILD, an analysis of the linear retreat rate model (described in Section 4.2) was carried out with the objective of finding the flow conditions most and least advantageous for headcut retreat resulting from plunge pool erosion. In the analysis, the first conditions are those that produce the largest difference between the intensity of the headcut retreat process and the intensity of the sheetwash process. The second conditions are those that result in the smallest intensity difference. These conditions were then simulated and compared in CHILD. The design of these simulations involved the parameterization of both the headcut-retreat and sheetwash models, and the geometric setting of the topographic surface where

they would act.

7.2.1 The 1D model analysis of shear stress

The analysis of the 1D retreat rate model consisted of a comparison between the shear stresses produced in the plunge pool and those produced by the sheetwash upstream of the headcut (henceforth referred to as *plunge pool and sheetflow shear stresses*) under the same circumstances of slope (S) and surface roughness (n), for a given headcut height (H) and shape factor (S_f) (see Figure 7-1). The shear stresses are assumed representative of the intensity of each process. The analysis also explored the effect of setting S_f to 0.5 and to 0.2, the first value derived from Stein and Julien's [36] observations as noted in Section 4.2, and the second representative of the S_f obtained from field measurements, as described in Chapter 3. The flows (q) analyzed were within the range of 0.0001 to $0.01 m^2/sec$ because that was the range of flows expected in the CHILD simulations. In the analysis, the sheetflow shear stress was estimated as

$$\tau_f = \rho g h S, \tag{7.1}$$

where ρ is the water density, g is gravity, and h is the depth of the flow.

Table 7.1 summarizes the conditions of the five examples of the 1D analysis, shown in Figures 7-2, 7-3, 7-4, 7-5, 7-6. From the analysis, several conclusions were obtained.

First, for $q < 0.01 m^2/sec$, $H > 0.25m$, $S_f \geq 0.2$, and any combination of n and

Table 7.1: Conditions of the 1D comparative analysis between the plunge pool and sheetflow shear stresses.

Name	S	n	H [m]	q [m^2/sec]	S_f
Slow flow conditions	0.03	0.05	0.5	0.0001 - 0.01	0.2
Fast flow conditions	0.09	0.01	0.5	0.0001 - 0.01	0.2
High shear stress conditions and Low shape factor	0.09	0.05	0.5	0.0001 - 0.01	0.2
Low shear stress	0.03	0.01	0.5	0.0001 - 0.01	0.2
High shape factor	0.09	0.05	0.5	0.0001 - 0.01	0.5

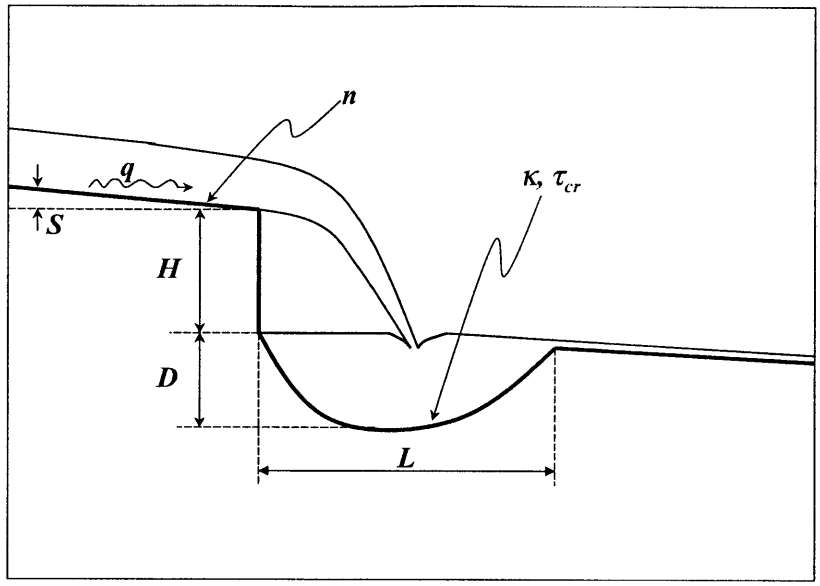

Figure 7-1: Hydraulic characteristics and soil properties considered in the retreat rate model.

S, the jet diffuses as it impinges the plunge pool. In the analysis $S_f = 0.2$, and any S_f larger than that would result in more diffusion. The plots in the right side of Figures 7-2 through 7-5 show that the diffusion/non-diffusion boundary is always below $0.25m$. The highest boundary in these plots corresponds to a subcritical regime (Figures 7-2 and 7-4), a regime in which the boundary is constant and maximum for any combination of S and n (for a given S_f). In diffusion, the shear stress at the bottom of the pool is independent of H, as discussed in Section 5.2.2. In the 3D CHILD simulations, all headcut heights were greater or equal to $0.42m$, $q < 0.1m^2/sec$, and $S_f = 0.2$. Thus all plunge pools are in a diffusion state. H is at least $0.42m$ because of the way a headcut is defined: the slope of a headcut must be larger than $40^o \cong 0.82$. Because the distance between cells is $0.5m$, in the simulations H must be larger than $0.42m$ in order for S to be larger than 40°.

Second, under these diffusion circumstances, the flow conditions that result most advantageous for the headcut retreat mechanism studied in this work (resulting from plunge pool erosion) are the *slow flow conditions*, which produce the largest difference

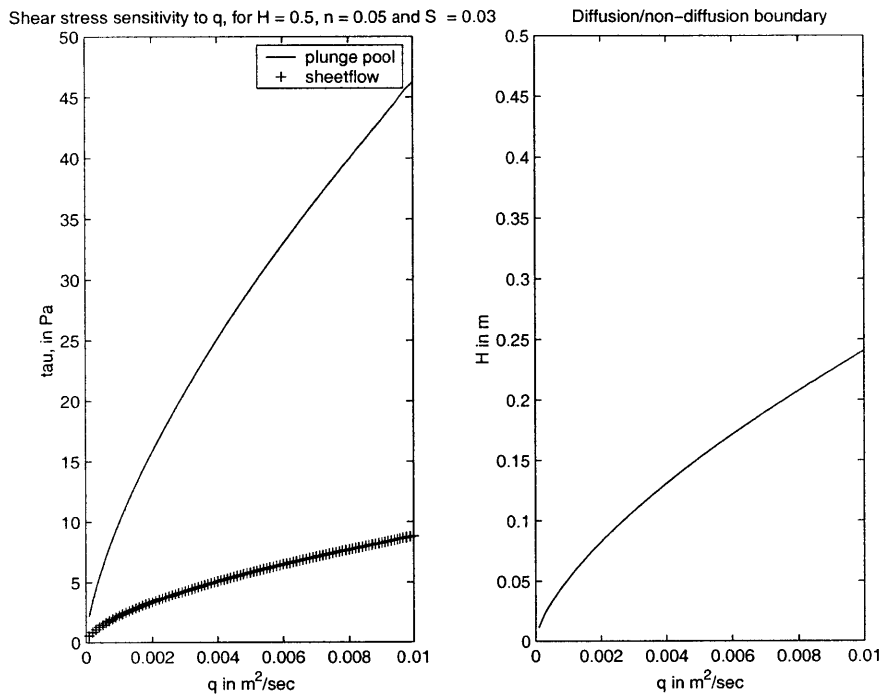

Figure 7-2: Plunge pool and sheetflow shear stresses for slow flow conditions.

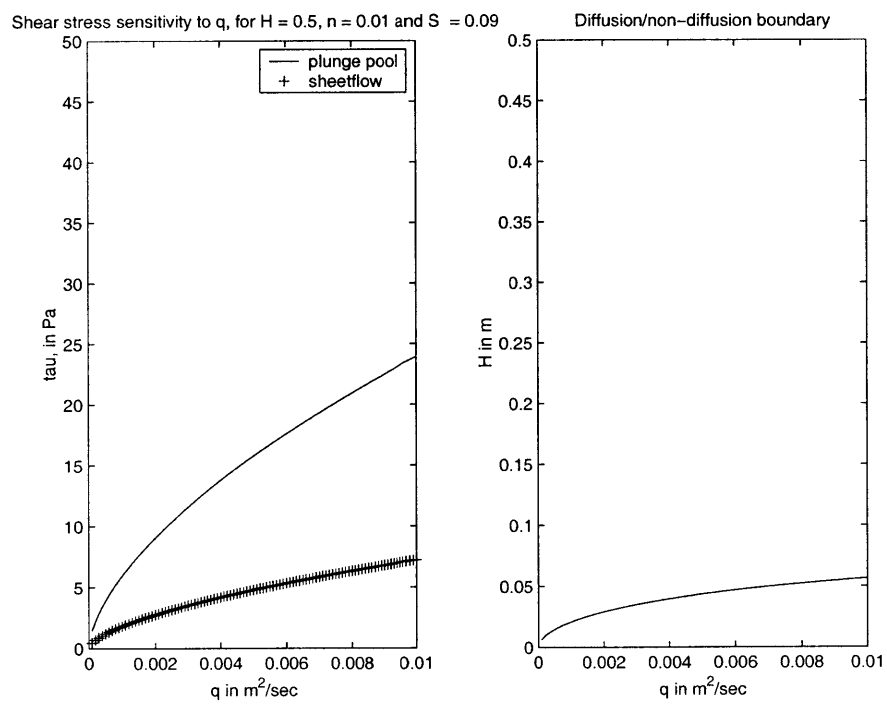

Figure 7-3: Plunge pool and sheetflow shear stresses for fast flow conditions.

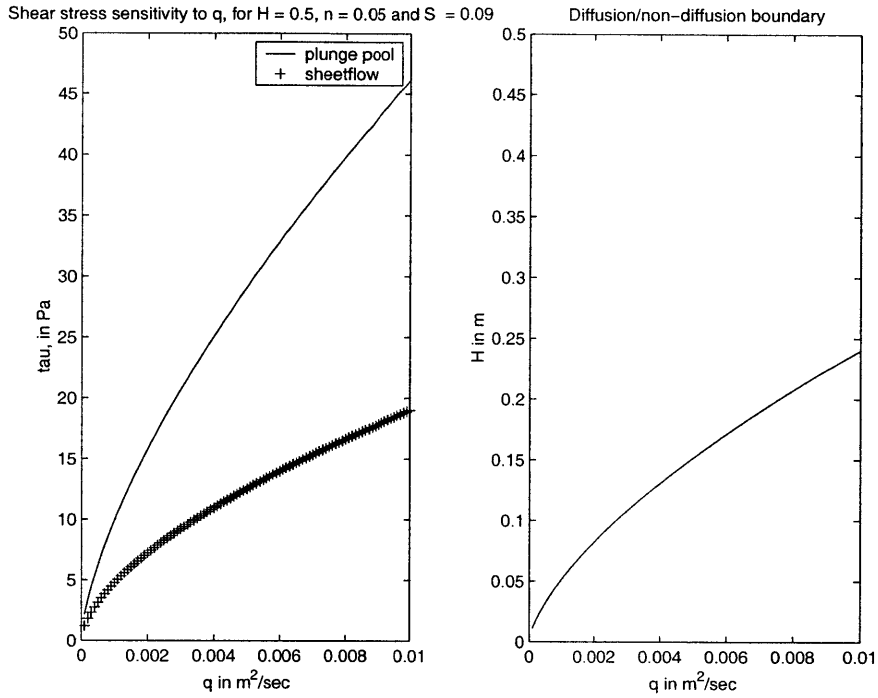

Figure 7-4: Plunge pool and sheetflow shear stresses for high [sheetflow] shear stress conditions.

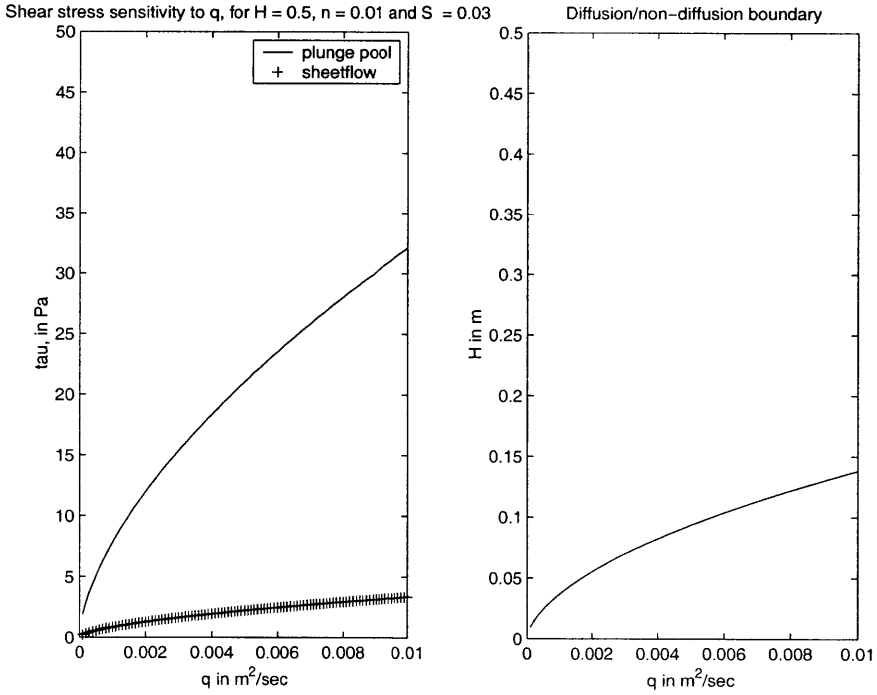

Figure 7-5: Plunge pool and sheetflow shear stresses for low [sheetflow] shear stress conditions.

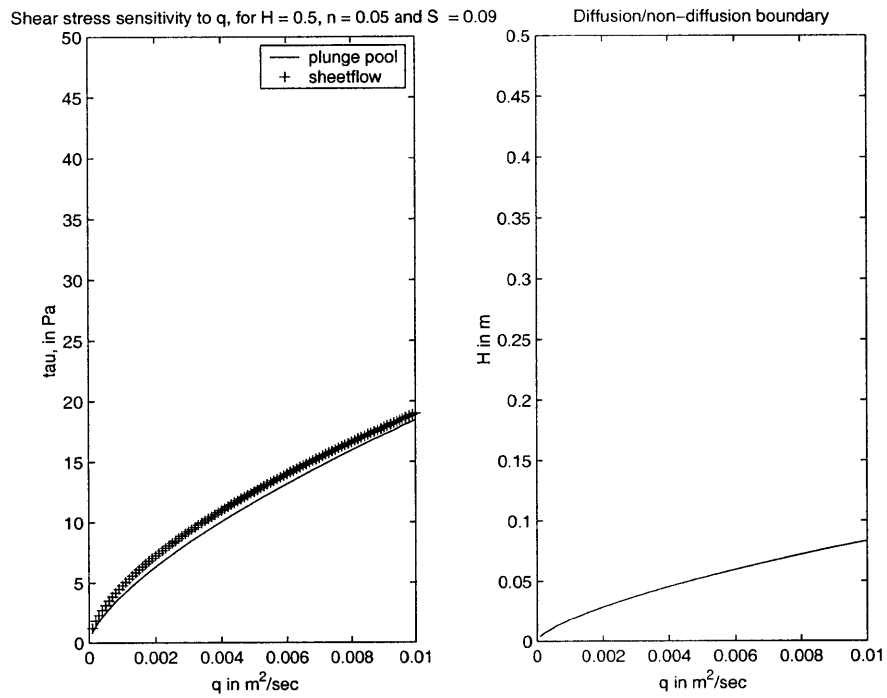

Figure 7-6: Plunge pool and sheetflow shear stresses for a shape factor (S_f) of 0.5 (large shape factor). All the previous examples consider an S_f of 0.2.

between plunge pool and sheetwash shear stresses. The slow flow conditions correspond to a large n and a small S. *Fast flow conditions* (small n and large S) were the least advantageous for the headcut retreat mechanism. They produce the smallest difference between plunge pool and sheetwash shear stresses. The plunge pool and sheetwash shear stresses produced under slow and fast flow conditions are shown in Figures 7-2 and 7-3. Table 7.2 reports the shear stress differences. *High shear stress* and *low shear stress* flow conditions (large values of n and S, and small values of n and S, respectively) result in a large shear stress difference between the plunge pool and the sheetwash shear stresses, as reported in Table 7.2, and thus headcut retreat via plunge pool erosion is favored under these conditions (even if sheetflow shear stress is large under high shear stress flow conditions). The difference in shear stresses, however, is higher under slow flow conditions. The plunge pool and sheetwash shear stresses produced under high shear stress and low shear stress flow conditions are shown in Figures 7-4 and 7-5. Changes in the plunge pool shear stress (and thus in

Table 7.2: Plunge pool, sheetflow shear stresses, and their difference, corresponding to the 1D shear stress simulations of this comparative analysis, for $q = 0.01m^2/sec$.

Name	Plunge pool $[Pa]$	Sheetwash $[Pa]$	Difference $[Pa]$
Slow flow conditions	47	9	38
Fast flow conditions	24	7	17
High shear stress conditions and Low shape factor	46	19	27
Low shear stress	32	3	29
High shape factor	18	19	-1

the headcut retreat rate rates) are the primary cause of the most and least favorable conditions for the headcut retreat mechanism. This is because the sheetflow shear stress changes little as it moves towards slower or faster flow conditions. When the flow changes towards a slow flow condition, the effects of an increase in n and a decrease in S on the sheetwash shear stress counteract each other because sheetflow shear stress is directly proportional to $n^{0.6}$ and $S^{0.7}$. The same counteraction occurs when the flow moves towards a faster flow condition. In the CHILD simulations, the upstream slope S changes as the sheetwash erodes the surface. The Manning's roughness n is constant in the model. In the field n depends on the vegetation cover and soil texture. Because vegetation cover changes rapidly over time (from one erosive event to the next), n is a parameter that in the field is variable over time.

Third, the headcut-retreat model is largely sensitive to the shape (S_f) factor when S_f increases from 0.2 to 0.5. The sensitivity of S_f was previously discussed in Section 6.2.1. In this analysis the difference in shear stresses obtained with $S_f = 0.5$ ($-1Pa$) resulted much smaller than that with $S_f = 0.2$ ($27Pa$) (See Figures 7-6 and 7-3, and Table 7.2). The first case results unfavorable for the headcut retreat mechanism, while the second results advantageous.

7.2.2 The experiments in CHILD

The conclusions of the above analysis of shear stresses guided the design of these experiments, which aim to show that: (a) under fast flow conditions and low headcut heights (a large S, a small n, and a small H), sheetflow is a dominant mechanism, and that under slow flow conditions and higher headcut heights (a small S, a large n, and a large H), the headcut retreat through plunge pool erosion is the dominant mechanism; (b) when the initial H is large, the headcut stays longer in the landscape; (c) the headcut retreat and fluvial erosion are correlated in time and space, at a scarp where considerable amounts of overland flow occur. The experiments also show the difference between considering or not considering headcut retreat in the development of the profile of a scarp, where sheetflow also occurs.

In these simulations sheetwash and headcut retreat through plunge pool erosion are the only land shaping processes considered. Both of these processes are driven by the runoff flow and they are assumed to be detachment limited. The headcut-retreat model used in this experiment is described in Chapter 4. The sheetwash model used in this experiment is described below.

The sheetwash model. The detachment limited sheetwash model in CHILD is derived from the commonly used empirical sediment detachment equation

$$D_c = \alpha_s(\tau_f - \tau_{cr})^a \tag{7.2}$$

where D_c is the detachment capacity per unit area in m/sec, α_s is erodibility and a is an experimental coefficient. D_c, α_s and a are equivalent to E, κ, and p of equation (4.20). The shear stress for the sheetflow, τ_f, is estimated with equation (7.1), while the rest of the parameters are those used in equation (4.20).

The experiments. In these experiments, S, q and H change as the topography of the simulated surface evolves. The values of n, τ_{cr}, and κ are fixed throughout the experiment. The six parameters mentioned above are the input parameters of

Table 7.3: Summary of the conditions simulated in CHILD.

Name	Initial S	n	Initial H $[m]$	runoff $[mm/hr]$	S_f
High initial H and Slow flow conditions	0.03	0.05	2	30	0.2
Low initial H	0.03	0.05	0.5	30	0.2
Headcut retreat *turned off*	0.03	0.05	2	30	0.2
Fast flow conditions	0.09	0.01	2	30	0.2
Examples of a headcut in a flat zone	< 0.03	0.05	2	30	0.2

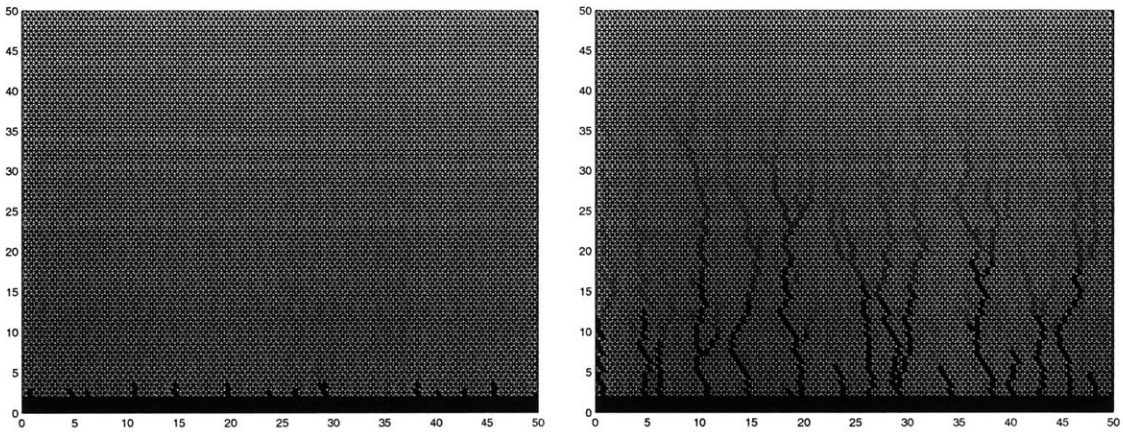

Figure 7-7: Example of a simulated surface in CHILD, view from above, where darker colors represent low elevations and lighter colors high elevations. The left and right figures are the surface conditions after one hundred and one thousand $1hr$ storms have occurred in the simulation, respectively. The dimensions shown are in meters.

the headcut retreat model, and all of them except H are input parameters into the sheetflow model. A summary of the CHILD simulations carried out in the experiment, under the settings described above, and under six different initial conditions, for a simulation of up to one thousand $1hr$ storms, is provided in Table 7.3.

7.3 Results from the CHILD simulations

The results from the simulations are shown as profiles extracted from the 3D surface representations. Figure 7-7 shows an example of these surface representations after one hundred and after one thousand $1hr$ simulations.

In this modeling exercise the channels do not widen because the instability of the slopes is not considered and because the channel width is set to the width of the Voronoi cells. The resulting channels thus, do not resemble field channels that widen due to instabilities and whose width is different from the Voronoi cell width set.

The results are described in terms of profiles because they provide a clear image of the effects of the sheetwash and headcut retreat in the land surface. These profiles correspond to the zones of maximum flow convergence, and it is along them where most of the erosive activity in the simulated surface occurs.

Along these profiles, as the surface is reshaped by the two erosion processes, the flow through the profile changes. The area that catches the flow that drains through any one point in the landscape is referred to as the *drainage area* of that point. Increases of flow in the downstream direction along the profile are due to increases in the drainage area corresponding to each of its points. The drainage area for points along the profile changes as the land is reshaped by the erosive processes. Figure 7-8 shows the changes in the drainage area at the profile's outlet as the profile evolves in time.

Three comparisons of profiles with a headcut and two examples of profiles where sheetflow erosion is practically negligible and a headcut forms, are described below.

1. **High vs low initial scarp height.** In this exercise the initial scarp along one of the sides of the plot (see Figure 7-7) is created with two different heights, 2 and $0.5m$. These profiles are shown in Figure 7-9. In the first case, the headcut is maintained during the first 1000 hours of the simulation, while in the second case, after 100 hours the headcut has become a gradual slope. This observation indicates that a larger headcut provides conditions that favor headcut retreat. This may seem obvious. Nevertheless it is a necessary element when determining whether headcut retreat is important or not in a particular zone. A channel or event that makes a channel incise deeper will favor gullying through headcut retreat through plunge pool.

2. **Active vs inactive (*switched off*) headcut retreat.** This exercise aims to

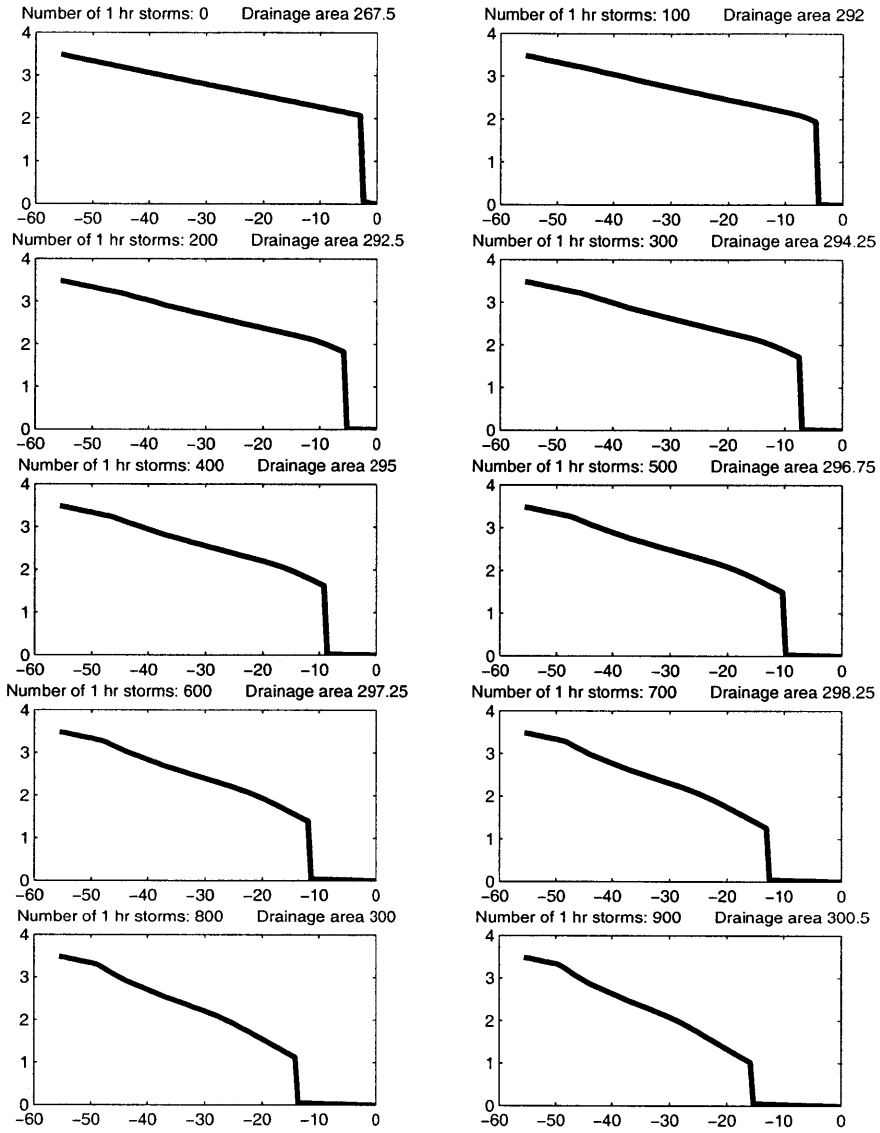

Figure 7-8: Evolution of a profile extracted from the simulated surface. The drainage area corresponding to the outlet of the profile changes as the profile evolves. The vertical and horizontal scales are elevation and negative distance from the outlet, respectively, in meters.

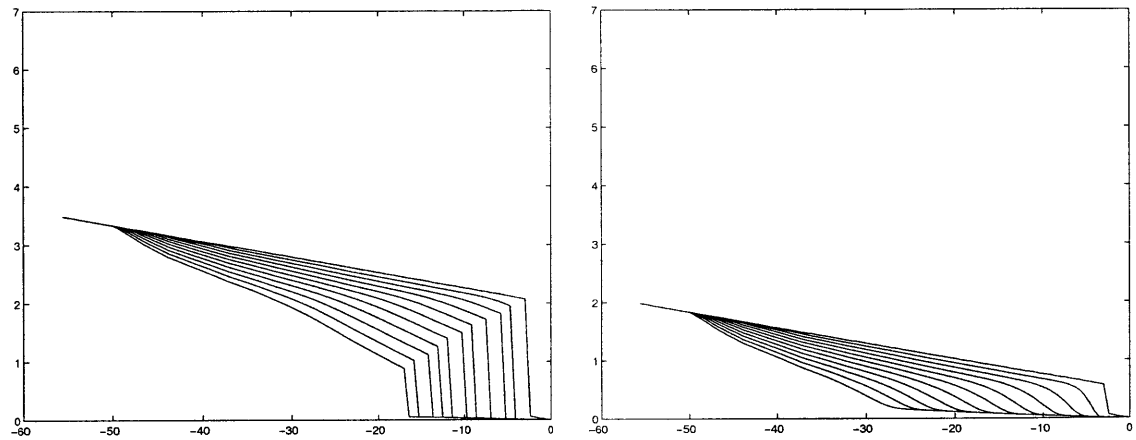

Figure 7-9: Comparison of the evolution of the profile extracted from two CHILD simulations: High initial H (on the left) and Low initial H (on the right) (see Table 7.3). The vertical and horizontal scales are elevation above and negative distance from the outlet, respectively, in meters.

test the relevance of the headcut retreat process through plunge pool erosion in the simulated scenario where the only other erosional process is sheetwash. Figure 7-10 shows that the profiles are similar, regarding the upstream of the headcut section. However, when the headcut retreat occurs, larger amounts of soil are removed from the landscape, which may cause sedimentation problems in downstream water bodies.

3. **Fast flow vs slow flow conditions.** This exercise compares the results from a scenario where the shear stresses produced at the plunge pool and those produced by the sheetflow are close (fast flow conditions), and the results from a scenario where the shear stresses produced at the plunge pool are much larger than those produced by the sheetflow (slow flow conditions). Figure 7-11 shows how a headcut of the same initial height diffuses faster in the first case than in the second case. This observation indicates that slow flow conditions favor headcut retreat, and that fast flow conditions favor sheetwash erosion.

4. **Example of a headcut in a flat zone.** This simulation is an example of what would happen if in a hillslope where sheetflow had acted for one thousand $1hr$ long storms, a channel incised $2m$ along its edge. During the one thousand

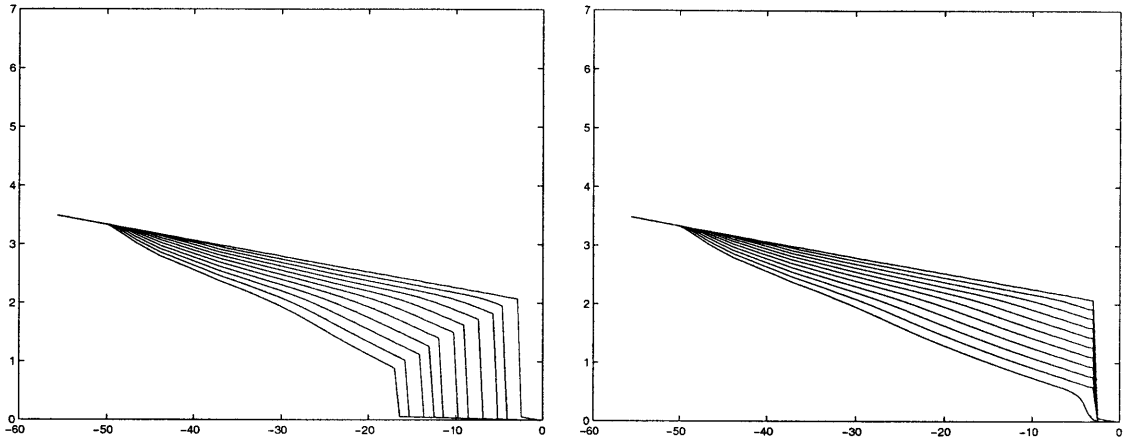

Figure 7-10: Comparison between the evolution of the profile extracted from two CHILD simulations, one considering headcut retreat and the other not considering it, for the same initial conditions (simulations High initial H on the left and No headcut retreat on the right) (see Table 7.3). The vertical and horizontal scales are elevation above and negative distance from the outlet, respectively, in meters.

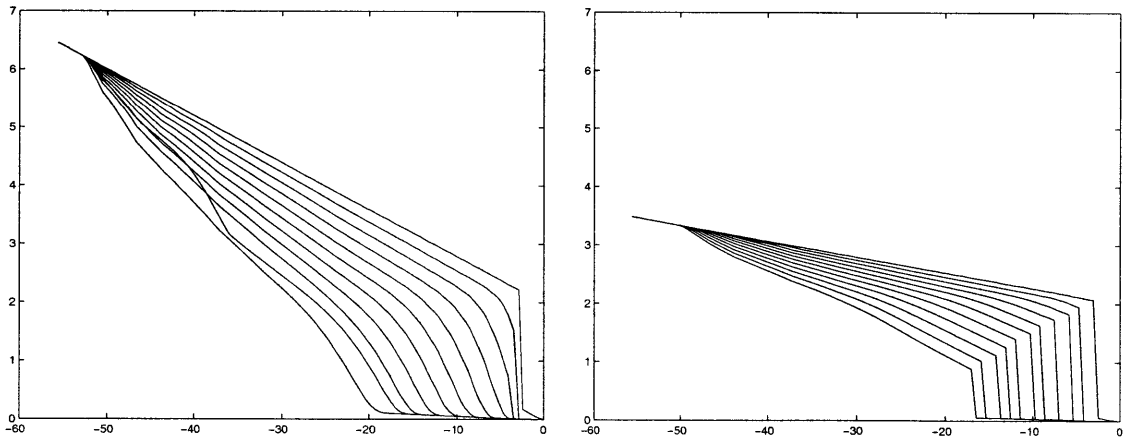

Figure 7-11: Comparison of the evolution of the profile extracted from two CHILD simulations: Fast flow conditions and Slow flow conditions (see Table 7.3). The vertical and horizontal scales are elevation above and negative distance from the outlet, respectively, in meters.

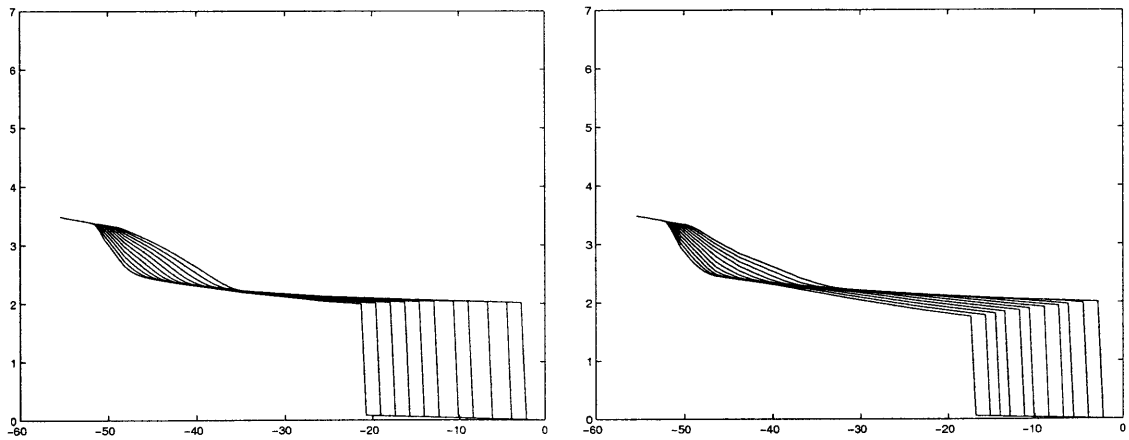

Figure 7-12: Examples of the evolution of two profiles extracted from a CHILD simulation where the initial slopes are little eroded by sheetflow because the slope gradients are small. Both profiles correspond to the simulation Examples of a headcut in a flat zone, summarized in Table 7.3. The vertical and horizontal scales are elevation above and negative distance from the outlet, respectively, in meters.

$1hr$ long storms, before the incision, the lower portions of the profile evolve to a low gradient where the sheetflow shear stress is not enough to cause erosion. Under these circumstances when a scarp is created in the lower portions of the profile, the headcut retreat will be a dominant process along the profile. The evolution of such slope profile is shown in Figure 7-12.

7.4 Conclusions

The following four conclusions drawn from the above analysis of the retreat rate model in 1D and the CHILD simulations in 3D provide insight into which zones of the landscape are more susceptible to headcut retreat through plunge pool erosion and thus to where in the landscape gullies are more likely to form, at least through the headcut retreat through plunge pool erosion mechanism.

First, for flows smaller than $0.01m^2/sec$, $S_f \geq 0.2$, and H larger than $0.25m$, the jet impinging the plunge pool diffuses.

Second, in the CHILD simulations the retreat is independent of H because the jet diffuses. Nevertheless, when the initial headcut is high, the headcut is maintained longer in the landscape, it does not become a smooth slope, as shown in Figure 7-9,

and thus the headcut retreat process is maintained for a longer period of time. Note that an upper limit to H is given by the H a soil can stand. In addition, as a profile evolves and its elevation decreases, the headcut tends to disappear. Therefore, a hillslope is more susceptible to headcut retreat and gullying through this mechanism shortly after the creation of a headcut than long after.

Third, headcut retreat is more competitive against sheetwash in slow flow environments than in fast flow environments, and in gentle slopes where the sheetwash shear stress is less than or equal to the critical shear stress.

Fourth, sheetwash and headcut retreat increase or decrease in magnitude as the drainage area at a point grows or shrinks. In the profiles presented in Figures 7-9 through 7-11, the effect of the increase in the magnitude of the sheetwash is evident because the elevations of the lower portions of the profile upstream of the headcut, a zone of large drainage areas, decrease faster than those in the upper reaches, a zone of small drainage areas.

Note about the flow acceleration at the brink of headcuts. When the flow approaches a headcut, it accelerates and causes larger shear stresses at the brink, the tip of the headcut. When such shear stress exceeds the surface's τ_{cr}, then the brink erodes and a slope steeper than that in the rest of its upstream surroundings appears. The increase in the steepness generates higher shear stresses and erosion rates and aggravates the difference in slopes between the brink and the rest of the land surface. The flow, approximating this steeper slope at the brink, accelerates and results in the propagation of a steeper slope in the upstream direction. This propagation was not considered in this work, but it is a relevant mechanism in the study of gully development because it contributes to the diffusion of headcuts. A more detailed description of this erosional process at the brink can be found in the experimental study of Gardner [13].

Chapter 8

Conclusions

8.1 Summary of the work

The purpose of this thesis was to improve our understanding of the gullying processes, in particular in the southwestern region in the United States. Gullying is a process driven by several erosive mechanisms. Headcut retreat through plunge pool erosion is one of them. Field evidence confirmed that headcut retreat contributes significantly to gully development in the region of interest. Headcut retreat was modeled in a 3D landscape evolution model, CHILD. In this novel modeling effort the effects of headcut retreat and sheetwash erosion were studied. It was hypothesized that headcut retreat in the landscape only occurs in places where the retreat is stronger than other processes that diffuse it, such as sheetwash erosion and diffusion.

The headcut-retreat model consists of the calculation of the retreat of an existing headcut and the transformation of the landscape due to such retreat. The retreat is calculated with a 1D retreat rate model that incorporates ideas developed by others regarding the impingement of a water jet falling from a headcut into a plunge pool and causing the headcut's retreat. The model predicted retreat rate, as a function of its parameters, was studied. This retreat rate model was compared to a series of headcut retreat flume experiments.

8.2 The retreat rate model

The retreat rate model analysis showed that two distinct states of behavior in the retreating headcut-plunge pool system may occur. The jet may be diffusing in the plunge pool before reaching the pool's bottom (diffusion state) or not (non-diffusing state). When the jet diffuses, it is insensitive to the headcut height (H) and very sensitive to the flow (q). In a non-diffusion state, the model is sensitive to H, and slightly sensitive to q. Therefore, if nature behaves this way, to mitigate gullying the approach should be to decrease q in a diffusion situation (e.g., by building a dam upstream) and to decrease H in a non-diffusion case (e.g., to reduce the slopes of headcuts).

8.3 The comparative analyses

The comparative analyses between the retreat rate model and the experiments carried out in a flume showed that the model's retreat rate (E) agrees relatively well with that of the experiments when a shape factor (S_f) representative of the experiments is used as an input to the model, even for cases where assumptions of the model are violated (i.e., the overfall water jet is submerged and the downstream flow depth (h_t) is not negligible). With constant soil erodibility (κ) and critical shear stress (τ_{cr}), the values of the modeled E closely follow the changes of the experimental E as the upstream slope (S), H, and q, increase.

These analyses highlighted the need for a way to estimate an appropriate value of S_f given the model's sensitivity to it and its variability observed in the field and in flume experiments.

The use of S_f is valuable. The assumption that the ratio between the depth of the pool (D) and the pool's mid length (X_m), S_f, is constant, was based on observations by Stein and Julien [36] and is discussed in Chapter 4. It permitted the application of a retreat rate model, similar to other models that required the plunge pool's depth as an input, into a 3D landscape evolution model, because it allowed for the calculation

of D based on H and the hydraulic characteristics upstream of the headcut, values known within the model.

Plunge pool erosion is largely sensitive to D in the diffusion state because the shear stress is directly proportional to D (4.18). The sensitivity to D makes the model, in turn, equally sensitive to S_f because D is directly proportional to S_f. This underscores the sensitivity of the model to S_f.

8.4 Zones of the landscape where headcut retreat through plunge pool erosion is likely to happen

The CHILD simulations indicated several landscape conditions where headcut retreat is likely to be a relevant erosive process. Headcut retreat only occurs where flow converges, and thus, it competes against wash processes. If the conditions favor sheetwash instead of headcut retreat, then, the headcut is likely to rapidly become a gradual slope and thus the headcut retreat process is likely to be of little importance.

The CHILD simulations suggest that the headcut retreat is more competitive against sheetwash a) in slopes where the slope is gentle and the sheetwash shear stress is less or equal to the soil's critical shear stress (τ_{cr}), b) where H is large, c) immediately after the creation of the headcut, and d) in the diffusion case, in slow flow environments rather than in fast flow environments. In areas where the sheetwash shear stress is less than or equal to τ_{cr}, the headcuts are likely to remain in the landscape and propagate without the diffusing effects of sheetwash, as Figure 7-12 shows. When H is large, the headcut remains longer in the landscape. A large value of H, however, is limited by the H a soil can stand.

Headcut retreat is more important immediately after the creation of a headcut since with time diffusion processes like sheetwash take over. In diffusion, rough zones with gentle slopes (slow flow zones) will favor headcut retreat through plunge pool erosion over sheetwash, where as smooth zones with steep slopes (fast flow zones) will favor sheetwash.

8.5 Future work

This modeling work provides a basis for testing the effects of headcut retreat through plunge pool retreat in the landscape, and the effects of the landscape in the plunge pool (e.g., topography, flow convergence, vegetation, soil properties, etc.).

Vegetation, when involved in the modeling, would affect the Manning's roughness n, as well as the critical shear stress τ_{cr} and the erodibility κ of the surface, on top of the headcut or at the bottom of the plunge pool. Vegetation should be variable in time and space, as observed in the field. Vegetation should also play a role in the rates of diffusion in the land.

The role of moisture in the soil is known to be a factor in the stability of a slope, and thus, it must be incorporated into gully modeling where slope stability is relevant.

The model uses a S_f to describe the shape of the pool and is largely sensitive to it, thus knowing what S_f to use is critical for correct results. S_f can be obtained from field observations and laboratory flume experiments, but it is not well understood what determines it, and under what circumstances a constant value of S_f is applicable. Further knowledge about it is needed.

In this work, only the plunge pool's diffusion state was explored in the CHILD simulations (but both the diffusion and non-diffusion state were explored in a 1D scenario in Chapter 5) because for the small region of 50 by $50m$, the maximum flow (q) generated is so small that the non-diffusion state is never achieved. Nevertheless, the non-diffusion state occurs at larger q and thus, needs to be explored with an analysis parallel to the analysis of the diffusion state in Chapter 6.

In this model, only two of the several mechanisms that compose gullying are taken into account: headcut retreat through plunge pool modeling and sheetwash erosion. In the future, more mechanisms of gullying and hillslope processes should be incorporated. The main gully mechanism to incorporate is slope instability. The incorporation of diffusion into the modeling would contribute to the transformation of headcuts into gentle slopes, and thus to a reduction of headcut retreat erosion.

Several simplifications were made to simulate the headcut-retreat mechanism. In

the future, relaxation of these assumptions should lead to the analysis of a more realistic climate, soil, and hydraulic conditions (i.e., stochastic precipitation events, soil layering and heterogeneities, and non-ventilated overfall jet and tail water depth considerations at the plunge pool).

Bibliography

[1] Carlos V. Alonso, Sean J. Bennett, and Otto R. Stein. Predicting head cut erosion and migration in concentrated flows typical of upland areas. *Water Resources Reserach*, 38(12), December 2002.

[2] Sean J. Bennett. Effect of slope on the growth and migration of headcuts in rills. *Geomorphology*, 30:273–290, 1999.

[3] Sean J. Bennett, Carlos V. Alonso, Shyam N. Prasad, and Mathias J. M. Römkens. Experiments on headcut growth and migration in concentrated flows typical of upland areas. *Water Resources Research*, 41(7):1911–1922, July 2000.

[4] Sean J. Bennett and Javier Casalí. Effect of initial step height on headcut development in upland concentrated flows. *Water Resources Research*, 37(5):1475–1484, May 2001.

[5] Rafael L. Bras. *Hydrology, An Introduction to Hydrologic Science.* Addison-Wesley Publishing Company, United States of America, 1990.

[6] Ven Te Chow. *Open-channel hydraulics.* McGraw-Hill, New York, 1959.

[7] A. J. C. Collison. The cycle of instability: stress release and fissure flow as controls on gully head retreat. *Hydrological Processes*, 15:3–12, 2001.

[8] Andrew Collison. *Unsaturated strength and preferential flow as controls on gully head development*, volume 2 of *Advances in Hillslopes*, chapter 34, pages 753–769. John Wiley & Sons Ltd., 1996.

[9] Soil Moisture Equipment Corp. *Guelph Permeameter 2800K1 Operating Instructions.*

[10] J De Ploey. A model for headcut retreat in rills and gullies. In A. Yair and S. Berkowicz, editors, *Arid and Semi-arid Environments Geomorphological and Pedological Aspects*, number 14 in Catena Supplement, pages 81–86. Catena Verlag, Jerusalem, 1989.

[11] Ashis Kumar Dey, Tetsuro Tsujimoto, and Tadanori Kitamura. Growth and migration of headcut in heterogenous soil stratum. *Annual Journal of Hydraulic Engineering*, 45:823–828, February 2001.

[12] Edwin T. Engman. Roughness coefficients for routing surface runoff. *Journal ofIrrigation and Drainage Engineering*, 112(1):39–53, February 1986.

[13] Thomas W. Gardner. Experimental study of knickpoint and longitudinal profile evolution in cohesive, homogeneous material. *Geological Society of America Bulletin*, 94:664–72, May 1983.

[14] Willi H. Hager. Hydraulics of plane free overfall. *Journal of Hydraulic Engineering*, 109(12):1683–1697, December 1983.

[15] G. J. Hanson and A. Simon. Erodibility of cohesive streambeds in the loess area of the mid western usa. *Hydrological Processes*, 15:23–38, 2001.

[16] Alan D. Howard. Groundwater sapping experiments and modeling. In A. D. Howard, R. C. Kochel, and H. E. Holt, editors, *Sapping Features of the Colorado Plateau, a Comparative Planeteary Geology Field Guide*, chapter 5, pages 71–83. NASA Scientific and Technical Information Division, 1988.

[17] Alan D. Howard. Simulation modeling and statistical classification of escarpment planforms. *Geomorphology*, 12:187–214, 1995.

[18] Alan D. Howard. *Simulation of gully erosion and bistable landforms*, pages 277–299. Incised River Channels. John Wiley & Sons Ltd., 1999.

[19] P. D. Jungerius, J. Matundra, and J. A. M. Van de Ancker. Impact of road building on gully erosion risk: a case study from the northern ethiopian highlands. *Earth Surface Processes and Landforms*, 27:1237–1247, 2002.

[20] David R. Montgomery and William E. Dietrich. *Landscape dissection and drainage area-slope thresholds*, pages 221–246. Process Models and Theoretical Geomorphology. John Wiley & Sons Ltd., 1994.

[21] R. Montgomery, David. *Erosional processes at an abrupt channel head: impications for channel entrenchmentand discontinujous gully formation*, pages 247–276. Incised River Channels. John Wiley & Sons Ltd., 1999.

[22] M. A. Nearing, J. R. Simanton, Norton L. D., Bulygin S. J., and J Stone. Soil erosion by surface water flow on a stony, semiarid hillslope. *Earth Surface Processes and Landforms*, 24:677–686, 1999.

[23] Jan Nyssen, Jean Poesen, Jan Moeyersons, Maude Veyret-Picot, Jozef Deckers, Mitiku Haile, and Gerard Govers. Impact of road building on gully erosion risk: a case study from the northern ethiopian highlands. *Earth Surface Processes and Landforms*, 27:1267–1283, 2002.

[24] D. J. Oostwoud Wijdenes and R. Brian. Gully-head erosion processes on a semi-arid valley floor in kenya: a case study into temporal variation and sediment budgeting. *Earth Surface and Landfroms*, 26:911–933, 2001.

[25] Dirk J. Oostwoud Wijdenes, Jean Poesen, Liesbeth Vandekerckhove, Jeroen Nachtergaele, and Jo de Baerdemaeker. Gully-head morphology and implications for gully development on abandoned fields in a semi-arid environment, sierra de gata, southeast spain. *Earth Surface Processes and Landforms*, 24:585–603, 1999.

[26] Anthony J. Parsons, John Wainwright, and Athol D. Abrahams. *Runoff andn erosion on semi-arid hillslopes*, volume 2 of *Advances in Hillslopes*, chapter 48, pages 1061–1078. John Wiley & Sons Ltd., 1996.

[27] Dale F. Ritter. Landscape analysis and the search for geomorphic unity. *Geological Society of America Bulletin*, 100(7):160–171, February 1988.

[28] Dale F. Ritter, Kochel R. Craig, and Jerry R. Miller. *Process Geomorphology.* Mac Graw Hill, New York, NY, fourth edition, 2002.

[29] K. M. Robinson, K. R. Cook, and G. J. Hanson. Velocity field measurements at an overfall. *Transactions of the ASAE*, 43(3):665–670, 2000.

[30] K. M. Robinson and G. J. Hanson. Gully headcut advance. *Transactions of the ASAE*, 39(1):33–38, 1996.

[31] Kerry M. Robinson. Hydraulic stresses on an overfall boundary. *Transactions of the ASAE*, 32(4):1269–1274, 1989.

[32] K. M. Robison. Predicting stress and pressure at an overfall. *Transactions of the ASAE*, 35(2):561–569, 1992.

[33] Glenn O. Schwab, Delmar D. Fangmeier, William J. Elliot, and Richard K. Frevert. *Soil and Water Conservation Engineering.* Wiley, New York, fourth edition, 1993.

[34] M. J. Selby. *Hillslope materials and processes.* Oxford University Press, Oxford, England, second edition, 1991.

[35] O. R. Stein and P. Y. Julien. Criterion delineating the mode of of headcut migration. *Journal of Hydraulic Engineering*, 119(1):37–50, January 1993.

[36] O. R. Stein and P. Y. Julien. Sediment concentration below free overfall. *Journal of Hydraulic Engineering*, 120(9):1043–1059, September 1994.

[37] O. R. Stein, P. Y. Julien, and C. V. Alonso. Mechanics of jet scour downstream of a headcut. *Journal of Hydraulic Research*, 31(6):723–738, 1993.

[38] O. R. Stein and D. D. Nett. Impinging jet calibration of excess shear sediment detachment parameters. *Transactions of the ASAE*, 40(6):1573–1580, 1997.

[39] Otto R. Stein and Dean A. La Tray. Experiments and modeling of head cut migration in stratified soils. *Water Resources Research*, 38(12), December 2002.

[40] Colin R. Thorne. *Bank processes and channel evolution in the incised rivers of north-central mississippi*, pages 97–121. Incised River Channels. John Wiley & Sons Ltd., 1999.

[41] Gregory E. Tucker. Drainage basin responses to climate change. *Water Resources Research*, 33:2031–2047, 1997.

[42] Gregory E. Tucker, Stephen T. Lancaster, Nicole M. Gasparini, and Rafael L. Bras. The channel-hillslope integrated landscape development (child) model. In R. S. Harmon and W. W. I. Doe, editors, *Landscape Erosion and Evolution Modeling*, pages 349–388. Kuwer Acad., New York, 2001.

[43] Garry R. Willgose. *A physically based channel network and catchment evolution model.* PhD thesis, Massachusetts Institute of Technology, 1989.